NTNU

Norwegian University of
Science and Technology

Effect of design specifications for off-design operation of low temperature Rankine cycles using zeotropic mixtures and pure working fluids

Goran Durakovic

Master of Science in Mechanical Engineering
Submission date: June 2018
Supervisor: Petter Nekså, EPT
Co-supervisor: Trond Andresen, SINTEF Energy Research
Brede Andre Larsen Hagen, SINTEF Energy Research

Norwegian University of Science and Technology
Department of Energy and Process Engineering

NTNU
Norwegian University
of Science and Technology

Department of Energy
and Process Engineering

EPT-M-2018-24

MASTER THESIS

for

Student Goran Durakovic

Spring 2018

Effect of design specifications for off-design operation of low temperature Rankine cycles using zeotropic mixtures and pure working fluids

Effekt av design spesifikasjoner for off-design drift av lav-temperatur Rankine prosesser med zeotropiske blandinger og rene arbeidsmedier

Background and objective

In lack of competitive options, vast amounts of industrial surplus heat are dumped to the ambient all over the globe. If a local or internal need for heat exist, direct use of the heat will most often be a cost efficient option, but in general the need is very low compared to available amounts of heat. The COPRO project, led by SINTEF Energy Research, primarily targets recovery of industrial waste heat in the temperature range of 125-250 °C for conversion to electricity. This is a temperature range where profitable energy recovery currently is challenging, but with large amounts of heat available.

The long term goal within this scientific field is to find mixtures of fluids that have ideal thermophysical properties for use in Rankine cyles for the intended applications, and exploit these properties as much as possible with specifically designed components, cycle configurations, and optimal operating conditions. Exploration of potential fluids and mixtures at variable conditions and cases are highly valuable, but identifying a basis for fair comparison without resorting to exhaustive detailed component design is challenging.

Building on the previous project work, the aim of this Master work is to systematically explore the effect of "locking down" optimal design specifications and simulate the system operated in off-design conditions, for example representing changing conditions over a year of operation. Fluid mixture composition and heat exchanger area distribution are defined from design point investigations, and further operating points could typically include varying heat source/sink temperatures and/or flow rates. The goal is to identify industrial scenarios, context, and conditions where mixed fluid cycles out-perform pure-fluid cycles. The potential for improvement should be quantifiable.

The following tasks are to be considered:

1. Explore and define relevant industry scenarios and realistic (seasonal) variation in conditions

2. Define case studies to be investigate including "good" design points. The design point is used to set up heat exchanger geometry, expander performance, and working fluid composition
3. Literature study on off-design behavior of power cycles – e.g. impact on heat exchangers and expanders
4. Describe and discuss a methodology for using discrete simulation points to represent a desired timespan or otherwise variable conditions in a balanced, representative manor
5. Topics for more in-depth studies:
    a. A scenario may exist where surplus heat may be used for either district heating or power production, and seasonal variation on electricity and heat price can be used to determine how to best combine the two over a year.
    b. Discuss the impact of system design and selection of design conditions. System design: E.g. heat exchanger areas and pressure drops in design point. Design conditions: E.g. heat source/sink state. What is the most cost-efficient design? Discuss the impact of design point selection on the off-design results and eventual system comparisons.
6. Summarize the work in a draft scientific article
7. Propose topics for further research

-- " --

Within 14 days of receiving the written text on the master thesis, the candidate shall submit a research plan for his project to the department.

When the thesis is evaluated, emphasis is put on processing of the results, and that they are presented in tabular and/or graphic form in a clear manner, and that they are analyzed carefully.

The thesis should be formulated as a research report with summary both in English and Norwegian, conclusion, literature references, table of contents etc. During the preparation of the text, the candidate should make an effort to produce a well-structured and easily readable report. In order to ease the evaluation of the thesis, it is important that the cross-references are correct. In the making of the report, strong emphasis should be placed on both a thorough discussion of the results and an orderly presentation.

The candidate is requested to initiate and keep close contact with his/her academic supervisor(s) throughout the working period. The candidate must follow the rules and regulations of NTNU as well as passive directions given by the Department of Energy and Process Engineering.

Risk assessment of the candidate's work shall be carried out according to the department's procedures. The risk assessment must be documented and included as part of the final report. Events related to the candidate's work adversely affecting the health, safety or security, must be documented and included as part of the final report. If the documentation on risk assessment represents a large number of pages, the full version is to be submitted electronically to the supervisor and an excerpt is included in the report.

Pursuant to "Regulations concerning the supplementary provisions to the technology study program/Master of Science" at NTNU §20, the Department reserves the permission to utilize all the results and data for teaching and research purposes as well as in future publications.

The final report is to be submitted digitally in DAIM. An executive summary of the thesis including title, student's name, supervisor's name, year, department name, and NTNU's logo and name, shall be submitted to the department as a separate pdf file. Based on an agreement with the

supervisor, the final report and other material and documents may be given to the supervisor in digital format.

☐ Work to be done in lab (Water power lab, Fluids engineering lab, Thermal engineering lab)
☐ Field work

Department of Energy and Process Engineering, 15. January 2018

Adjunct Prof. Petter Nekså
Academic Supervisor

Research Advisor(s):
Brede A. L. Hagen, SINTEF Energy Research
Trond Andresen, SINTEF Energy Research

Summary

Using organic Rankine cycles to produce power from low temperature heat sources seems like a promising solution to lower our reliance on environmentally damaging energy sources. By introducing this technology to new and existing industrial processes, it is possible to increase the energy efficiency of the industry, and thereby reduce their consumption of energy. In order to make the cycles' implementation more attractive to the industry, an analysis on their performance variation with the changing seasons must be conducted. The aim of this work is to evaluate the yearly performance of organic Rankine cycles using butane, pentane and a 50%-50% mixture of these as the working fluids, and gauge their sensitivities to their design specifications and conditions. This work is a continuation of a project work from the preceding fall, from which the three working fluids have been chosen to be investigated more deeply.

A literature study has been performed to identify the cycle components that play a key role in the off-design performance of the organic Rankine cycle, and to explore the influence of changing varying heat source and sink characteristics. Furthermore, a major focus in the literature study was to find the most appropriate expander technology for the pressure ratios and power outputs of the cycles in this work. To gauge the approximate values of these, the results from the project work were utilized. Ultimately, it was decided that screw expanders matched well with the needs of this cycle. Using models discovered in the literature study, an off-design model of the expander, which took into account non-design volumetric flows and pressure ratios, was developed and implemented.

With a working off-design model, a design point was chosen for each fluid and their yearly performance optimized. The off-design performance at each data point was compared with its corresponding on-design optimization, which has the optimal set of parameters for that data point. It became clear that pentane was much worse-performing than both butane and the mixture, and so the subsequent analyses favored these two working fluids, while pentane was neglected.

The chosen design points for butane and the mixture were evaluated on whether they were feasible operationally, and no problems were found. Afterwards, their performances were each compared with an alternative design point, which found that the original design points were thermodynamically better. Having accepted the original design points as optimal, the cycle was evaluated under different conditions to investigate how the off-design performance varied with such changes.

Because the model used in this work is unable to model the waste heat recovery unit, the temperature difference in this entire heat exchanger was set to 17.5 K. The influence of this choice was investigated by changing the temperature difference with $\pm$7.5 K. Implicit in this is that the size of the waste heat recovery unit has changed: a larger temperature difference means a smaller waste heat recovery unit and vice versa. For butane, decreasing the temperature difference in the waste heat recovery unit from 25 K to 10 K increased the exergy efficiency of the cycle from 30.9% to 41.1%, while this increase was from 30.8% to 41.4% for the mixture. Having a non-constant temperature difference in the waste heat recovery unit was also investigated for the mixture. Using the data from the project work, the maximum and minimum temperature of the indirect water was set to the optimal solution found in those results. This did not perform better than the constant temperature difference of 17.5 K, primarily because of much

more unused exergy being left in the heat source. The performance was estimated where there was no unused exergy left in the heat source, and this showed that the non-constant temperature difference performed better than the cycle with constant temperature difference.

District heating is part of the system, and the heat for this is extracted upstream of the organic Rankine cycle. The performance impact of this has been estimated, and it shows that if there were no district heating, the electric energy output could be increased with 15.1% for butane, and 19.3% for the mixture. However, despite the increased electric power output, it is not clear that this is economical, as the district heating accounts for roughly 60% of the yearly energy output – when it is included. For it to be economical to neglect the district heating, it was calculated that the price of the district heat would have to be less than roughly 10% of the price of electricity. Other designs for extracting the district heat, where the high-temperature and low-temperature heat would be spent on power production, and medium-temperature heat would be dedicated to district heating, were also qualitatively discussed.

The effect of increasing the temperature of the heat source was also investigated, along with the response of increasing the allowable heat exchanger area for the evaporator, recuperator and condenser. Unlike with the waste heat recovery unit, the optimizer can modify the areas of these heat exchangers while optimizing, and choose the optimal distribution by itself. In increasing the temperature, the mass flow was reduced so that the heat content relative to the ambient was maintained. It was found that by just increasing the heat exchanger area from 230 m^2 to 300 m^2, the net power of butane would increase by 13% relative to the normal case, while the mixture would experience an increase of 17%. Increasing only the temperature from 150°C to 180°C increased the power for a cycle using butane with 43%, while the mixture increased its power output by 37%. Finally, increasing both simultaneously yielded a 63% increase for butane and 56% increase for the mixture.

Sammendrag

Å bruke organiske Rankine sykler til å produsere kraft fra lavtemperatur varmekilder virker som en lovende løsning til å redusere vår avhengighet på ikkemiljøvennlige energikilder. Ved å introdusere denne teknologien til nye og eksisterende industrielle prosesser, kan vi øke energieffektiviteten til industrien, og redusere deres energiforbruk. For å gjøre teknologien mer appellerende til industrien må det undersøkes hvordan ytelsen på slike systemer varierer med årstidene. Målet i dette arbeidet er å evaluere den årlige ytelsen til organisk Rankine sykler som bruker butan, pentan og en 50%-50% blanding av disse som arbeidsmedium. Arbeidet er fortsettelsen på et prosjekt fra høsten som kom før, hvor de tre arbeidsmediene er datapunkt som ble valgt ut til å undersøkes dypere.

En litteraturstudie har blitt utført for å identifisere komponentene i syklusen som spiller en stor rolle i off-design ytelsen til systemet, samt å utforske hvilken innflytelse varmekilden og varmesluket har på sykelparametrene. Et stort fokus i litteraturstudiet var å finne passende expander-teknologier for trykkforholdene og kraftproduksjonsnivåene til syklusene i dette arbeidet. For å estimere hvor store disse ville være, ble resultatene fra prosjektoppgaven brukt. Til slutt ble det bestemt at skrue-expandere passet godt med behovene til denne syklusen. En modell for off-design ytelsen til expanderen, som tok hensyn til volumstrømmer og trykkforhold som var ulike sammenlignet med design, ble utviklet basert på modeller funnet i litteraturstudiet, og implementert i optimalisatoren.

Et on-design punkt ble valgt for hvert fluid, og deres årlige ytelse ble optimalisert med den nye modellen. Off-design ytelsene for hvert datapunkt ble sammenlignet med den tilsvarende on-design optimaliseringen, som har det optimale settet med parameterverdier for det spesifikke datapunktet. Det ble tydelig at pentan hadde mye lavere ytelse enn både butan og blandingen, og dermed ble kun disse to arbeidsmediene analysert i større detalj senere i arbeidet, mens pentan ble forkastet.

De valgte design-punktene for butan og blandingen ble evaluert på om det er mulig å drifte en reell prosess med de sykelparameterne optimalisatoren hadde funnet, og ingen problemer ble oppdaget med disse. Den årlige ytelsen deres ble senere sammenlignet med et alternativt design-punkt hver. Dette viste at det originale design-punktet var fortsatt optimalt for begge fluidene. Nå som et design punkt hadde blitt funnet, ble syklusen evaluert ved forskjellige forhold for å utforske hvordan off-design ytelsen endret seg.

Det ble antatt at temperaturdifferansen mellom varmekilden og den indirekte varmekretsen i ”waste heat recovery unit”-en var 17.5 K gjennom hele varmeveksleren, fordi modellen som ble brukt i dette arbeidet er ikke i stand til å modellere denne varmeveksleren. Modellen ble brukt til å anslå hvor stor effekt denne temperaturdifferansen har på ytelsen til helse systemet ved å finne resultater for når denne temperaturdifferansen ble endret med $\pm$7.5 K. Når temperaturdifferansen blir endret slik, er det implisitt at størrelsen på ”waste heat recovery unit”-en endres, da man får en større temperaturdifferanse med en mindre ”waste heat recovery unit”, og motsatt. Ved å senke denne temperaturdifferansen fra 25 K til 10 K, så økte eksergivirkningsgraden til syklusen med butan fra 30.9% til 41.1%, mens syklusen med blandingen opplevde en økning av den samme virkningsgraden fra 30.8% til 41.4%. En ikke-konstant temperaturdifferanse i ”waste heat recovery unit”-en ble også utforsket for blandingen, hvor data for maksimum- og minimumstemperaturer for den indirekte vannkretsen ble hentet fra resultater i prosjektopp-

gaven. Dette førte ikke til en økt ytelse, og hovedgrunnen viste seg til å være at veldig mye eksergi ble ikke tatt ut av varmekilden og ble dermed tapt. Et estimat ble gjort for hvor mye kraft ville ha vært produsert dersom all eksergien i varmekilden ble brukt, og da var ytelsen høyere for en syklus med en ikke-konstant temperaturdifferanse i "waste heat recovery unit"-en.

Fjernvarme er også en del av systemet, og varmen til dette er tatt ut fra varmekilden oppstrøms til den organiske Rankine syklusen. Innflytelsen dette har på ytelsen av syklusen ble anslått, og dette viser at dersom varme ikke ble fjernet for fjernvarmen, så ville den elektriske kraftproduksjonen økt med 15.1% for butan, og 19.3% for blandingen. Til tross for den økte elektriske kraften, så er det ikke entydig at det er økonomisk lønnsomt å neglisjere fjernvarmen, ettersom den representerer omtrent 60% av den årlige energieksporten – når den er inkludert. For at det skal være lønnsomt å ikke levere fjernvarme, så har det blitt regnet ut at prisen på fjernvarmen må være mindre enn omtrent 10% av prisen for strøm. Andre design for å hente fjernvarmen fra varmekilden har blitt diskutert. I de alternative designene blir høy- og lavtemperaturvarmen brukt til kraftproduksjon, mens mellomtemperaturvarmen blir brukt til fjernvarmen.

Effekten av å øke temperaturen på varmekilden og å øke det tillate varmevekslerarealet for fordamperen, rekuperatoren og kondensatoren ble også utforsket. I motsetning til "waste heat recovery unit"-en, kan optimalisatoren endre på arealene til disse tre varmevekslerne mens den optimaliserer syklusen, og dermed kan den velge fordelingen av areal på egen hånd. Når temperaturen ble økt, så ble massestrømmen av varmekilden minket slik at varmeinnholdet sammenlignet med omgivelsene ble holdt konstant. Resultatene fra denne analysen viser at ved å øke varmevekslerarealet fra 230 m^2 til 300 m^2, så øker netto kraft for syklusen med butan med 13% sammenlignet med det normalet caset, mens syklusen med blandingen økte med 17%. Når kun temperaturen ble økt fra 150°C til 180°C, så økte kraftproduksjonen med 43% for butan, og med 37% for blandingen. Når begge ble økt samtidig, så førte det til en 63% økning i kraftproduksjon for butan, og 56% for blandingen.

Preface

This work is my master's thesis, and it is the culmination of my five year tenure as a student at the Norwegian University of Science and Technology. It is written at the Department of Energy and Process Engineering in collaboration with SINTEF Energy Research for the project COPRO. Readers familiar with thermodynamic power cycles and the evaluation of these should have no issue following the contents of this work, but readers that have not been introduced to the deeper analyses of such cycles may also gain new insights by following the figures that are familiar to them.

The finishing of this thesis marks the conclusion of some of the most transformative years of my life, and the university and its faculty deserve credence for facilitating the character development and academic growth of their students. I am fortunate to have been given the opportunity to use the tools for learning that this institution has provided.

My sincere thanks are extended to my supervisors Trond Andresen, Brede Hagen and Petter Nekså for their unlimited patience and skillful mentoring. By always being available to quickly rectify any confusions, problems or lacks of inspiration, their influence on this work has been monumental.

Acknowledgments are also given to SINTEF Energy Research and all the partners of COPRO for enabling me to work on and contribute to the project.

Goran Durakovic

Table of Contents

List of Tables

List of Figures

Nomenclature

Symbols

A	Area, m^2
E	Energy, MWh
$\dot{E}_x$	Exergy, kW
e_{x}	Specific exergy, $\frac{kJ}{kg}$
h	Specific enthalpy, $\frac{kJ}{kg}$
$\dot{I}$	Exergy destruction rate, kW
$\dot{m}$	Mass flow rate, $\frac{kg}{s}$
n	Rotational speed, rpm
P	Pressure, bar
s	Specific entropy, $\frac{kJ}{kg \times K}$
V	Volume, m^3
$\dot{Q}$	Heat transfer, kW
$\dot{W}$	Power, kW

Subscripts

0	Ambient
avail	Available
cond	Condenser
design	Design specification
DH	District heating
E	Energy
el	Electric
evap	Evaporator
exp	Expander
gen	Generator
in	Inlet
loss	Loss
min	Minimum
net	Net
out	Outlet
pump	Pump
recup	Recuperator
s	Heat source
tot	Total
WHRU	Waste heat recovery unit

Abbreviations

NC	Non-constant
LMTD	Log mean temperature difference
ORC	Organic Rankine cycle
WHRU	Waste heat recovery unit

Greek symbols

Δ	Difference
η_{Ex}	Exergy efficiency
η_{is}	Isentropic efficiency
η_t	Thermal efficiency
η_V	Volumetric efficiency
ρ	Density, $\frac{kg}{m^3}$

Chapter 1

Introduction

1.1 Motivation

In light of the growing consciousness on the effect of greenhouse gases on the environment, a great emphasis has been placed on developing solutions to limit emissions that may harm the environment. One source of emissions is found in the procurement of energy which oftentimes originates from fossil fuels, and limiting such pollution seems like a worthwhile strategy to minimize the footprint of our industries and private lives. Pursuing the goal of limiting our energy needs, one approach is to make current and future energy use more efficient, so as to limit the consumption of polluting non-renewable fuels. The industry has begun exploring this proposal, wishing to lower the environmental impact of their business.

Together with its industrial partners, SINTEF Energy Research has started the project CO-PRO, to develop and improve technologies that convert waste heat to electrical power. One focus in the project is modifying the Rankine cycle to suit the specific industrial needs, such as better utilization of waste heat from various processes. Seeing as how waste heat is often released at low temperatures, it is not effective to use the traditional steam Rankine cycle, and investigating the performance of alternative technologies becomes paramount. Finding appropriate and effective solutions will make these technologies more attractive to the industry, a critical step before they are adopted and can begin limiting the industry's environmental damage.

The application of Rankine cycles for low temperate heat sources has garnered some attention in the literature, and most notably the organic Rankine cycle – a cycle that utilizes organic fluids rather than water as the working fluid – seems promising. In a preceding project, the organic Rankine cycle was studied using various working fluids, and the top fluids were singled out. The motivation of this work is to investigate the organic Rankine cycles using these fluids in off-design conditions, to illuminate how its performance varies over the course of the year, as well as seeing how this performance varies with other industrial characteristics. This provides an indication of what the industry can expect in implementing such technologies. Additionally, in studying how the performance correlates with surrounding system parameters, the work will show how the performance can be improved when applied to realistic contemporary cases. This information is valuable to any members of the industry considering applying such technologies, as it allows them to appraise them more accurately.

1.2 Objective and scope

The objective of this work is to investigate the off-design performance of organic Rankine cycles using butane, pentane and a 50%-50% mixture of these two fluids as the working fluids. Defining a realistic and industry-applicable off-design specifications for the heat source and sink are important to the work, and is one of the earlier objectives. With the yearly variation in surrounding temperatures set, a literature study is done to discover the impact of cycle components on the performance of the cycle. In particular, the role of the expander is given a large focus, and finding an appropriate expander technology for the range of cycle pressures and power outputs is one of the goals of the literature study. After choosing an expander technology for the cycle, a model is developed to realistically evaluate how the performance of the expander changes as the operating point deviates from the design point.

With the expander model developed, and with the yearly variation of relevant parameters defined, a design specification of the cycle has to be made. It is important that this design point is chosen such that the system is able to operate all year, and also that the off-design operations work with an efficiency that is as high as possible. With these goals in mind, the design point is evaluated to ensure that they are upheld.

With the off-design optimizations for the year completed, the system's response to changes in some of its parameters are evaluated, for both the mixture and a pure fluid. First, the presence of district heating is identified as deteriorating the performance of the cycle, and so it is quantified how much the cycle performance improves if there were no district heating. More efficient ways of extracting the thermal energy for the district heat are also qualitatively discussed. Subsequently, the performance of the system is evaluated with varying sizes of the heat exchangers, and the temperatures of the heat source. These performance changes are analyzed and explained.

1.3 Background theory

1.3.1 The Rankine cycle

The Rankine cycle is a thermodynamic cycle that utilizes a temperature difference between a heat source and sink to produce electric power. The most elementary Rankine cycle consists of four components connected with pipes: the pump, the evaporator, the expander and the condenser. The process diagram illustrating these components is depicted in Figure 1.1a. The Rankine cycle operates by evaporating the working fluid in the evaporator before the fluid enters the expander. Here the energy in the vapor is converted into rotational mechanical energy, which can drive an electrical generator or other mechanical equipment. After the expander, the fluid is passed into the condenser, where heat is released from the working fluid to the heat sink. Afterwards, the liquid working fluid enters the pump, which increases the pressure of the working fluid and drives it to the evaporator, completing the cycle. Traditionally, the working fluid of a Rankine cycle has been water.

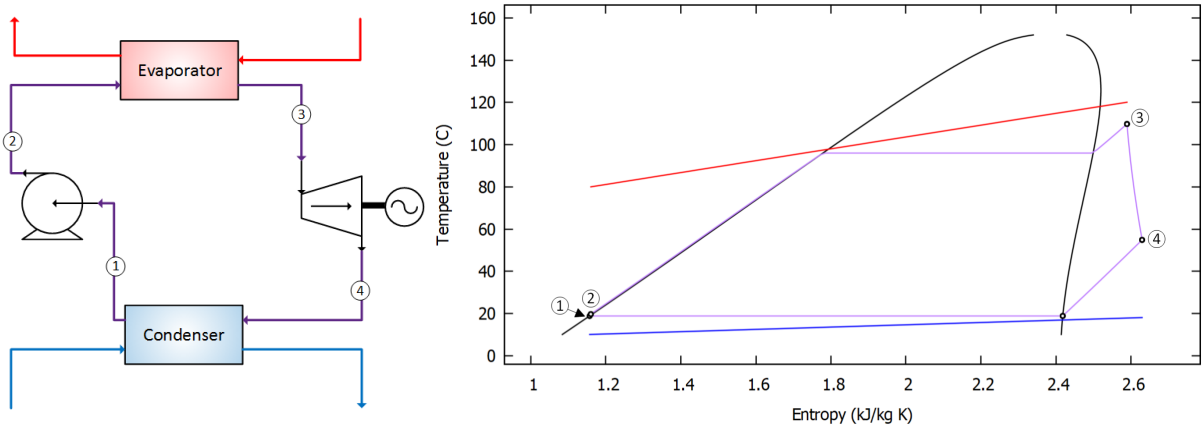

(a) Process diagram.

(b) Temperature - entropy diagram.

Figure 1.1: Elementary Rankine cycle.

In Figure 1.1b, the temperature - entropy diagram of the Rankine cycle is shown. This particular diagram is for butane rather than water, but shows how such a diagram generally looks. This diagram helps in the analysis of the process by showing the state that the working fluid is in at various points during the cycle. Notice how in Figure 1.1b, the numbers at each point correspond to the numbers in Figure 1.1a, and shows how the fluid evaporates between points 2 and 3, expands to point 4 and condenses to point 1. The fluid is subsequently pumped from point 1 to point 2, but this is imperceptible in the diagram. Also shown in Figure 1.1b are the temperature changes of the heat source in red and heat sink in blue. The black curve represents the phase envelope of the working fluid, showing where the phase change occurs in the cycle.

It is possible to modify the Rankine cycle in various ways in order to increase the efficiency or safety of the cycle. One such modification is to add an internal heat exchanger, which is also known as a recuperator. The recuperator works by allowing the hot low pressure gas exiting the expander to heat the colder high pressure liquid coming from the pump. This means that less energy needs to be extracted from the heat source for the same net power output from the cycle, leading to a greater efficiency. The process diagram of a Rankine cycle with a recuperator is

shown in Figure 1.2a, and its corresponding temperature - entropy diagram is shown in Figure 1.2b.

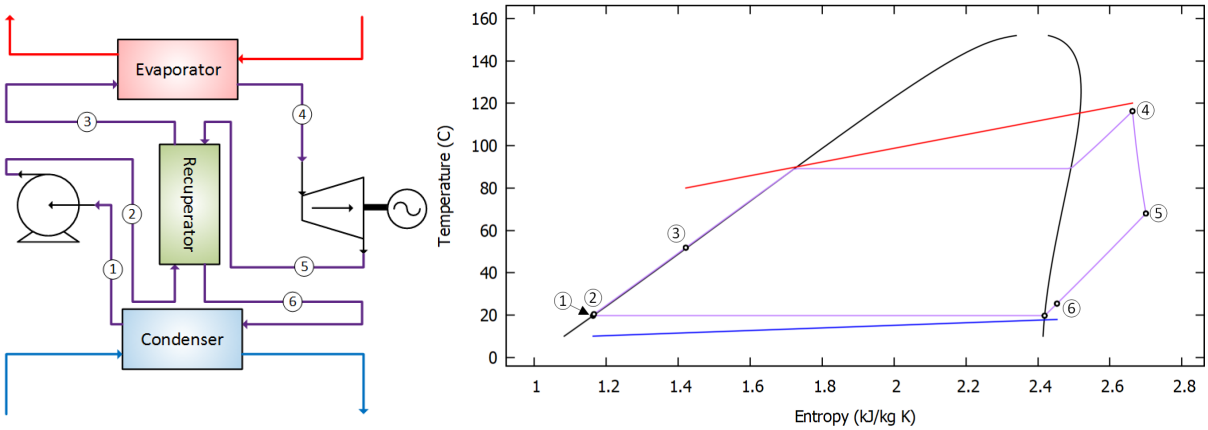

(a) Process diagram.

(b) Temperature - entropy diagram.

Figure 1.2: Rankine cycle with recuperator.

From Figure 1.2a, it is clear how the system becomes more complex when a recuperator is added, owing chiefly to the added heat exchanger and extra required piping. While the recuperator decreases the load on the evaporator and the condenser, allowing for smaller heat exchanger designs and thus cheaper components for these two, the total investment is likely to increase when using a recuperator. The added costs may however be offset by the added cycle efficiency that the recuperator offers.

To improve the operational safety of the Rankine cycle one can add an intermediate heating loop between the heat source and the evaporator. The indirect loop is heated by the heat source in a waste heat recovery unit (WHRU), and is cooled in the evaporator as it heats the working fluid of the Rankine cycle. This design is particularly advantageous when one wants to avoid leaking the working fluid into the heat source stream, or if the working fluid is flammable and one wants to minimize its exposure to open flames or other high temperature objects by moving the cycle away from these. Other advantages of an indirect cycle is that it is easier to control the temperatures in the WHRU, which is for example important in scenarios where there is the risk of reaching the acid dew point of the hot stream, or that it may minimize the impact of thermal fluctuations in the heat source, leading to a more stable operation of the Rankine cycle.

The general process diagram and the temperature - entropy diagram are shown in Figures 1.3a and 1.3b. In the temperature - entropy plot for the design with an indirect heating loop there are now two red lines; one for the heat source, and one for the indirect loop. The heat source is always the hottest stream in the cycle, and is thus the red line that is highest in the diagram, with the bottom red line showing the temperature change of the indirect fluid.

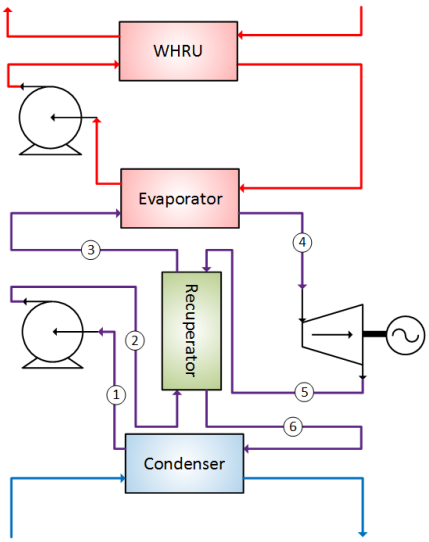

(a) Process diagram.

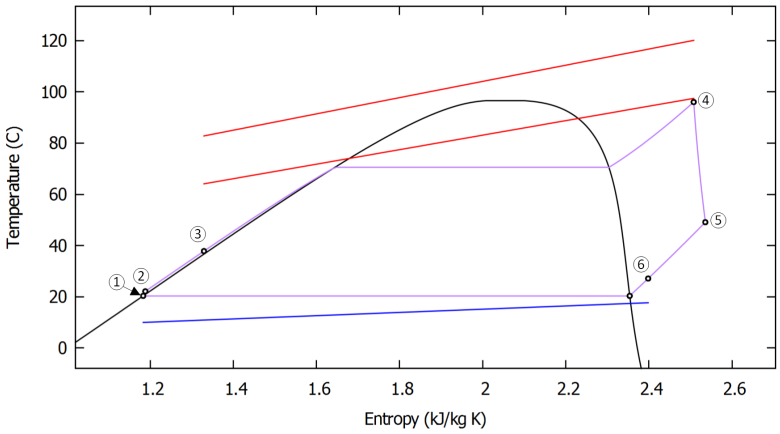

(b) Temperature - entropy diagram.

Figure 1.3: Indirect Rankine cycle with recuperator.

Similarly to the recuperator, this design also increases complexity and investment cost, because one needs to add a new heat exchanger and pump for the indirect fluid. Unlike with the recuperator, this design has a negative impact on the efficiency of the cycle, because of the losses in the WHRU. This is evident in Figure 1.3b, where there is a temperature drop from the heat source temperature profile to the indirect fluid temperature profile. This temperature difference could instead have been used to heat the working fluid, but is instead lost to irreversibilities in the WHRU.

Another modification to the Rankine cycle is changing the working fluid. Typically, when working with low temperate heat sources one employs organic fluids rather than water, and this is the characteristic that chiefly separates an organic Rankine cycle from the traditional Rankine cycle. The general principles of the traditional Rankine cycles still apply to the organic Rankine cycle, with the main difference being that the organic fluids are more suitable for low temperature use than water.

It is also possible to use zeotropic mixtures instead of pure fluids. A zeotropic mixture is a mixture of fluids that have different saturation temperatures at a given pressure. These behave differently than pure fluids in that they evaporate and condense with a temperature glide rather than at a constant temperature. This makes it possible to reduce losses in the evaporator and condenser by having a closer temperature match between the working fluid temperature profile and that of the heat source and sink.

The temperature - entropy diagram of a zeotropic mixture is shown in Figure 1.4, where the temperature glide in the evaporator and condenser are evident. Since the process equipment is the same as with a pure fluid, the numbers in Figure 1.4 correspond to the numbered states in the process diagram given in Figure 1.3a. Notice how when using a zeotropic fluid, the temperature glide makes it possible for the working fluid to start condensing in the recuperator, thereby further reducing the load on the condenser. This allows for a more efficient use of the heat sink.

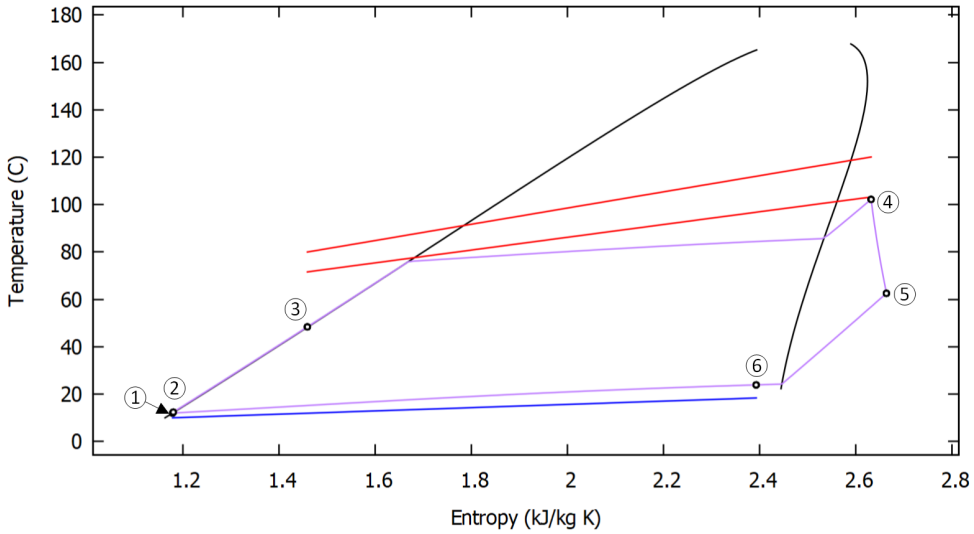

Figure 1.4: Temperature - entropy diagram of an indirect Rankine cycle with recuperator using a zeotropic mixture.

1.3.2 Volumetric expanders

In evaluating the off-design performance of the Rankine cycle, it is important to differentiate whether one is using a volumetric expander or a turbine, as these will have very different off-design characteristics. These differences arise because of the different ways that volumetric expanders and turbomachines convert energy contained in the fluid to rotational energy.

Volumetric expanders expand the flow in pre-designed chambers that sequentially increase in volume, thereby decreasing the pressure and producing work. The ratio of the discharge volume to the inlet volume is known as the volume ratio, and seeing as how these are part of the design of the expander, every volumetric expander will have a built-in volume ratio that is constant.

The built-in volume ratio is an important design parameter, as the expander will operate with the highest efficiency when the process parameters match this built-in volume ratio. If the process parameters are such that the volume ratio of the flow deviates from the built-in volume ratio of the expander, then losses will incur in the expander and its performance will deteriorate.

The volume ratio of the flow is closely related to the pressure ratio, and so there exists an optimal pressure ratio for each individual expander. Expanding beyond or below this pressure ratio will result in over-expansion and under-expansion respectively, and will lead to an efficiency loss. The effect of over-expansion is shown in a pressure - volume diagram in Figure 1.5a, and the same for under-expansion is shown in Figure 1.5b. $P_{2,\,i}$ and $V_{2,\,i}$ are what the designed outlet conditions are for the expander, whereas P_2 and V_2 are the actual outlet conditions. As a result of this mismatch, there will be a net loss of power, which is the area enclosed by the red lines.

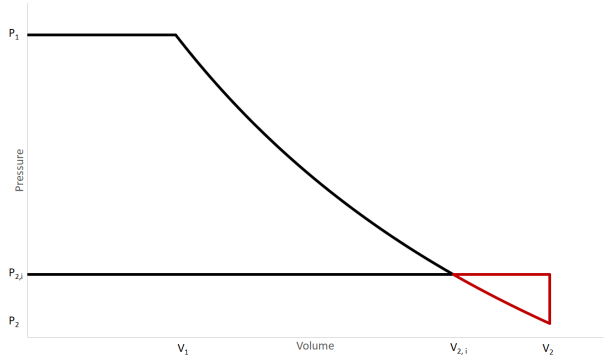

(a) Over-expansion

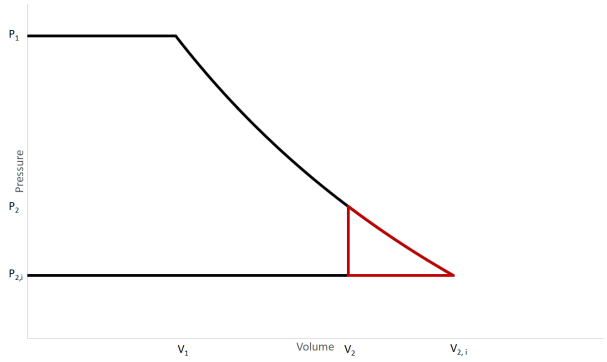

(b) Under-expansion

Figure 1.5: Pressure - volume diagrams showing over- and under-expansion in a volumetric expander.

1.3.3 Turboexpanders

Turboexpanders produce work by converting a part of the pressure energy to kinetic energy, before the flow drives rotors attached to a shaft. This conversion occurs in static nozzles called stators, and the share of pressure energy that is converted varies between different types of turbines, and is dictated by the shape of the rotors. A reaction turbine is a type of turbine that utilizes some of the pressure in the rotors to make them rotate, while an impulse turbine converts most of the pressure energy to kinetic energy before the flow passes through the rotors. Modern turboexpander combine these methods of extracting energy from the stream in a single blade to evenly distribute the load on the rotors.

Turboexpanders do not have a built-in volume ratio like their volumetric counterparts, and as such do not experience the same performance degradation when pressure ratio varies. Instead, the velocity triangles of the flow entering and leaving the rotors dictate the performance of a turbine, and the angles in these should be kept as similar as possible to those of the design velocity triangle to maintain high efficiency. Seeing as how a part of the pressure energy in the flow is converted to kinetic energy, a change in the pressure ratio will result in different velocities entering and leaving the rotor section of the turbine. The losses associated with pressure ratio changes can therefore be somewhat mitigated by changing the rotational speed of the rotors. This provides a way to preserve the designed angles of the velocity triangles, and so reduces the efficiency loss associated with off-design operation. Another strategy is to use turbines that have variable inlet guide vanes, which enable the stators to change the angle at which the flow enters the rotor section. This will also improve the turbine's off-design performance.

1.3.4 Exergy calculations

In this work, the distribution of available exergy has been analyzed for different design parameters. The exergy of a system is the total amount of energy that can be converted to work, before the system reaches a base state, oftentimes being ambient pressure and temperature. This is also the base state in this work, so the base temperature is 10°C and the base pressure is 1 bar. Ignoring the changes in kinetic and potential energy, the specific exergy of a point is given by Equation 1.1.

$$e_x = (h - h_0) - T_0 \times (s - s_0) \tag{1.1}$$

In the equation above, e_x is the specific exergy, h is the specific enthalpy, s is the specific entropy and T_0 is the ambient temperature in Kelvin. h_0 and s_0 are the enthalpy and entropy at the base state, respectively. Multiplying Equation 1.1 with the mass flow through that point yields the exergy of that point. This is shown in 1.2 with E_x being the exergy and $\dot{m}$ representing the mass flow.

$$\dot{E}_x = \dot{m} \times e_x \tag{1.2}$$

Similar to the energy balance, there exists a balance for the exergy as well. However, unlike with energy, exergy can be destroyed, and this occurs in all real processes. This may arise in several ways; for example in a heat exchanger, one source of exergy destruction is the temperature difference, which makes the cold stream leave the heat exchanger with lower exergy than the hot source entered with. In an expander it may be non-isentropic expansion, which comes about as a result of various losses in the expander. Regardless, the sum of exergy entering a system must be equal to the exergy that either leaves the system or is destroyed. Exergy leaving the system may take the form of work which is transported elsewhere, such as in the expander, or exergy that simply follows the stream and exits a given control volume. The exergy balance is shown in Equation 1.3.

$$\sum \dot{E}_{x\,in} - \sum \dot{E}_{x\,out} - \dot{W}_{net} - \dot{I} = 0 \tag{1.3}$$

Here $\dot{W}_{net}$ is the net power being produced in the given control volume, and $\dot{I}$ is the exergy destruction.

The exergy efficiency of the cycle is calculated by dividing the net work production with the available exergy. Because the heat source has a lower temperature limit, the available exergy is not the work one can develop by bringing the heat source inlet to ambient conditions, but instead the work one can develop by cooling the heat source to the lower limit. This is shown algebraically in Equation 1.4.

$$\eta_{Ex} = \frac{\dot{W}_{net}}{\dot{E}_{x\,s,\,in} - \dot{E}_{x\,s,\,out,\,min}} \tag{1.4}$$

To ensure that the exergy calculations are correct, it is helpful to have a reference with which one can compare the calculations with. One such reference may be the Carnot efficiency, which provides the theoretical maximum amount of work one could produce in such a system. The Carnot efficiency of a system where the heat source has a temperature glide and is also subject to a lower temperature limit is given by Equation 1.5, where all the temperatures are given in Kelvin.

$$\eta_{Carnot} = 1 - \left(\frac{T_0}{T_{s,\,in} - T_{s,\,min}}\right) \times \ln\left(\frac{T_{s,\,in}}{T_{s,\,min}}\right) \tag{1.5}$$

With the Carnot efficiency, one can calculate the theoretical available exergy content of the system, using Equation 1.6.

$$\dot{E}_{x\,avail,\,Carnot} = \eta_{Carnot} \times \dot{m}_s \times (h_{s,\,in} - h_{s,\,min}) \tag{1.6}$$

The sum of all the exergy spent in the system, whether converted to work, destroyed or otherwise lost, must equal to the available exergy given by the Carnot cycle, and this is used to check the calculations in this work.

Some discrepancies may arise in this work due to how the model used is numerical, and so a solution may use more exergy than theoretically available. These violations are small however, and do not change the main conclusions of the work.

1.4 Review of project work

This work is a continuation of a project done during the preceding autumn. The objective of the project work was to find optimal zeotropic mixtures for three cases consisting of various combinations of heat source inlet temperature and minimum heat source temperature. The three cases are summarized in Table 1.1.

Table 1.1: Cases from project work.

Case	$T_{s,\,in}$ (°C)	$T_{s,\,min}$ (°C)
Case 1	120	80
Case 2	120	100
Case 3	150	80

The mixtures that were evaluated are shown in Table 1.2.

Table 1.2: Mixtures evaluated in project work.

Cyclopropane - propane	Isobutane - cyclopropane
Isobutane - propane	N-butane - cyclopropane
N-butane - propane	Isopentane - isobutane
N-pentane - n-butane	

To find optimal mixtures, the system was optimized using software provided by SINTEF, which attempts to find the optimal values of each free variable set, under the given constraints. In the project work, the total heat exchanger area, A_{tot}, was constrained to various levels for each case, and the optimal fluid was found for each of these areas for every case. The optimal mixtures for all the different values of A_{tot} were found because A_{tot} is closely correlated with investment costs of the system, and so it was seen as interesting to find the optimal mixtures for these different levels of investment. The results are succinctly presented in Figure 1.6, where only the best mixtures are shown for each case and the lesser mixtures discarded. Interestingly, the optimal mixture for every data point is one involving the heaviest hydrocarbons investigated, consisting of a mixture between isomers of pentane and butane.

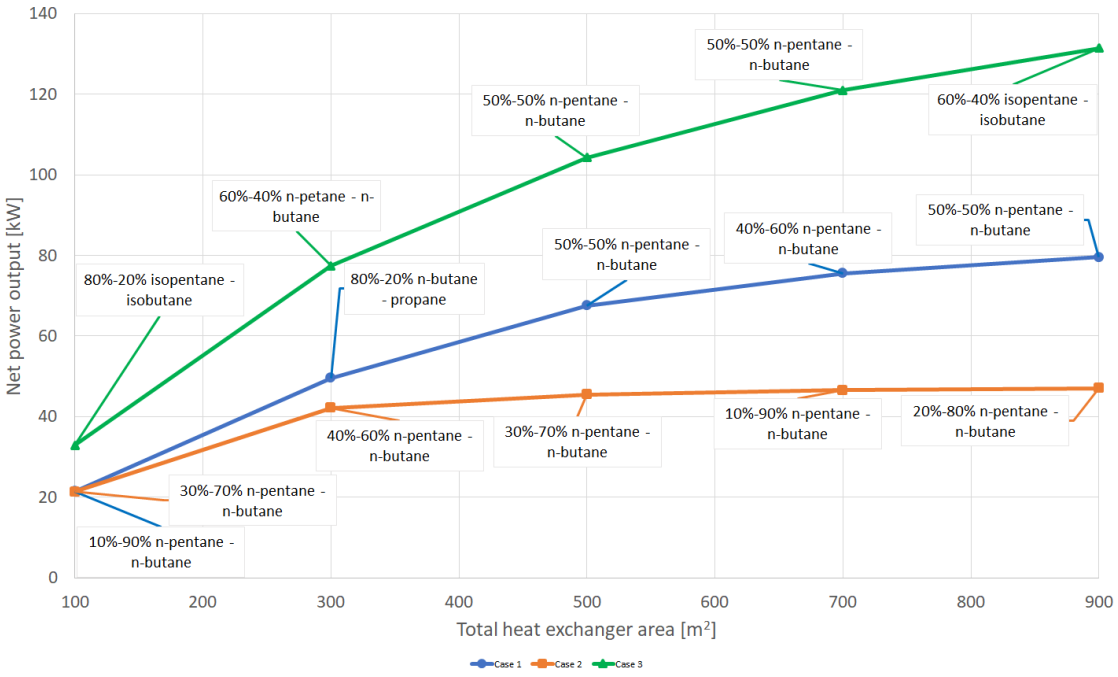

Figure 1.6: Optimal mixtures for each total area.

The results were further analyzed to investigate the net work decrease if a single mixture was used across the cases. This was an introductory off-design analysis, as the different cases could represent different activity levels in the surrounding system. The mixture that was locked across the cases was the one that minimized the decrease in power output in the other two cases. The results of this analysis are shown in Table 1.3.

Table 1.3: Changes in net power output when a single mixture is used across all cases for each value of A_{tot}.

A_{tot} (m^2)	Mixture (-)	$\Delta\dot{W}_{net}$ for Case 1 (%)	$\Delta\dot{W}_{net}$ for Case 2 (%)	$\Delta\dot{W}_{net}$ for Case 3 (%)
100	30%-70% n-pentane - n-butane	~ 0	0	-0.16
300	40%-60% n-pentane - n-butane	-3.38	0	-0.32
500	50%-50% n-pentane - n-butane	0	-0.56	0
700	50%-50% n-pentane - n-butane	-3.87	-0.68	0
900	50%-50% n-pentane - n-butane	0	-1.47	-0.64

From this analysis, it seems that mixtures between n-pentane and n-butane are the most effective off-design mixtures for this system, as they minimize the net power decrease in the other two cases for all A_{tot}. Based on this, mixtures with these two fluids seem like ideal candidates for further investigations into off-design performance.

Chapter 2

Literature Review

The performance of organic Rankine cycles is well-documented in literature, and its viability in low temperate settings has been studied and affirmed. Before the designed cycles can be implemented in the industry, their behavior in off-design environments must also be evaluated, and this aspect has been given some, but limited attention in literature. This section will summarize studies that have focused on the off-design analysis of organic Rankine cycles and their findings.

In addition to looking into previous work on the off-design performance of entire cycles, some time has also been dedicated to investigate the characteristics of various expanders under off-design operation. The focus when investigating expander technology was to try to find suitable expanders for the system in this work. The findings from this review is summarized below.

2.1 Off-design performance of volumetric expanders

He et al. (2017) experimentally studied the off-design performance of a 50 kW organic Rankine cycle that employed a twin screw expander. The off-design operation was the result of changing environmental temperatures throughout the year, which affected the temperatures of the heat source and heat sink. Both the heat source and sink are water, where the hot water arrives at temperatures between 65 and 95°C, and the cooling water enters at temperatures between 13 and 32°C. The working fluid in the study was an organic fluid called TY-1. The built-in volume ratio of their expander was 3, and their results show that the maximum efficiency occur at a pressure ratio a little higher than 3.2, at which point the efficiency is 67.5%. As predicted by theory, the efficiency deteriorates as the pressure ratio is both lowered and increased, and the authors comment that higher efficiencies are easier to be reached when operating in under-expanded conditions. This follows their findings that the peak efficiency was found when the flow was slightly under-expanded. They also recommend to operate the expander in under-expanded conditions for higher shaft power and stability.

Zhu et al. (2014) modelled and studied the off-design performance of a screw expander for six different organic fluids. Their expander model involved multiplying the maximum efficiency with a correction factor that varied with pressure ratio, thereby simulating the declining efficiency of volumetric expanders as the cycle pressure ratio moves away from the design pressure ratio. This correction factor would be equal to 1 at the design point, and would gradually decline as the pressure ratio differed from that of the design. The general curve of the correction

factor shows that it declines with a larger gradient when the flow is over-expanded than when it is under-expanded, which is in accordance with the findings by He et al. (2017). Zhu et al. (2014) also found that the fluid used also has a great influence on the performance, where the heat capacity ratio has a great influence on the shape of the curve. Their findings show that the higher the heat capacity ratio is, the more sensitive the performance is to changes in pressure ratio.

Tian et al. (2017) modelled the off-design performance 118 kW twin-screw expander. The system consisted of steam that required throttling, and they proposed that instead of using a valve, an expander can perform the same function while also producing mechanical work or electricity for other uses. Under design conditions, the steam enters the process at 165°C and 0.7 MPa, with a mass flow rate of 1258 $\frac{kg}{h}$. However, the suction pressure, discharge pressure and mass flow are all subject to variations, and the effects of these changes are investigated. Their results show that there is a linear relationship between the mass flow rate and the isentropic efficiency of the expander, where the highest efficiency is achieved at the lowest mass flow rate. When operating at design pressure ratios, the isentropic efficiency decreases from 83% to 77% as the rotational speed increases from 60% to 140% of the design rotational speed. The authors explain that this is a result of higher suction pressure loss and friction loss when the rotational speed increases. The researchers also investigated how the isentropic efficiency varied with rotational speed when the flow is both over- and under-expanded. They found that when the flow is over-expanded, the isentropic efficiency decreases from 81% to 73% over the same span of rotational speeds, while the under-expanded efficiency varied between 83% and 78%. This shows that operating in over-expanded conditions are more taxing on the performance than under-expansion according to the authors. Their results from when the suction and discharge pressures are varied support this conclusion. An increase in the suction pressure or a decrease in the discharge pressure will lead to the flow being under-expanded after the expansion process, and either one of these lead to higher efficiencies compared to when the flow was over-expanded. Their analysis on varying pressure ratios thus reaffirm the conclusions reached in the previous studies.

The results by Tian et al. (2017) are corroborated in experimental studies performed by Hu et al. (2017) and Hsu et al. (2014). In the experiment conducted by Hu et al. (2017), the system comprised of R245fa being heated by hot water, before entering a twin-screw expander. In the study, the researchers investigated how the performance of the expander varied as the rotational speed and suction pressure diverged from the design point. From a design rotational speed of 1500 rpm, they studied the isentropic efficiency of the expander for rotational speeds between 900 and 1900 rpm, corresponding to an interval of 60% to 126.67% of the design rotational speed. In concordance with the results found by Tian et al. (2017), the results from this study also show that the efficiency decreases with rotational speed, from a maximum efficiency of 84.6% to a minimum of 61.7%. These losses are mainly as a result of friction losses and suction losses, the authors explain. The linear relationship between the rotational speed and isentropic efficiency is further supported by Tang et al. (2015), in a study that studied a twin screw expander both experimentally and using a model. To calculate the isentropic work, they measured the pressure and temperature at the inlet of the expander to find the enthalpy and entropy using REFPROP. The isentropic efficiency was subsequently found by calculating the isentropic enthalpy using the measured pressure at the outlet and the entropy.

Despite these studies showing a negative correlation between rotational speed and isentropic efficiency for screw expanders, there are studies that also show the opposite trend. For example, Li et al. (2018) experimentally studied a prototype single screw expander in which the isentropic

efficiency linearly increased with rotational speed. However, it is not entirely clear why this relationship arises, and the researchers do not explain well how they calculate the isentropic efficiency to begin with. It is possible that in adjusting the rotational speed, other parameters of the systems have changed. Li et al. (2018) comment that in their study, the back pressure of the expander increases with the rotational speed, while Tang et al. (2015) point out that they ensured constant suction and back pressures as they varied the rotational speed. This gives credence to the studies that show that the isentropic efficiency decreases with rotational speed.

In investigating the effects of the suction pressure, Hu et al. (2017) operated the expander with pressures between 550 kPa and 750 kPa, with the design pressure of 658 kPa roughly in the middle of these two limits. The discharge pressure was kept constant at the design pressure throughout these experiments. They found that at under design operations, the efficiency was 84.9%, and that the efficiency dropped to 78.4% as the suction pressure was reduced to 550 kPa. Conversely, when the pressure was increased to 750 kPa, the efficiency was reduced to 78.9%. Increasing the suction pressure will lead to under-expansion in the expander whereas decreasing the suction pressure will cause the flow to be under-expanded, and so the results by Hu et al. (2017) reaffirm previous results that show that under-expansion is more favorable than over-expansion in a twin-screw expander, although with an almost negligible difference for this particular expander. Hsu et al. (2014) experimentally studied the influence of pressure ratios on the performance of a hermetic screw expander. Similarly to the results from the study by Tian et al. (2017), the isentropic efficiency deteriorates much quicker during over-expansion conditions compared to under-expansion conditions. The data also show that the maximum efficiency is located at pressure ratios slightly higher than the built in pressure ratios of the investigated expander. The authors argue that this is a result of friction losses and supply pressure drop, so that the total pressure drop in the expander is higher than the designed expander pressure ratio would suggest. Consequently, the researchers recommend designing the expander so that the design pressure ratio is slightly lower than the pressure ratio in the design cycle.

2.2 Off-design performance of turboexpanders

Cho et al. (2014) investigated how well a radial inflow turbine using R245fa performed when the turbine inlet temperature was varied by simulating changing available heat energy from the heat source. The turbine inlet temperature varied between 70°C and 120°C in increments of 10°C. Because the working fluid is modelled to be saturated gas at each of these temperatures, the pressure also increases for each of these turbine inlet temperatures. The researchers modelled a turbine with a fixed geometry, and for each investigated temperature, they tried to keep the turbine output power constant. This was achieved by varying the amount of active nozzles that admit the working fluid into the rotors. Their analysis on the efficiency of the turbine shows that it drops from a maximum of roughly 78% at 70°C to 62% at 120°C. Over a narrower temperature span of about 15°C, the smallest efficiency drop is 6%, from 68% to 62% in the temperature interval of 105°C to 120°C.

Zheng et al. (2017) also numerically investigated the off-design performance of a radial inflow turbine with a set geometry. Using R134a as the working fluid, they investigated the performance of their designed turbine when the turbine inlet temperature and turbine rotational speed varied, while the pressure ratio was kept constant at the design value. Their data show a relatively level curve for the total to static isentropic efficiency for when the rotational speed is at design and with the turbine inlet temperature increasing from the design value of 360K to 420K.

Curiously, the efficiency increases from the design efficiency of 80% to roughly 81% at 10K over the design turbine inlet temperature, before falling to the final value of about 79.5%. When increasing the rotational speed to 120% of the design speed, there is a much larger variation in the efficiency, where it continually increases from 75% to 81.5% over the same temperature range. When the turbine inlet temperature is at about 395K, the efficiency is higher for the higher rotational speed compared to design rotational speed, suggesting that one should increase the rotational speed as the turbine inlet temperature increases. Their data imply that the reverse is also true for when the turbine inlet temperature is below the design temperature. They also investigated the efficiency when the rotational speed was 80% of the design speed for the same temperature range, and found that it continually decreases. Unfortunately, the researchers did not investigate turbine inlet temperatures below the design temperature, but the trend seems to show that there is a temperature for which 80% rotational speed has a higher efficiency than the design speed. Their data thus suggest that off-design operation can be accounted for by varying the rotational speed of the rotors.

In addition to investigating the relationship between turbine inlet temperature and rotational speed at the designed pressure ratio, Zheng et al. (2017) also investigated the effect of varying the pressure ratio across the turbine at design rotational speed. The range of pressure ratios that was investigated were from 2.1 to 2.9, where the design pressure ratio was 2.63. Their results show that the total to static isentropic efficiency decreases as the pressure ratio increases, for all three values of turbine inlet temperatures. For the design inlet temperature, the efficiency decreased from 83% to 78% over the investigated range of pressure ratios. The researchers went on to investigate how the efficiency was correlated with pressure ratio and rotational speed at the design turbine inlet temperature. They found that for a rotational speed of 80% of the design speed, the efficiency decreases almost linearly, but at design speed, the efficiency begins to level off, before starting to decrease linearly again. For a rotational speed of 120% of the design speed, the curve takes a parabolic shape, with a maximum point between the two limits. The data also shows that at a specific value of pressure ratio, the efficiency is higher when the rotational speed is 120% of the design speed, as compared to the design speed. This reaffirms that varying the rotational speed of the turbine can minimize the performance deterioration in off-design operation.

Kim and Kim (2017) performed a similar analysis as Zheng et al. (2017), but their radial inflow turbine had different dimensions, design conditions and utilized a different working fluid. They investigated using R143a in a turbine that has a design power output of 400 kW, whereas the turbine in the study by Zheng et al. (2017) had a design output of 643 kW. From a design turbine inlet stagnation temperature of 413 K, Kim and Kim (2017) investigated the effect of changing the rotational speed and turbine inlet temperature by varying the temperature between 393 K and 433 K and the rotational speed between 80% and 120% of the design rotational speed, in increments of 10%. These data points were generated at the design pressure ratio. The results are in concordance with those by Zheng et al. (2017), where the efficiency decreases across the entire range of temperatures for the low rotational speeds, and continually increases for the high rotational speeds. At the design rotational speed, the curve also take a parabolic shape, where the maximum at the design temperature. Because this study investigates temperatures below the design temperature, it is possible to investigate whether the efficiency is higher for low rotational speeds when the temperature is below the design temperature, as was predicted from the data by Zheng et al. (2017). The results by Kim and Kim (2017) show that this is true. At roughly 400K, the curve for the rotational speed that is 90% of the designed rotational speed shows a higher efficiency than the curve for the nominal rotational speed. Furthermore, the relationship

found by Zheng et al. (2017) between pressure ratio and rotational speed at design temperature is also present here, but there are certain differences. The curve for the design rotational speed is a parabola with a maximum point in this study, whereas it decreased continually in the study by Zheng et al. (2017). Furthermore, the curves for the high rotational speeds increase continually, instead of having parabolic shapes. The curves for the low rotational speeds are similar however, and decrease over the entire range. The differences between the studies may have to do with the study by Zheng et al. (2017) using a range of pressure ratios that are too small. The design pressure ratio in the study by Kim and Kim (2017) is 2.72, and the maximum of the efficiency at nominal rotational speed is when the pressure ratio is roughly 2.65. If Zheng et al. (2017) decreased the minimum pressure ratio that they investigated, perhaps their data would show a maximum as well. These differences may also be a result of the different geometries of the expanders. Despite the discrepancies between the two studies, the numerous similarities in their data strongly suggest that their results are general trends of radial inflow turbines, and not only characteristics of their particular turbines.

2.3 Investigations into the off-design performance of entire cycles

Where the previous studies have focused on the detailed off-design performance of various expanders, others have maintained a larger perspective by investigating entire cycles. These studies have analyzed different aspects of off-design operation. For example, some have attempted to find general guidelines for choosing optimal design points, whereas others have looked into optimal control strategies during off-design operation. Some studies have also focused on the parameters of the cycle, investigating how different parameters affect each other, and finding how the parameters affect the performance of the entire cycle.

2.3.1 Cycles using turbines

Wang et al. (2014) studied how an organic Rankine cycle performed when the heat source characteristics changed. Their system employed solar radiation, where thermal oil would be heated and stored in a thermal tank, before being passed to the evaporator to heat the working fluid. The working fluid in this system was R245fa. Changes in environmental temperature were investigated, as well as how the entire cycle performed when the flow rate of thermal oil into the evaporator varied. They found that as the environmental temperature increased, the mass flow of the working fluid in the cycle increased, along with the temperature in the thermal storage unit and the turbine inlet pressure in the organic Rankine cycle. Despite the higher turbine inlet pressure and mass flow rate, the net work in the organic Rankine cycle decreased, because when the ambient temperature increased, the condensation pressure followed. The ultimate effect is that the enthalpy difference across the turbine decreased, leading to decreased net power output and exergy efficiency of the cycle. The effect of increasing the flow rate of the thermal oil into the evaporator was also investigated. In essence, this means extracting more heat from the thermal storage and delivering this to the organic Rankine cycle, and so the mean temperature of the thermal storage predictably fell. However, they found that the turbine inlet pressure and the working fluid mass flow rate both increased. The combined effect of this was increased work output and exergy efficiency. The researchers compiled their individual results to model how their cycle would perform over the course over a year, using weather data from Xi'an for the

average environmental temperatures. The data from this analysis is consistent with the data of varying individual parameters, where higher environmental temperatures lead to higher thermal storage temperature and mass flow rate in the organic Rankine cycle. The cycle performance is worst in the hottest month, as predicted by their earlier results. The highest exergy efficiency is reached in the coldest month, further confirming their previous data.

Calise et al. (2014) studied a similar system as Wang et al. (2014), where solar radiation is collected and heats diathermic oil in an indirect loop that ultimately heats the working fluid in the organic Rankine cycle. The working fluid in this study is n-butane. The study consists of two parts, where the researchers first perform a techno-economic analysis to find optimal heat exchanger geometries to maximize the yearly profit of the system. Included in this analysis is the income from the power generated, and an estimate for the total investment cost of the system, which is distributed across the operational years using an annuity factor. The investment cost of the system consists of estimates for the cost of the heat exchangers as well as the working fluid and the expander. There are five heat exchangers in the system, all of which are designed as shell and tube heat exchangers. The condenser ensures that the fluid exits as a saturated liquid, before being pumped to the recuperator. Following the recuperator is the economizer, which heats the fluid until it is saturated liquid at the higher pressure. The fluid then enters the evaporator, and exits as saturated vapor before being further heated in the superheater. The study optimizes the geometry of all the heat exchangers except for the condenser, whose geometry is locked. The researchers find that for the recuperator, economizer and superheater, the profit always increases in the investigated range as the number of tubes increase and as the tube length increases. This means that it is profitable to set these parameters to their maximum values. For the evaporator, the study finds that the profit curve is parabolic, both for the number of tubes and the tube length. The researchers therefore chose not to set these parameters to the maximum limit.

Following the techno-economic optimization of the heat exchangers, the researchers investigated the off-design performance of their cycle by changing the temperature and flow rate of the diathermic oil. These are varied from their respective design values of 160°C and 20 $\frac{kg}{s}$ to between 155°C and 185°C and 18 $\frac{kg}{s}$ and 24 $\frac{kg}{s}$. Their results show that the highest net power output is achieved when the flow rate of the oil is at its minimum and the temperature is at its maximum, and the least power is produced when both are at their maximum. This suggests that the flow rate of the heat source has a major effect on the performance of the system. The results also show that the maximum thermal efficiency is reached when both of these are at their minimum, yielding a thermal efficiency of 14.52%. Their data also show that the heat source characteristics affect the pressure levels in the condenser and evaporator as well. Increasing the temperature of the oil at constant flow rate increases both the pressure levels, but the evaporator pressure increases faster, thereby the net effect is to increase the pressure ratio across the turbine. When the temperature of the heat source is constant, but the flow rate increases, both pressure levels increase again, but now the condensation pressure increases at a higher rate. This decreases the pressure ratio across the expander. Since the net power developed in the expander is related to the pressure ratio across it, this analysis offers a possible explanation why the maximum and minimum values of net power produced are both found when the temperature is highest, but the values for the flow rate are at their minimum and maximum respectively.

Mazzi et al. (2015) modelled a system where thermal oil is heated by exhaust gases rather than solar radiation, before passing this heat to the working fluid of the organic Rankine cycle. All the heat exchangers in this study are shell and tube heat exchangers, and each has their geometrical parameters locked throughout the investigation. The researchers investigated how the performance of the cycle varied with the thermal oil mass flow rate and the heat sink inlet

temperature. From a design thermal oil flow rate of 58.5 $\frac{kg}{s}$, they investigated the power output and thermal efficiency at flow rates equal to 80%, 100%, 110% and 115% of the design flow rate. Furthermore, for each of these flow rates, they also investigated how the performance varied for heat sink inlet temperatures of 15°C, 20°C, 25°C and 30°C, where the design temperature is 20°C. Their results show that maximum power output is achieved by maximizing the thermal oil flow rate and minimizing the heat sink inlet temperature and conversely, minimum net power is produced when the thermal oil flow rate is minimized while the heat sink inlet temperature is maximized. While net power continually increases with mass flow rate, their data for the efficiency show that for all heat sink inlet temperatures, the efficiency is maximized when the thermal oil flow rate is equal to the design flow rate. At design heat sink inlet temperature, this efficiency is 24.56%, and decreases slightly to 24.21% when the thermal oil flow rate decreases to 80% of the design flow rate, and to 24.45% when the flow rate increases to 110% of the design flow rate. The authors argue that this almost imperceptible difference shows that the flow rate of the oil has little effect when the relative difference from the design point is small. Changing the heat sink inlet temperature yields a more significant effect – increasing this from 20°C to 30°C at design oil flow rate lowers the efficiency to 23.56%. The contradicting conclusions regarding the influence of the oil flow rate between the studies by Mazzi et al. (2015) and Calise et al. (2014) seem to suggest that the significance of the heat source flow rate vary from one system to another, and it is difficult to draw any general conclusions.

Manente et al. (2013) investigated the off-design performance of a system using geothermal fluid as the heat source. The flow rate of the fluid is set at 100 $\frac{kg}{s}$, and varies in temperature between 130°C and 180°C, from a design temperature of 160°C. They have also set a lower temperature limit of 70°C on the heat source to avoid issues with silica scaling. The heat sink in this investigation is air, which enters the condenser at ambient temperature, and the researchers also investigate the effect of varying this temperature as well. Unlike the flow rate for the heat source, the flow rate of the heat sink is not locked and can vary to satisfy the energy and mass balance of the system. From a design temperature of 20°C, the ambient temperature is varied from 0°C to 30°C. The study investigates using isobutane and R134a as working fluids, where the respective turbine inlet conditions are subcritical and supercritical. In either case, a radial turbine is used as the expander for the cycle. Their results show that for both working fluids, the net power increases with increasing heat source temperature and decreasing ambient temperature. For isobutane, when the ambient temperature is 20°C, the net power increases from 3806 kW to 6050 kW – a 59.0% increase – when the geothermal fluid temperature increases from 160°C to 180°C. When the geothermal fluid temperature instead falls to 130°C, the net power decreases to 2641 kW, meaning a decrease of 30.6%. Furthermore, if the geothermal fluid is kept at its design value of 160°C and the ambient temperature falls to 0°C, the net power increases to 4872 kW, yielding an increase of 28.0%, but if the ambient temperature rises to 30°, the net power output will fall by 19.5% to 3063 kW. When R134a was used, similar results were found despite that cycle being supercritical. In the majority of the results found in this study, the minimum heat source temperature constraint is reached, and limits the performance of the system. The researchers explain that if this constraint were not present, the performance could have been even better, especially for the cases where the ambient temperature was low.

2.3.2 Cycles using volumetric expanders

The previous chapters have primarily used turbines as the expander in the cycle. It is however important to also investigate whether the general trends found in the preceding studies also apply to cycles with volumetric expanders, and studies using this technology have therefore also been looked into. Liu et al. (2017) modelled an organic Rankine cycle in which R123 was heated by hot air at temperatures between 373 K and 473 K, before entering a scroll expander and generating work. Following the expander, the working fluid is cooled by water at 293 K, before being pumped back into the evaporator. The study employs a geometrical approach to calculate the performance of the expander, pump and heat exchangers, where the evaporator is a fin-tube heat exchanger and the condenser is a shell and tube heat exchanger. The researchers varied the required output of the expander, and investigated how the system responded when this constraint was set. This constraint was varied from a design value of 3000 W down to 1500 W in steps of 300 W. Furthermore, this study also investigates the working fluid charge in the cycle, which is represented as the sum of the mass in the evaporator and condenser. From a design charge of 33.6 kg, they vary this to 1 and 2 kg above and below the design, and investigate the efficiency and amount of heat transferred from the heat source. The system performed with the highest thermal efficiency at the design expander power output for all working fluid charges, and with the lowest efficiency for the lowest expander power output. The variation in thermal efficiency between different working fluid charges at a given expander output level increases with the expander power output, as the curve is nearly flat at 1500 W, but varies most at 3000 W. This suggests that when the expander operates at levels far below its design output, one may change the charge to perhaps save cost on pumping power, without sacrificing thermal efficiency. Their analysis on the heat transfer in the evaporator shows that more heat is transferred for low charges than for high charges. This information is important when designing systems where cooling the heat source is critical, showing that if the current level of cooling is not sufficient, one can decrease the working fluid charge for the same level of expander output.

Ibarra et al. (2014) analyzed the off-design performance of an organic Rankine cycle incorporating a scroll expander. Two working fluids were considered in the study, R245fa and Solkatherm ES36 (SES36). The model they developed assumes that the heat source is infinite at a temperature that is equal to the temperature of the working fluid at the outlet of the evaporator, and so rather than varying the mass flow or temperature of a hypothetical heat source, they instead vary the temperature and pressure at the turbine inlet. For R245fa, the pressure varies between 500 and 3000 kPa and for SES36, the maximum pressure is lowered to 2000 kPa. For both fluids, the maximum temperature is varied between 120°C and 150°C. Additionally, the expander speed is varied between 1000 RPM and 5000 RPM, and the condensation temperature is varied between 15°C and 35°C. The heat sink is considered infinite as well, similarly to the heat source. As in the previous studies, Ibarra et al. (2014) found that the thermal efficiency of the cycle increases with increasing turbine inlet temperature and decreasing condensation temperature for both fluids. They also found that the performance of the cycle, which is measured in terms of thermal efficiency in this study, is strongly influenced by the isentropic efficiency of the expander. It is therefore vital to have an expander that performs well in the scenarios were it may operate.

2.3.3 Investigating different control strategies

Whereas the previous studies have focused on investigating the performance of a system under a single control strategy, Hu et al. (2015) looked into how a system performed under different control strategies, and attempted to identify which one worked best for their system. The heat exchangers used are plate heat exchangers, and the expander is a radial inflow turbine. The performance of the turbine and evaporator are each calculated using separate sub-models, which are based on the geometric characteristics of the equipment. The cycle uses R245fa as the working fluid, and geothermal fluid as the heat source. The heat source enters the evaporator at a design flow rate and temperature of 10 $\frac{kg}{s}$ and 90°C. In the off-design analysis, the flow rate and temperature vary between 5 and 15 $\frac{kg}{s}$ and 84 and 96°C respectively. The study compares three different control strategies. The first is called constant pressure operation, where the evaporating pressure is kept constant, but the variable inlet guide vanes of the turbine are controlled to change the flow rate of the working fluid to maintain the energy balance. The second control strategy is called sliding pressure operation, where the evaporation pressure may change, but the inlet guide vane settings are kept constant. The final control strategy is called the optimal control strategy, where both the evaporation pressure and the inlet guide vane settings may change, essentially combining the two previous control strategies. They found that for all three control strategies, the net power generally increased with heat source mass flow and inlet temperature, in a very similar way. However, because the restrictions for constant evaporation pressure and constant inlet guide vane setting were strictly obeyed under constant pressure and sliding pressure control respectively, they found that certain combinations of heat source flow rate and inlet temperature were not possible to fulfill, and therefore the cycle could not operate under such conditions. They found however, that the optimal control strategy was able to accommodate such combinations. They therefore argue that the optimal control strategy is easiest to control.

Walnum et al. (2013) investigated the performance of an organic Rankine cycle using R123 and a transcritical cycle using CO_2 under different control strategies for when the heat source flow rate and temperature changed. The heat source in this study was air, at design mass flow of 1 $\frac{kg}{s}$ and temperature of 100°C, and these respectively varied between 0.7 $\frac{kg}{s}$ and 1.6 $\frac{kg}{s}$ and 90°C and 120 °C. They modelled three control strategies in this study. The first strategy involved having a constant volumetric flow through the expander, thereby having a constant flow rate of the working fluid. The latter is achieved by having the pump run at a constant speed. The effect of this strategy is that the evaporation pressure and amount of superheating must vary, so that the density at the inlet of the expander is equal to that of the design density. The second control strategy was to vary the expander speed and keep the evaporation pressure constant, similar to constant pressure operation in the study by Hu et al. (2015). The pump speed was still kept constant in this case. The final strategy that is investigated is one where both the expander speed and pump speed are varied. This allows for changes in evaporation pressures and mass flows, and is similar to the optimal control strategy in the preceding study. When the heat source mass flow increases, but the temperature is kept at 100°C, the results show that for small changes in mass flow, there is very little difference between the control strategies, but large differences arise when the flow rate experiences larger variations. For CO_2, the two "simple" control strategies both rapidly level out, and perform worst among all the combinations of fluids and control strategies. However, using the optimum control strategy, CO_2 is the top performer in this investigation, significantly outperforming even R123 using the optimal control strategy. Applying the simpler control strategies to R123 yields poorer performance than the optimal strategy, but not as bad as with CO_2. Where for CO_2 the performances when using the

two simple control strategies were indistinguishable, when they are applied to R123 it is clear that the constant high pressure control strategy outperforms using constant expander speed. Decreasing the heat source flow rate predictably leads to less work output, and R123 using the optimal control strategy experiences the smallest performance degradation, followed by CO_2 using the same control strategy. Using the two simple control strategies with CO_2 leads to a more rapid performance deterioration, but it is still theoretically possible to operate under these conditions. The same cannot be said for R123. In Walnum et al. (2011), it was shown that when the flow rate was lowered, R123 could quickly enter an infeasible region because condensation would form at the inlet of the expander, or it would be present at the outlet. This was not an acceptable result, and so these results are not included. That CO_2 is able to operate at these lower heat inputs with the simpler control strategies highlights its versatility as a working fluid. When the temperature of the heat source is changed rather than its mass flow, some different results emerge. When the temperature is lowered significantly, R123 will again reach an inoperable region with the simpler control strategies. However, for the remaining valid data, the results are very similar to each other. This means that for CO_2, one can operate in this scenario using the simpler control strategies with a very small loss of performance compared to the optimal strategy. When the temperature is instead increased, the results show that the control strategy has a much greater effect. Again, the optimal control strategy performs best, and there is very little difference between the two fluids. Using the simpler control strategies, R123 with constant high pressure performs worst, whereas R123 with constant expander speed performs best. The performances of the cycles using CO_2 with these two control strategies are again very similar.

Chapter 3

System overview and model details

3.1 System overview

The heat source in this system is waste heat found in exhaust gases in an aluminum production plant. For safety and environmental reasons outlined in Section 1.3.1, the working fluid is indirectly heated with water acting as the intermediary fluid. The temperature of the flue gas varies with the ambient air temperature, and in this work this variation is modelled to be one-to-one, meaning that a 1 K decrease in the ambient air temperature leads to a 1 K decrease in the heat source temperature. The variation of the ambient temperature is modelled as a sinusoidal curve between the maximum and minimum average monthly temperatures, with the maximum temperature being reached on the 1st of July and the minimum temperature occurring at the start of January. The maximum and minimum ambient air temperatures are 14.8°C and -1.7°C, taken from weather data from Sunndalsøra (Yr.no, 2018). The flow rate of the exhaust gases is 40,000 $\frac{Nm^3}{h}$, regardless of the temperature of the stream.

Along with the changes in ambient air temperature, one must also consider the temperature variations in the surrounding water, which is used as the heat sink in this system. This seasonal variation is also modelled sinusoidally with a maximum and minimum temperature of 14°C and 4°C respectively. Furthermore, the months that the maximum and minimum occur in are shifted one month ahead, so that the minimum water temperature is reached in February, and the maximum is reached in August. The temperature variations of the ambient air and water are shown graphically in Figure 3.1.

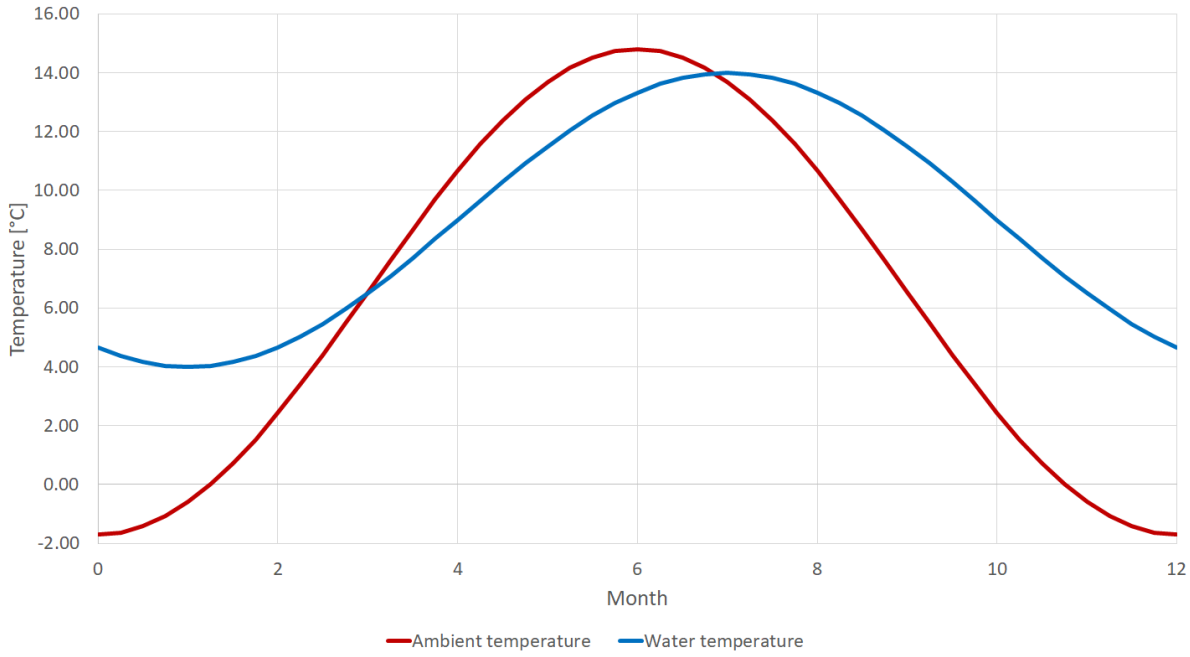

Figure 3.1: Seasonal temperature monthly average variation of ambient air and surrounding water.

This work also takes into consideration that the hypothetical aluminum production plant is a source of district heating to surrounding customers. Data for the district heating load has been provided by one of SINTEF's industrial partners, and has been used as the source for the magnitude of heat given to district heating. The district heating load increases with decreasing ambient temperature, and is predictably largest during the coldest months. In this work, the aluminum plant is thought to be contractually obligated to provide the district heating, and so this load will take precedence over the power production cycle. Therefore, the heat for the district heating is extracted upstream of the power cycle. Decreasing temperature of the heat source during the colder months naturally leads to less power being developed during such periods, and this phenomenon is amplified by the district heating, as energy is beings used for district heating in lieu of power production. This further worsens the performance during wintertime.

In the autumn project work, three separate cases were investigated, distinguished by the heat source inlet temperature and minimum heat source outlet temperature. In this work, Case 3 is further delved into. This means that in the warmest month, the gas enters the waste heat recovery unit (WHRU) at 150°C and is cooled as it heats the water in the indirect loop. To ensure that the conditions in the exhaust gas stream are above the acid dew point, the heat source has a minimum temperature of 80°C. Seeing as how the heat source enters at a low temperature and also has a minimum temperature requirement, it is important that the system utilizes the available energy to the greatest degree. For this reason, the option to include a recuperator is available to the optimizer, so that the recuperator will be present in scenarios were this is beneficial.

In this work, a twin screw expander is used as the chosen expander technology. This choice comes as a result of the data from the project work during the preceding autumn. As seen in 1.4, the expander capacity was in the approximate range between 20 kW and 130 kW. The required capacity varied much with the inlet temperature of the heat source, as well as the

maximum value of the total heat exchanger area. For the purposes of the design investigated in this work, an expander that is able to sustain a power output up to around 90 kW with the ability to also perform well with lower loads should suffice. From the literature study, it seems twin screw expanders are favored for this level of power output. Furthermore, the results from the project work show that the expander must be able to handle large pressure ratios, as these were found to sometimes reach up to 6. The literature study showed that screw expanders are able to withstand such large pressure ratios in a single stage, whereas turbines would require several stages. Furthermore, Lemort et al. (2013) found that in this range for pressure ratios, screw expanders were able to operate with high values of peak isentropic efficiencies. Screw expanders are thus selected in favor of turbines for this system to reduce cycle complexity as much as possible while maintaining high efficiencies.

No specific technology has been chosen for the heat exchangers in this work. This is because they are not implemented in the model, and so one cannot accurately evaluate their performances. Instead, a simpler heat exchanger model has been developed by SINTEF, which is described in greater detail in Section 3.2.2.

3.2 Model details

The optimizer is a program developed by SINTEF Energy Research, and was shared with me to use in this work. It employs the NLPQL routine to find the extremum of an objective function that is subject to a series of constraints. These constraints can be either equality constraints, where a parameter has to be equal to a set value, or inequality constraints, where a parameter must be greater or smaller than a set value, depending on the type of inequality. Because the routine estimates functions such as gradients numerically, it is conceivable that the solver finds a solution that very nearly – but not entirely – satisfies the constraints, and so the user can also specify a tolerance for such errors. The algorithm finds the extremum by varying the parameters that are set as variable, where the maximum and minimum values of each variable parameter are set.

The objective function in this work is net power. The model only evaluates the steady state performance of the system, and transient conditions are not considered. For the solver to evaluate this parameter and the effect of changing each of the variable parameters, it needs to be able to retrieve thermodynamic data for all the fluids employed. The optimizer supports a variety of thermodynamic libraries, and the user is free to choose the appropriate one. In this work, REFPROP 9.1 is used for its support of a large number of fluids, in addition to its robustness and thermodynamic accuracy.

3.2.1 Expander off-design performance evaluation

The evaluation of the expander's off-design performance is done using results found by Tian et al. (2017) and Zhu et al. (2014). The procedure to evaluate the performance was designed by myself and implemented by SINTEF Energy Research in their model.

The off-design performance of the screw expander varies primarily for two reasons: the pressure ratio of the cycle is different from the built-in pressure ratio of the expander, and variations in the rotational speed lead to differences in losses due to for example friction and leakages. Both of these influences have to be taken into account when investigating the expander's off-design performance. In the present model, these are handled in two steps: first the

impact of rotational speed at design pressure ratio is evaluated, and subsequently the impact of pressure ratio is considered.

The influence of changing the rotational speed is found with help of the results by Tian et al. (2017). They showed a near linear relationship between the isentropic efficiency of the expander and the rotational speed, where it decreased throughout. In the aforementioned study, the rotational speed varied between 60% and 140% of the design rotational speed, and these are set as the lower and upper limits in this model as well.

To find the relative change in rotational speed, the equation relating the mass flow to the rotational speeds for volumetric expanders is employed. This equation is shown in Equation 3.1.

$$\dot{m} = \eta_V \times \rho \times \dot{V} = \eta_V \times \rho \times V \times \frac{n}{60} \tag{3.1}$$

In Equation 3.1, ρ is the density of the fluid, V is the displacement volume of the expander and n is the rotational speed. η_V is the volumetric efficiency of the expander, which describes how much of the volume in the expansion chamber is used relative to that of the available volume.

Because the expander model does not take into consideration any geometrical parameters, it is difficult to evaluate the off-design performance using the rotational speed directly. However, by applying the affinity laws and evaluating the rotational speed in relative terms to the design point, it becomes possible to quantify the performance change due to changing rotational speeds. In this model, for a given process, the design mass flow rate, density and volumetric efficiency are known, and when investigating an off-design scenario for the same process, the flow rate, density and volumetric efficiency will be available for that case as well. The expansion volume will be the same for both cases. Using 3.1, one can therefore find the ratio of off-design rotational speed to the design rotational speed. This is done by first dividing the off-design mass flow with the design mass flow, as shown in Equation 3.2.

$$\frac{\dot{m}}{\dot{m}_{design}} = \frac{\eta_V \times \rho \times V \times \frac{n}{60}}{\eta_{V,\,design} \times \rho_{design} \times V \times \frac{n_{design}}{60}} \tag{3.2}$$

Equation 3.2 can further be simplified to Equation 3.3, which gives us the ratio of the off-design rotational speed to the designed one. As in the study by Tian et al. (2017), the off-design rotational speed cannot deviate with more than 40%, so the ratio found in Equation 3.3 must be between 0.6 and 1.4.

$$\frac{n}{n_{design}} = \frac{\dot{m} \times \eta_{V,\,design} \times \rho_{design}}{\dot{m}_{design} \times \eta_V \times \rho} \tag{3.3}$$

This approach was chosen because it utilizes parameters that are easily available from the model, namely the density of the fluid and the mass flow rate. This makes it easier to implement in the existing model. It should be noted that just like the isentropic efficiency, the volumetric efficiency will also vary with the rotational speed. Because the off-design volumetric efficiency is used in finding the off-design rotational speed, the optimizer will solve these two simultaneously through iteration.

To evaluate the isentropic efficiency, it is assumed that the relationship between isentropic efficiency and rotational speed is linear when the relative rotational speed varies between 0.6 and 1.4, as found by Tian et al. (2017) and supported by Hu et al. (2017). The same is assumed for the volumetric efficiency. To find the isentropic and volumetric efficiencies, one needs

to specify the maximum and minimum values of these, from which it is possible to linearly interpolate later. These can be given as input in the model, but the default values are the same as those found by Tian et al. (2017) for the design pressure ratio. For the isentropic efficiency, this maximum is 83% and the minimum is 77%. The corresponding values for the volumetric efficiency are 88% and 82% respectively. Figure 3.2 shows how the isentropic efficiency varies with the mass flow, with all other parameters kept constant. Notice that while the lower and higher limits for the rotational speeds are 60% and 140% relative to the design rotational speed, the mass flow in Figure 3.2 only varies between 70% and 130%. This is because as Equation 3.3 shows, a relative difference in mass flow does not correspond to a one-to-one difference in rotational speed, due to the effect of changing volumetric efficiencies.

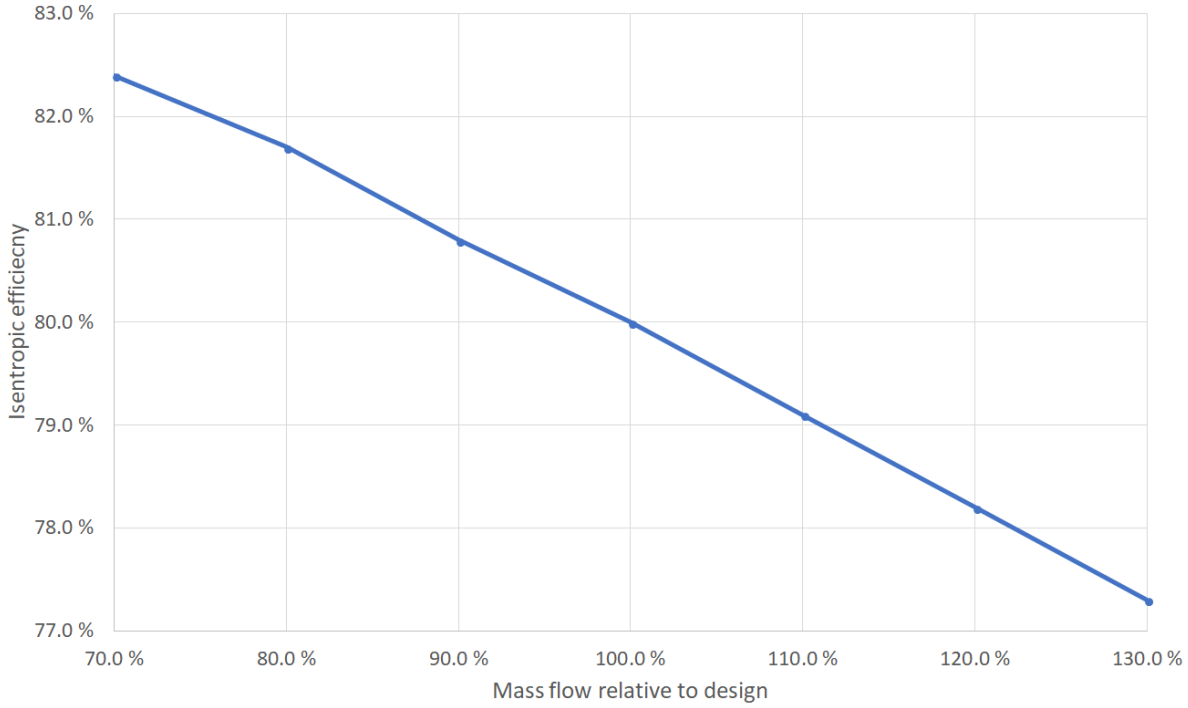

Figure 3.2: Isentropic efficiency versus relative mass flow.

To account for mismatch between the pressure ratio of the cycle and the built-in pressure ratio of the expander, the work by Zhu et al. (2014) is used. Using the relationship between pressure, volume and power for volumetric expanders, they derived an expression for a correction factor that is multiplied to the design isentropic efficiency. When the pressure ratio is equal to the design pressure ratio, this factor is equal to 1, and it decreases as the pressure ratio in the cycle changes. This model is also sensitive to the fluid in question, as the heat capacity ratio is also a parameter in the calculation of the correction factor. The heat capacity ratio, and the pressure ratio of the cycle are readily available to the model, while the built-in pressure ratio is an input to the off-design model. Unlike with the performance evaluation for off-design rotational speed, there are no upper and lower limits for the deviation in pressure ratios. The logical limit for this curve is when the correction factor reaches 0, but it is unlikely that the pressure ratio will vary so much that this limit is reached. Figure 3.3 shows how the isentropic efficiency varies with the relative pressure ratio, when all the other parameters are kept constant. The design efficiency in this figure is 80%.

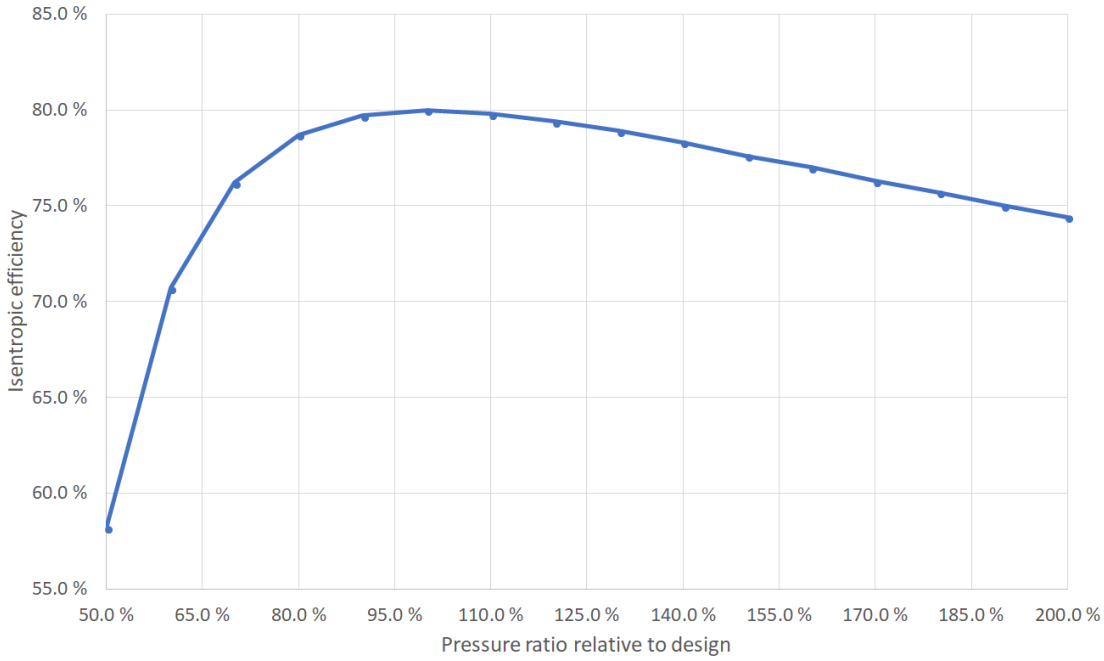

Figure 3.3: Isentropic efficiency versus relative pressure ratio.

Combining these results, we can create a performance map for any off-design scenario. The isentropic efficiency for a given scenario is first calculated for the given rotational speed through linear interpolation as described earlier. Subsequently, the correction factor for the pressure ratio is calculated, and multiplied to to the isentropic efficiency for that rotational speed. Figure 3.4 shows what the performance curve looks like across the range of pressure ratios for three values of relative mass flows.

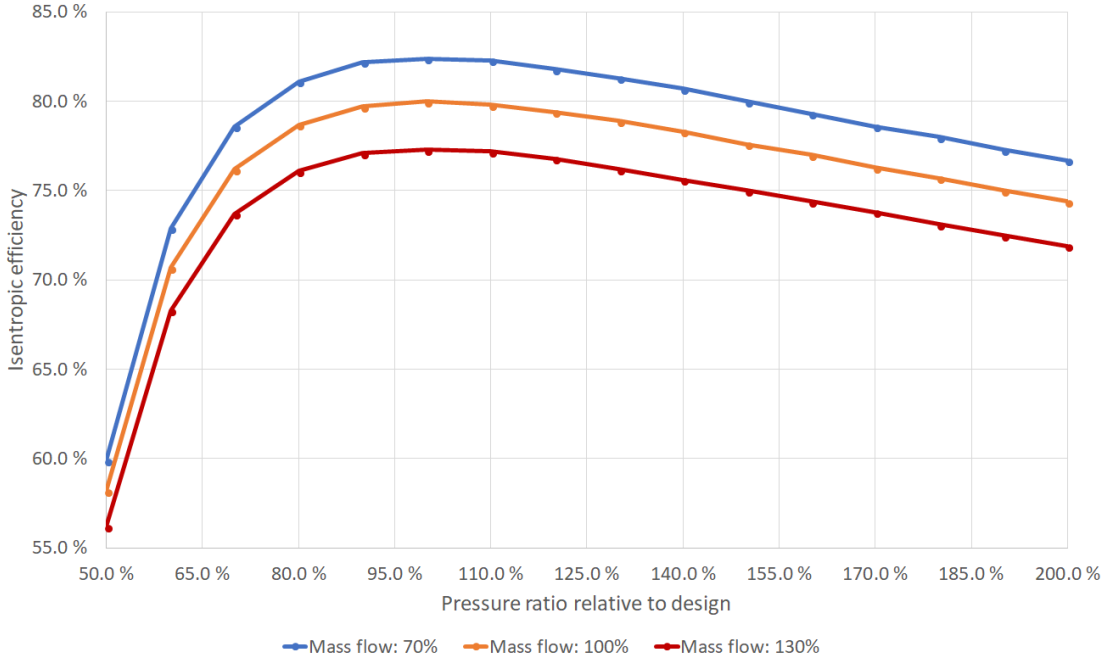

Figure 3.4: Variation of isentropic efficiency with both changing mass flow and pressure ratio.

3.2.2 Heat exchanger performance evaluation

The heat exchanger model in the optimizer does not take into account any specific heat exchanger technology. Instead, it models the heat exchange from the hot fluid to the cold fluid more simply, by assuming that there are a number of tubes of a specific diameter for either fluid. The diameter and number of tubes can independently be set for the hot and cold stream, but the length must be equal for them both. The space between the pipes is modelled to be filled with an infinitely thermally conducive material, meaning that it offers no thermal resistance in the heat exchange. Furthermore, all heat is assumed to pass from the hot to the cold fluid, and no heat is lost to the surrounding environment in the heat exchangers or elsewhere in the system. Figure 3.5 shows a cross section of a heat exchanger in the model, with the hot stream in red and the cold stream in blue. The figure illustrates the different number of hot and cold tubes, and the dissimilar diameters between the two streams.

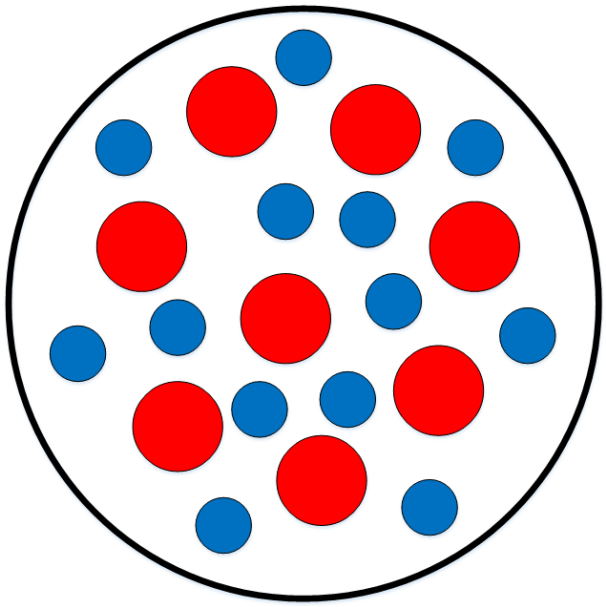

Figure 3.5: Example of a cross section for a modelled heat exchanger. (Recreated from model description.)

From the geometry of the tubes and the parameters of each flow, the heat transfer coefficient and pressure drop is calculated using appropriate correlations. Because the heat transfer coefficient changes much during phase change, the calculation will be sensitive to the amount of sections that the heat exchangers are subdivided into. This number is set by the user.

It may occur that the optimizer struggles to converge to a solution when many parameters are set as variable, or it may take a long time to do so. It is therefore possible to set a constant heat transfer coefficient for the hot or cold side in each heat exchanger, bypassing the calculation with the correlations. This decreases the time to convergence, but may lead to highly erroneous conclusions depending on the quality of the set constant heat transfer coefficient.

3.3 Model assumptions and optimization approach

As described in Section 3.1, the system is indirectly heated using water in the indirect loop, in order to separate the organic Rankine cycle from the exhaust gas flow. However, this version of the optimizer unfortunately does not feature the ability to model the indirect loop. To be able to make comparisons with the work from the fall project work, this work tried to model an indirect cycle using an optimizer for direct cycles, where the modelled heat source is the indirect water loop. Because the WHRU is not modelled, some assumptions must be for how the indirect water loop is heated by the heat source. In this work, it is assumed that the temperature difference in the WHRU was constant. This constant temperature difference was found by using the data from the fall project work and calculating the LMTD in the WHRU for the three working fluids, and taking the average of these. This temperature difference is found to be 17.5 K. Because it is assumed that there is a constant temperature difference in the WHRU, it means that it is possible to calculate the corresponding maximum and minimum temperatures of the indirect loop by taking the corresponding values from the exhaust gas stream and subtracting the constant temperature difference. Recall that the minimum temperature in the exhaust gas is 80°C, and this means that the minimum temperature of the indirect loop is 62.5°C. Simultaneously, the inlet temperature of the exhaust gas in the hottest month is 150°C, corresponding to a temperature of 132.5°C in the indirect water loop. The mass flow of the water in the indirect loop was calculated so that the heat content in the indirect loop matched that which was available in the heat source, and was calculated to be roughly 3.3 $\frac{kg}{s}$.

One of the goals from the autumn project work was to identify which values for total heat exchanger area seemed most interesting to further study for each of the three cases. Two such points were found for Case 3, namely total heat exchanger areas of 700 m^2 and 900 m^2. This work focuses on the scenario where the total heat exchanger area is 700 m^2. This total heat exchanger area also includes the heat exchanger area for the WHRU, and so the present work must restrict the total heat exchanger area to only represent the area used by the evaporator, condenser and hypothetical recuperator. This was done by finding the average area dedicated to the WHRU in the project work results, and subtracting this from the aforementioned total. From a total heat exchanger area of 700 m^2, this calculation leaves only 230 m^2 to the remaining heat exchangers. With regards to the geometries of each heat exchanger, it should be noted that the diameters – while adjustable – have been to a constant value for each stream in each heat exchanger, because the optimizer struggles to converge to a solution when these are variable. For the same reason, the geometry of the hot fluid in the evaporator has not been evaluated either, and so the heat transfer coefficient in this fluid is set to 5000 $\frac{W}{m^2 \times K}$. This value is most likely higher than what a real evaporator would experience, but it is chosen to be so high so as to not be the limiting characteristic in the evaporator. The number of cold side tubes in the condenser is also not variable, and is locked to 150, again because of limitations in the optimizer. This number is close to the number of hot-side tubes in this heat exchanger, and is therefore deemed acceptable.

As shown in the results from the project work in Section 1.4, for this value of total heat exchanger area, the working fluid that produced the most power was a 50%-50% mixture of n-butane and n-pentane. For this reason, this is also the mixture investigated in this work. Furthermore, using pure n-butane and n-pentane are also investigated and compared with the mixture.

There are several free variables in the optimizer, three of which define the recuperator geometry; the recuperator length, the number of cold side tubes and the number of hot side tubes. For every optimization, the minimum length of the recuperator is set to 0, so that in the event that the optimal solution is one without the recuperator, the length will be set to 0 and no area

will be dedicated to this component. Furthermore, the optimizer is constrained so that no two phase flow may either enter or leave the expander, ensuring single-phase operation. While the expander has a sub-model dedicated to its off-design performance, the pump operates with a constant isentropic efficiency. This approach has been chosen because the work used by the pump does not represent a significant share of the net power. The minimum pressure in the cycle is also constrained to always be greater than 1 bar, to avoid sub-atmospheric operation and risking to have air leak into the flow.

Figure 3.6 shows the temperature profiles of the heat source and heat sink throughout the year. Note that while the heat source in the entire system is the flue gas from the aluminum cells, the heat source that is referred to in Figure 3.6 is the water in the indirect loop, which is always 17.5 K colder than the flue gas.

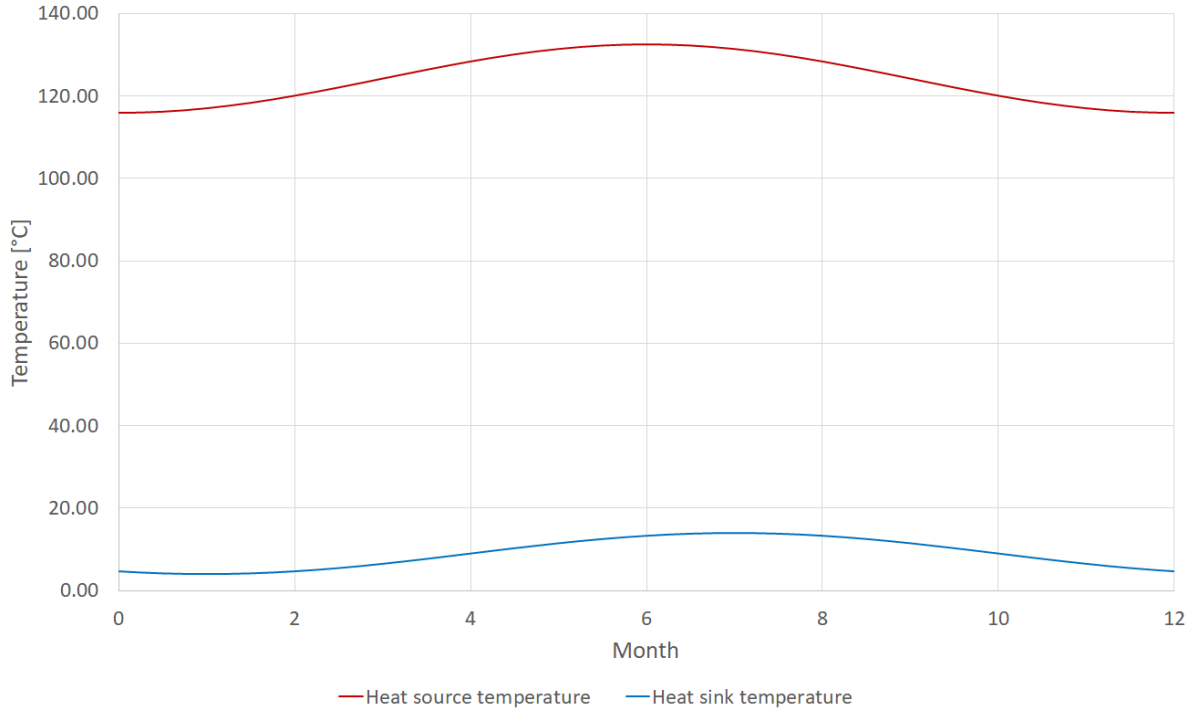

Figure 3.6: Temperature profile of the heat source and heat sink.

To evaluate the performance throughout the year, eight evenly distributed points have been simulated, beginning at the start of January, and ending in the middle of November. It is assumed that the length of each of these periods is 45 days. Using the data for the district heating, the required temperature difference of the hot air to provide the heat was calculated using Equation 3.4. The inlet temperature of the indirect water was lowered by this temperature difference to simulate the less available heat due to required district heating.

$$\Delta T = \frac{\dot{Q}_{district\ heat}}{\dot{m}_{air} \times c_{p,\,air}} \tag{3.4}$$

Figure 3.7 shows how the distribution of available heat to district heating and power production varies throughout the year. The district heating requirement is assumed to be constant from the start of one period to the next, and the load is read from the data provided by the industry partner.

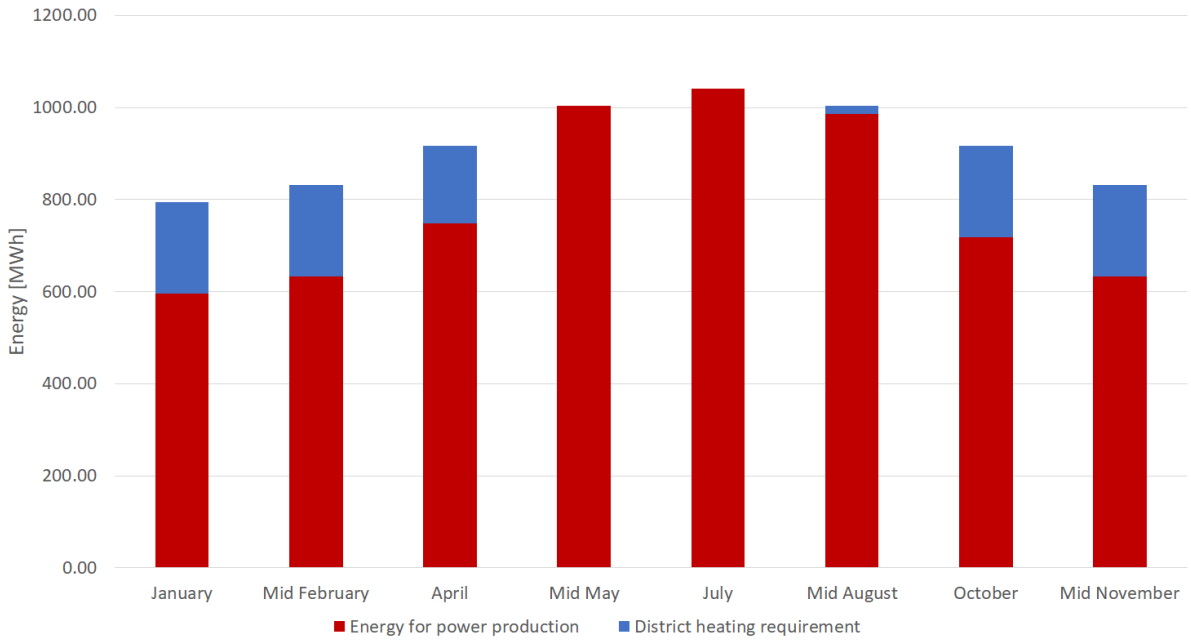

Figure 3.7: Distribution of available heat to district heating and power production

The on-design operating point was found by optimizing for all the variables – including the heat exchanger geometries – for every point from the year, and choosing one of these as the design for the cycle. The off-design performance evaluation for the other points was then carried out by locking the heat exchanger geometries to those of the design point, and enabling the off-design performance evaluation for the expander. Table 3.1 shows all the variables in the optimizer, and differentiates between those that can be varied during both on-design and off-design operation and those that are disabled during off-design cases. The other constant parameters of the optimizer are shown in Table 3.2. Again, like in Figure 3.6, the heat source referred to is the water in the indirect loop.

Table 3.1: Variables in the optimizer.

Parameter
Variable in both on-design and off-design optimization
Working fluid maximum pressure
Working fluid mass flow rate
Working fluid maximum temperature
Working fluid minimum pressure
Heat sink mass flow rate
Variable only in on-design optimization
Evaporator length
Evaporator cold side number of tubes
Condenser length
Condenser hot side number of tubes
Recuperator length
Recuperator cold side number of tubes
Recuperator hot side number of tubes

Table 3.2: Constant parameters in the optimizer.

Parameter	Value	Unit
Heat source and sink characteristics		
Heat source fluid	Water	-
Heat source flow rate	3.275	$\frac{kg}{s}$
Heat source minimum temperature	62.5	°C
WHRU temperature difference	17.5	K
Heat source inlet pressure	5[a]	bar
Heat sink fluid	Seawater	-
Heat sink inlet pressure	5[b]	bar
Heat exchanger diameters		
Evaporator cold side	10	mm
Recuperator hot side	20	mm
Recuperator cold side	10	mm
Condenser hot side	20	mm
Condenser cold side	10	mm
Other constants		
Pump isentropic efficiency	70	%
Generator efficiency	95	%
Motor efficiency	95	%
Evaporator hot side heat transfer coefficient	5000	$\frac{W}{m^2 \times K}$
Condenser cold side number of tubes	150	-

[a] Where there was a risk of the water being vapor at the maximum temperature at 5 bar, this pressure was increased to 20 bar. Because water is incompressible, it is unlikely that this plays a major role on the results.

[b] 5 bar was chosen to avoid issues with high pressure loss in the model. In evaluating the pump work for the heat sink, the model only takes into account the work needed to pump the fluid from the outlet conditions back to the inlet conditions, so a high inlet pressure here does not affect the results. In reality, the inlet pressure here would most likely be much lower to avoid having to needlessly pump the heat sink fluid to a high pressure.

Chapter 4

Results

4.1 On-design optimization

As mentioned in the preceding chapter, in order to find the design characteristics of the heat exchangers and the expander, the optimizer was used for all eight points in the year with every variable in Table 3.1 being available to the optimizer to change. That means that for each fluid, there are eight potential designs for the cycle, and one is chosen to be evaluated in the off-design cases. The off-design designs are evaluated by finding the total net work produced, which is calculated by estimating the integral across the year using the trapezoid rule. To compare with the best case, the trapezoid approximations for the on-design simulations are 644.35 MWh for butane, 472.07 MWh per year for pentane and 649.17 MWh per year for the 50%-50% mix between the two.

4.1.1 Choosing design point

In choosing the design point, the expander and the heat exchangers have been identified as the components around which the design characteristics must be considered. Lemort and Legros (2017) pointed out how the performance of the expander largely influences that of the whole system, and particular focus has thus been given to the off-design performance of the expander. In choosing the design point, the points with the higher heat source temperatures have been emphasized. It is important that the heat exchangers are able to harness the higher available heat during these periods, and so it is discouraged to choose one of the designs for the colder months, in fear that these heat exchangers are not able to effectively utilize the higher heat content available.

As shown in Section 3.2.1, two parameters influence the off-design performance of the expander in this work: the volumetric flow rate, and the pressure ratio. In choosing the design point, it has been assumed that these two parameters do not change much from the on-design simulations. Figure 3.2 shows that the performance of the expander increases with decreasing mass flow rate, which is closely connected to the volumetric flow rate. It is therefore advantageous to choose a design point so that the design flow rate is on the higher end of the range of mass flows. As for the dependency on pressure ratio, Figure 3.3 shows that the highest efficiency is achieved at the design pressure ratio, but that the decline in performance is not equal for over-expansion – when the built-in pressure ratio is higher than the pressure ratio in the cycle – as it is for under-expansion – the converse of over-expansion, when the built-in pressure

ratio is lower than the pressure ratio in the cycle. As can be seen in Figure 3.3, under-expansion is much more favorable than over-expansion, as a similar deviation in pressure ratio leads to a much lower performance when the flow is over-expanded. Choosing a design point thus involves balancing the losses due to over- and under-expansion across the year. Since under-expansion is favorable to over-expansion, it seems reasonable to expect that it is favorable to choose a design pressure ratio that is on the lower end of the range of pressure ratios across the year. However, it seems ill-advised to choose the smallest pressure ratio as the design pressure ratio, as large losses could be incurred when operating in scenarios where the cycle pressure ratio is high.

Figure 4.1 shows the variation of the pressure ratio and the mass flow rate for the three fluids across the year. Investigating each graph, it becomes clear that the goal of finding a design point with high mass flow and low pressure ratio is not always easy. For butane and the 50%-50% mixture it is relatively simple, as the pressure ratio is on lower end simultaneously as the mass flow rate is high during the warm months, as is evident from Figures 4.1a and 4.1c respectively. However, by inspecting Figure 4.1b it can be observed that the pressure ratio is the largest during the warmest months for pentane. It thus becomes clear that this pattern does not persist for all working fluids.

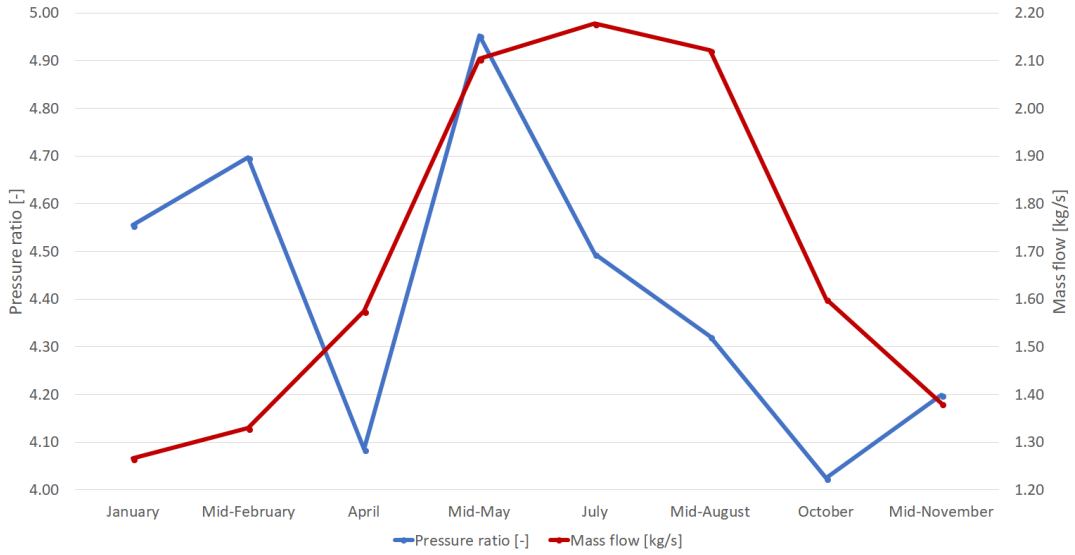

(a) Butane.

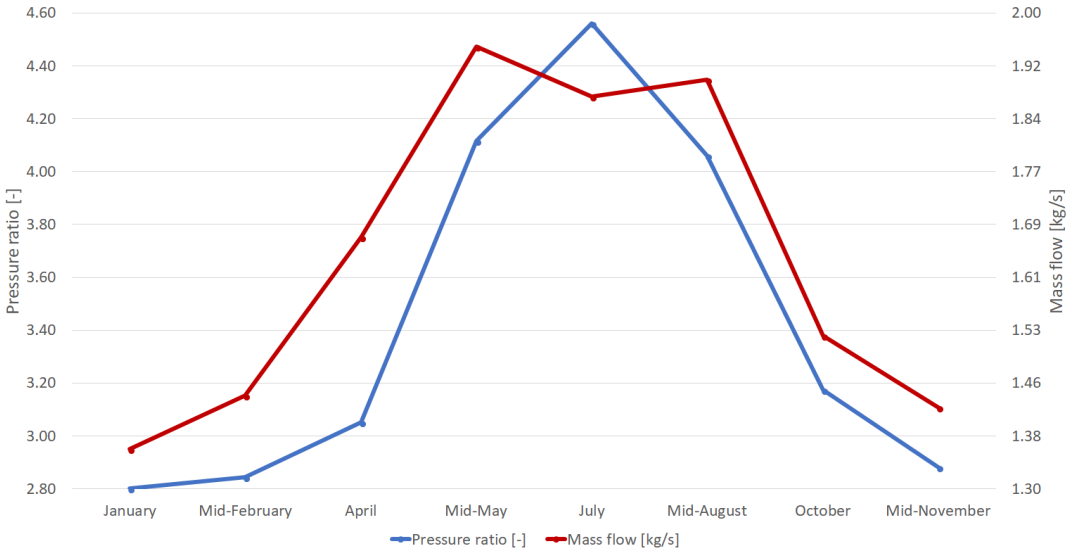

(b) Pentane.

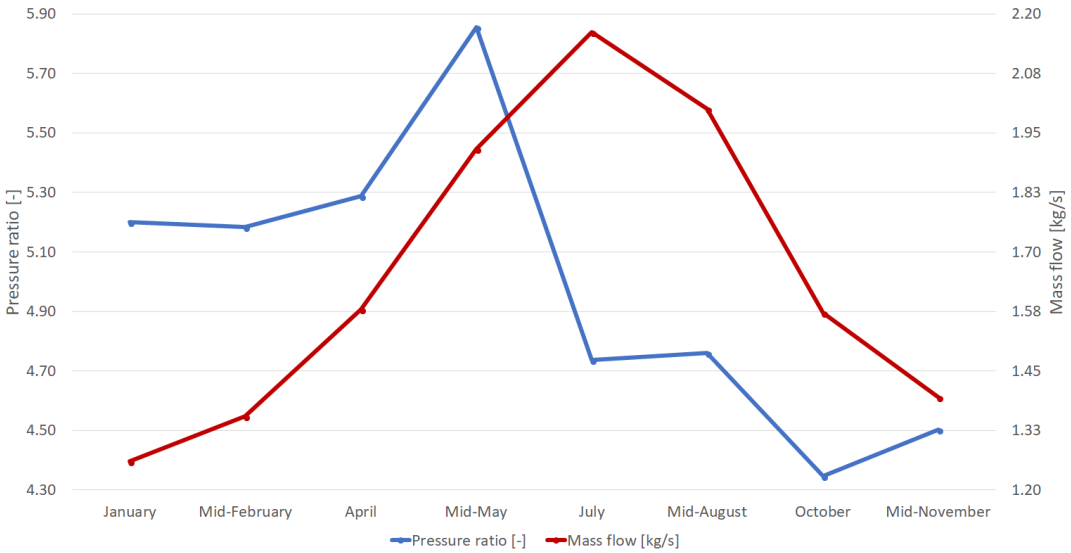

(c) 50%-50% mixture of butane and pentane.

Figure 4.1: Variation of optimized pressure ratio and mass flow rate throughout the year.

Based on the prior discussion on the choice of design points, the optimized design for mid-August has been chosen as the design point for butane. For the 50%-50% mix, the design point is in July. Both of these points are in one of the warmer months of the year, and both designs benefit from having high design mass flow rates and relatively low design pressure ratios. While there will be losses due to under-expansion during the colder months, it is believed that these losses will be offset by the higher performance of the expander due to lower mass flow rate. For pentane, April is chosen as the design point. This decision was based on the off-design characteristics of the expander, so the low pressure ratio is ideal. On the other hand, the mass flow rate at this point is roughly in the middle of the range, so during the periods where the pressure ratio is much higher than the design pressure ratio, the performance will deteriorate both from the pressure ratio mismatch and the increased mass flow. Additionally, April is not among the warmest months in the year, and there is a risk that the heat exchangers from this

design are inadequate for use in the warmest months.

The parameters for the design flow are summarized in Table 4.1.

Table 4.1: Design parameters for each fluid.

	Butane	Pentane	50%-50% mixture
Working fluid maximum pressure (bar)	11.07	3.10	6.80
Working fluid maximum temperature (°C)	84.08	73.35	89.02
Working fluid flow rate ($\frac{kg}{s}$)	2.12	1.67	2.16
Working fluid minimum pressure (bar)	2.45	1	1.33
Heat sink mass flow rate ($\frac{kg}{s}$)	23.64	13.87	21.73
Evaporator length (m)	25.77	25.81	23.81
Evaporator cold side number of tubes (-)	104	202	107
Condenser length (m)	26.11	7.39	22.46
Condenser hot side number of tubes (-)	85	142	97
Recuperator length (m)	1.34	0.09	2.38
Recuperator cold side number of tubes (-)	67	61	51
Recuperator hot side number of tubes (-)	126	100	141
Expander design isentropic efficiency (%)	80	80	80

4.2 Off-design

With the on-design points chosen, the seven other points were simulated with the heat exchanger geometries locked. Figure 4.2 shows how the off-design performance compares with the corresponding on-design optimization for each point of investigation. It is expected that the off-design points perform worse than their on-design counterparts, and this is true for the majority of the points for all three working fluids. With these design points, the total amount of electricity generated throughout the year is tabulated in Table 4.2, along with the district heating output in each case. Figure 4.2 shows how in the two earliest data points butane outperforms the mixture substantially, but in the other points, the mixture is equal to or slightly better than butane. Table 4.2 shows that the small superiority of the mixture in the latter months is not enough to make it the best performing working fluid across the year, however.

Table 4.2: Estimated yearly electric energy output for butane, pentane and the 50%-50% mixture of the two.

	Butane	Pentane	50%-50% mixture
Yearly E_{el} production (MWh)	643.6	441.1	640.0
Yearly E_t output (MWh)	982.5	982.5	982.5

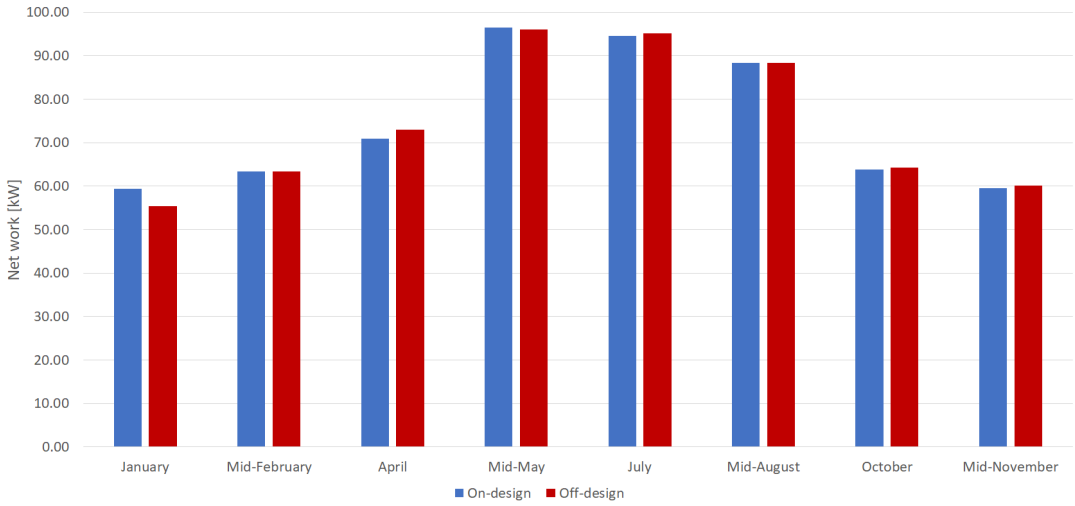

(a) Butane.

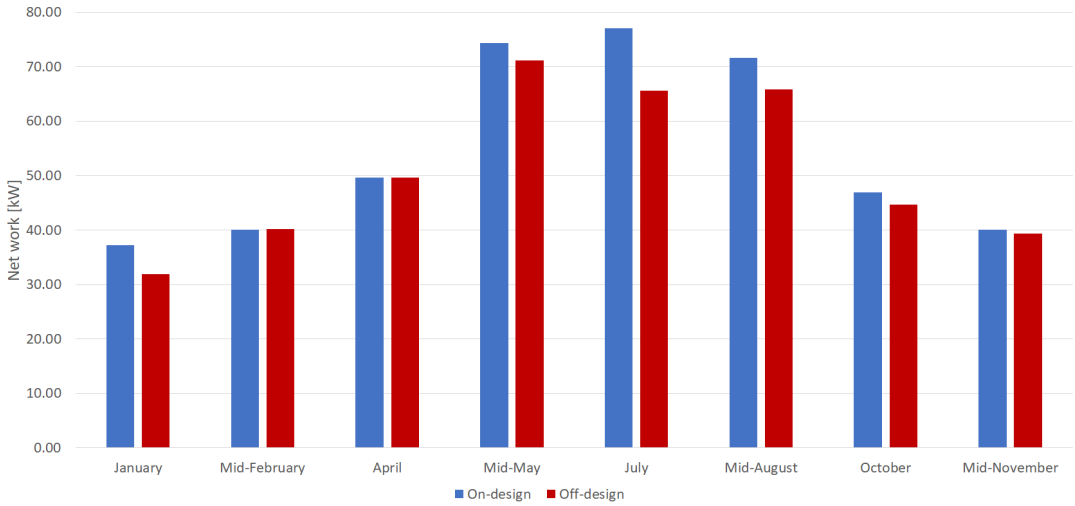

(b) Pentane.

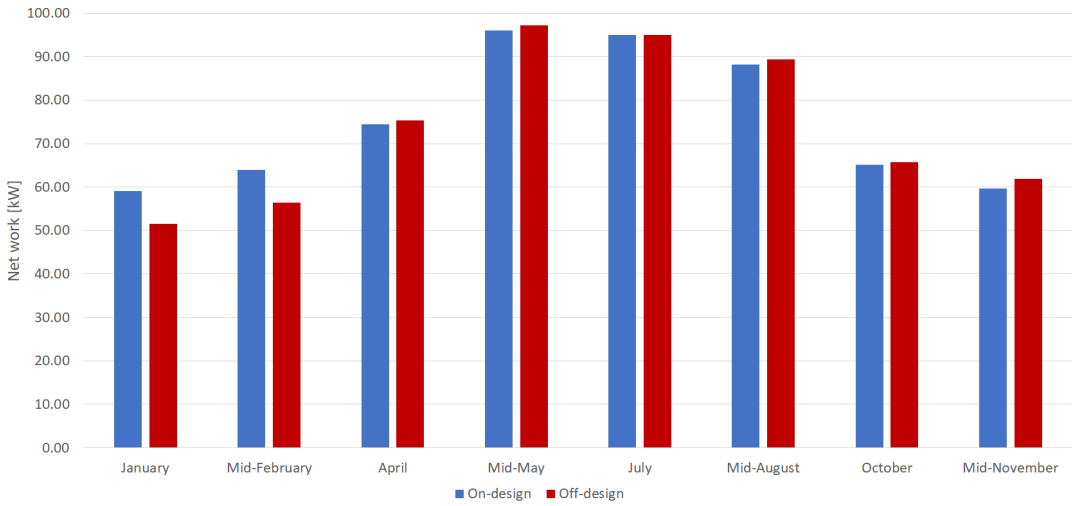

(c) 50%-50% mixture of butane and pentane.

Figure 4.2: On-design and off-design performance for each point of investigation.

Chapter 5

Analysis

5.1 Variation of process parameters with the chosen design

The previous results show how much net power it is theoretically possible to produce using each respective design, but it does not show how the various parameters change to reach those levels of power output. From an operational standpoint, it is important to ascertain these variations, to judge whether it is possible to operate the cycle safely and efficiently.

5.1.1 Changes in volumetric flow rate and pressure increases in the pump

One of the key parameters in the cycle is the volumetric flow entering the expander. This is one of the design parameters when making the expander, and a large deviation from the design point may lead to the cycle being practically infeasible to operate. Additionally, the variation in pressure increase in the pump has been investigated, as it is important that this component is also able to operate in all the changing conditions throughout the year. Figure 5.1 shows the variation of these two parameters throughout the year, for each working fluid.

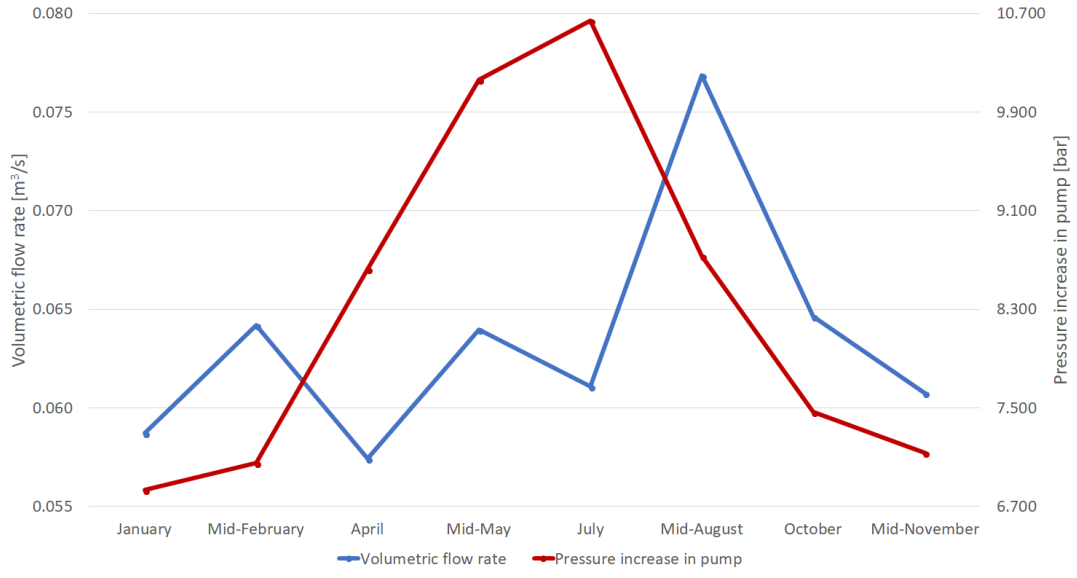

(a) Butane. (Design point: mid-August)

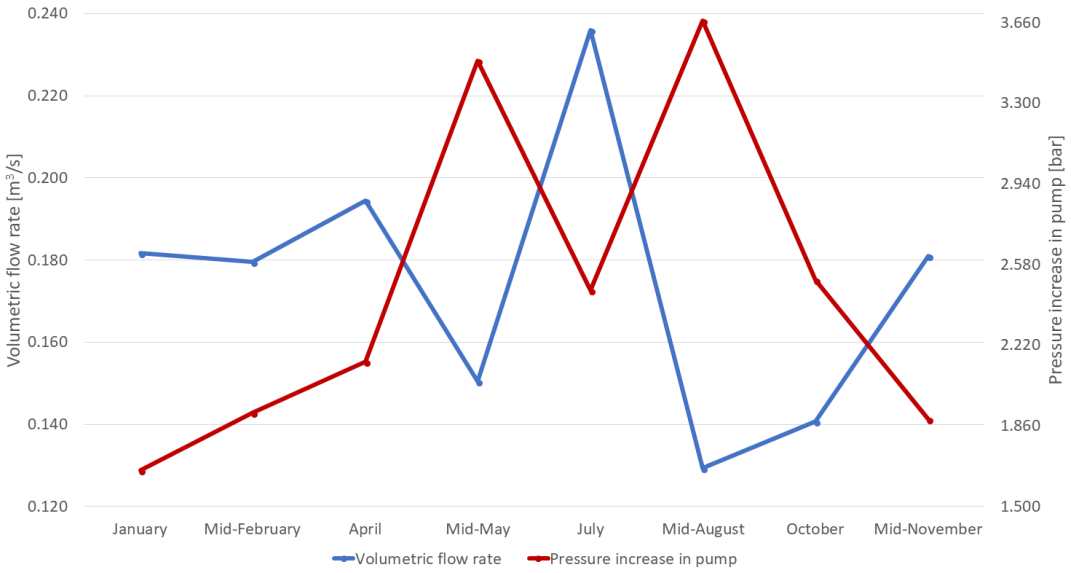

(b) Pentane. (Design point: April)

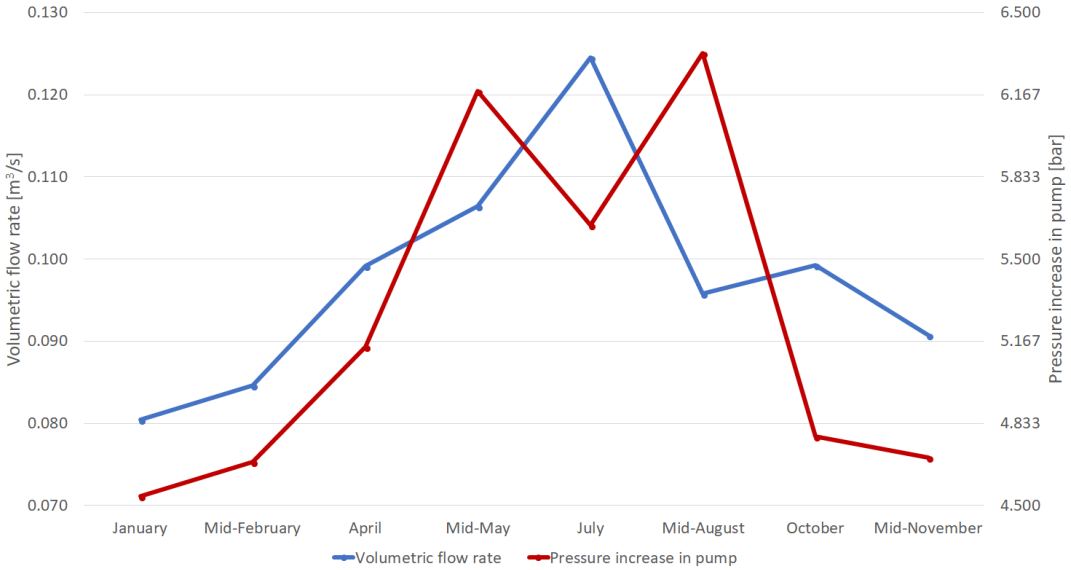

(c) 50%-50% mixture of butane and pentane. (Design point: July)

Figure 5.1: Variation of volumetric flow rate and pump pressure increase for each working fluid.

As Figure 5.1 shows, the volumetric flow rates are largest during the design points for both butane and the 50%-50% mixture. For pentane, the highest volumetric flow rate is reached in July, with the second highest volumetric flow rate being reached in the design point. For butane, the volumetric flow rate entering the expander is minimized in April, where it is 74.7% of the design flow rate. This should not offer any operational problems. The smallest flow rate for the 50%-50% mixture is 68.0% of the design flow rate, and this should not offer any challenges either. The volumetric flow for pentane has a greater relative range, because the volumetric flow is not maximized at the design point. For pentane, the maximum volumetric flow is 121.3% of the design flow rate, with the minimum flow rate being 66.5% of the design flow rate. By itself, this range should not lead to operational problems, but because the expander must be designed for both high and lower flow rates, perhaps the design will be more complicated compared to

the expanders for the cycles with butane and the mixture. Because greater variations have to be considered for the design of the expander with pentane, the cost of this particular expander may be higher compared to that of the cycle using butane or the mixture.

It was predicted that the flow rate in off-design mode would be very similar to the flow rate in the on-design optimization, but this is generally not the case. The flow rates in off-design mode are often significantly lower than they were after the on-design optimization. Given the implementation of the expander's off-design performance, it is reasonable to expect the optimizer to try and have the volumetric flow rate be largest during the design. As shown in Figure 3.4, the performance of the expander increases as the volumetric flow rate decreases, so when off-design operation is configured in the optimizer, one may expect that the flow rate will be low wherever possible.

For pentane in July, this explanation does not hold, as the flow rate spikes in this data point, as seen in Figure 5.1b. To explain the deviation, one must investigate which surrounding parameters influence the volumetric flow rate in the optimizer. The volumetric flow rate at a point in the cycle is essentially a function of the mass flow rate and the pressure and temperature at that point, where lower pressures and higher temperatures lead to higher volumetric flow rates for a given mass flow. While attempting to find a flow rate that increases the efficiency of the cycle, the optimizer is simultaneously subject to a series of constraints where for example the inlet to the expander must be superheated, and there cannot be any temperature crossing anywhere in the evaporator. To reduce the volumetric flow rate in July, the optimizer would have to lower the mass flow rate or increase the pressure. While changing these parameters, it also needs to satisfy the energy balance in the heat exchanger.

Because of these constraints, the optimizer cannot increase the pressure, because the pressure is already so high that the temperature pinch is only 0.3 K. Furthermore, decreasing the mass flow at the current pressure will, due to the energy balance, lead to increased temperature at the inlet of the expander, and thus risks a temperature crossing in the heat exchanger. Even if there is an opportunity to decrease the mass flow and simultaneously uphold all the constraints, it is not clear that this will lead to a higher performance. Because power output in the expander is a function of mass flow rate and enthalpy change, the net power may decrease even as the expander efficiency increases, thereby worsening the performance of the cycle.

Observing the graph for the pressure increases in the pump, it can be seen that unlike for the volumetric flow rate, the design points for all three months are not on either the maximum or minimum of the respective ranges. Compared to their respective design pressure increases, the maximum pressure increases are 121.9% for butane, 170.8% for pentane, and 112.4% for the mixture. Conversely, the minimum pressure increases are 80.8% for butane, 88.1% for pentane and 83.0% for the mixture. Again, the range is not large for butane and the mixture, whereas it is very large for pentane. However, as Zeleny et al. (2017) showed in an experimental study of a gear pump, it is not an issue to operate the pump with large variations in pressure increases and still have a relatively constant isentropic efficiency. The assumption of a constant efficiency in the pump thus holds.

5.1.2 Investigating pressure drops in heat exchangers

The pressure drop in the heat exchangers are investigated because these are an important characteristic to consider. The pressure drop of a heat exchanger is positively correlated with its heat transfer coefficient, meaning that some pressure drop may be beneficial to the performance of the system. However, the system will perform worse if the pressure drop is sufficiently high,

as an increased pressure drop will increase the pump power draw.

Figure 5.2 shows the pressure drop in every heat exchanger for each data point. The results are relative to the pressure increase in the pump, so that they give an indication of the power cost associated with the pressure loss. In inspecting the graphs, keep in mind that the left vertical axis is only for the evaporator and condenser, while the right vertical axis is for the two sides of the recuperator.

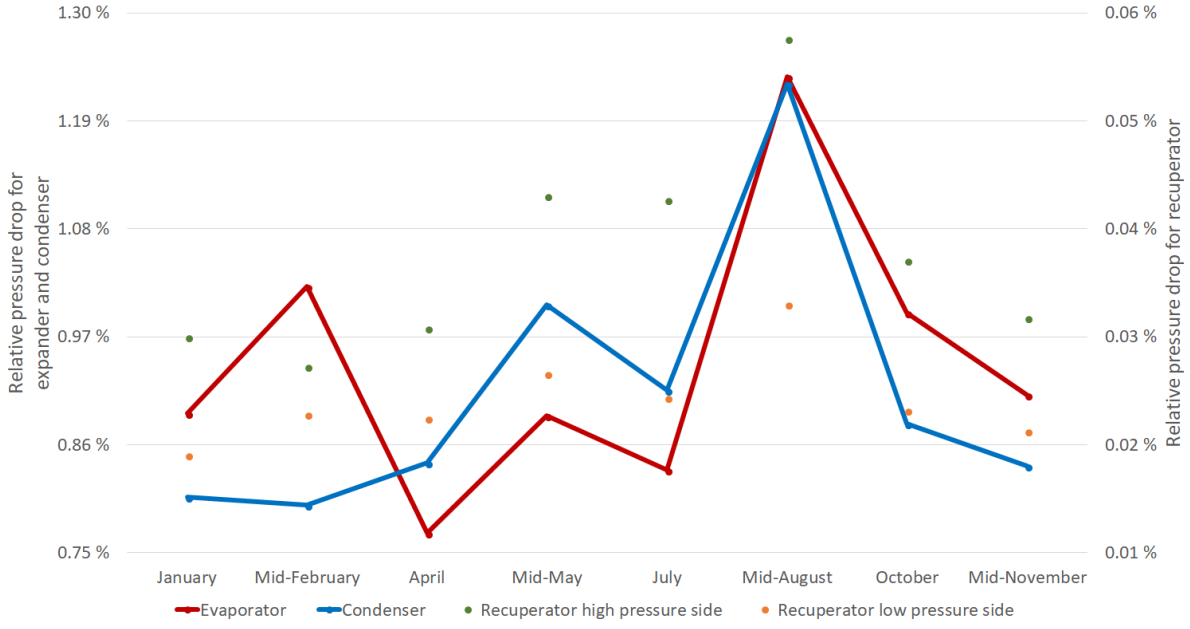

(a) Butane.

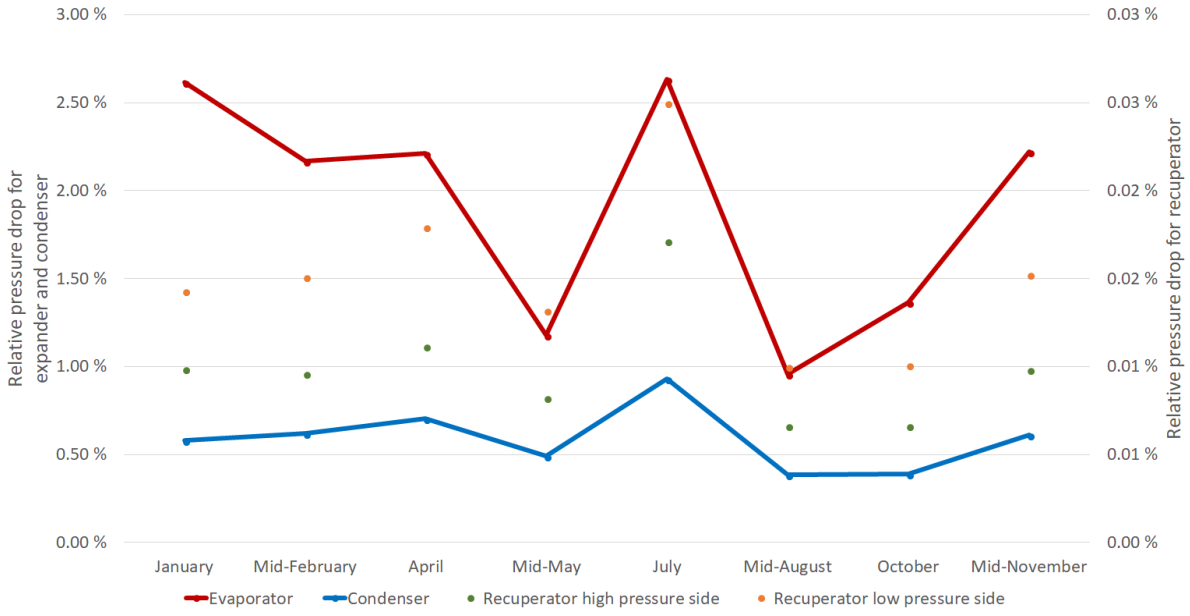

(b) Pentane.

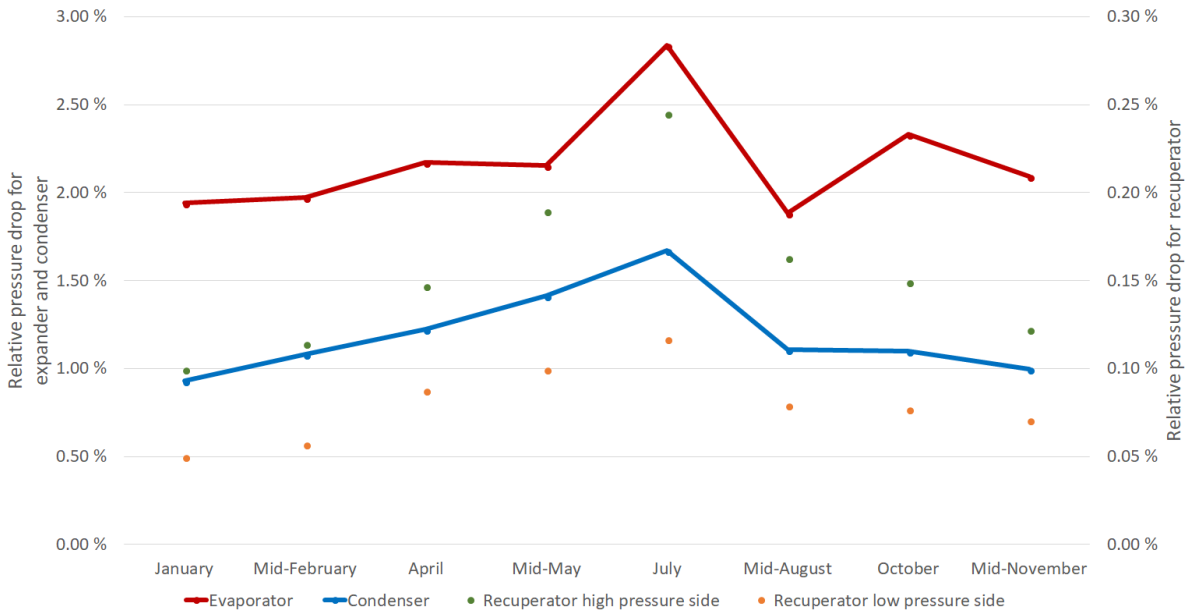

(c) 50%-50% mixture of butane and pentane.

Figure 5.2: Pressure loss relative to pump pressure increase in each heat exchanger for each data point.

Inspecting Figure 5.2, it is clear that the pressure losses in the evaporators and condensers are much more significant than those in either side of the recuperator. For butane and pentane, the losses in the recuperator are so small they may be considered negligible. However, the pressure losses in the condenser and evaporator are significantly high that they have an impact on the performance of the cycle.

Using the results for butane and the 50%-50% mixture during their design points[1], it is possible to roughly estimate the impact of the pressure losses in the heat exchangers. There are primarily two mechanism that lead to a performance loss due to pressure loss in the heat exchangers. The first is an increased temperature difference in the heat exchanger. For the evaporator, the working fluid enters the evaporator at a high pressure and high saturated temperature. As the pressure is reduced in the heat exchanger, the saturated temperature of the fluid is also lowered, leading to a higher temperature difference. In the condenser, because the model has a minimum pressure of 1 bar, pressure loss may force the model to choose a solution where the working fluid enters with a higher pressure and thereby higher saturated temperature. If pressure loss were not present, the optimizer may have found a solution where the working fluid enters the condenser with the minimum pressure, and thereby pressure loss leads to a higher temperature difference in the condenser also. On the other hand, in situations where there is not a feasible solution where the condenser outlet pressure is at the minimum limit, pressure loss may in fact decrease the temperature difference in the condenser as it lowers the saturation temperature of the fluid. In any case, a smaller temperature difference would result in a smaller exergy destruction rate in the heat exchanger.

The second aspect affecting the performance is how when there is pressure loss in the evaporator and condenser, the pressure ratio across the expander is reduced due to a lower pressure at the expander inlet and a higher pressure at the outlet. This will reduce the enthalpy difference

[1]Recall that the design point for butane was mid-August and the design point for the 50%-50% mixture was in July.

across the expander, leading to a smaller power output.

The examination of these two individual losses is done for the evaporator in Table 5.1. To calculate each individual effect, first the total effect was calculated using the increased outlet pressure and the same degree of superheating to find the increased enthalpy at the inlet of the expander. Then, the effect of only the pressure drop was found by calculating how much the exergy destruction rate was reduced when only the pressure was increased. The effect of lowering the temperature difference was then assumed to be the difference between the total loss and the estimated impact of the pressure loss.

Since it is not clear how no pressure loss in the evaporator and condenser would affect the recuperator, it is difficult to perform this analysis on the condenser, which is downstream from the low pressure side recuperator. Therefore, only the total potential increased work is evaluated when pressure loss is eliminated from the condenser. This has been estimated by using the constant isentropic efficiency, and calculating the enthalpy at the expander outlet with the outlet pressure being equal to the condenser outlet pressure. Implicit in this estimation is that the pressure loss in the low-pressure stream of the recuperator is negligible, as Figure 5.2 shows.

Table 5.1: Influence of pressure drop in evaporator and condenser on cycle performance, for butane and the 50%-50% mixture.

	Butane	50%-50% mixture
Evaporator		
$\dot{I}_{evap}$ with P_{loss} (kW)	40.71	46.03
$\Delta\dot{I}$ due to increased $P_{evap,\,out}$ (kW)	0.91	1.24
$\Delta\dot{I}$ due to reduced ΔT (kW)	0.32	2.01
Total reduced $\dot{I}_{evap}$ with no P_{loss} (kW)	1.23	3.25
Condenser		
Increased $\dot{W}_{net}$ with no P_{loss} (kW)	3.90	5.92
Total increased $\dot{W}_{net}$ potential (kW)	5.13	9.17
$\dot{W}_{net}$ with P_{loss} (kW)	101.96	107.04
Relative potential for $\dot{W}_{net}$ increase (%)	5.03	8.57

From these estimates, it appears that the mixture is hindered more by pressure loss than the pure fluid. For the mixture, it is clear from the analysis of the evaporator in Table 5.1 that the largest deteriorating effect of the pressure loss is due to the increase in temperature difference. The benefit of using a mixture versus a pure fluid is that the temperature profile of the working fluid matches more closely with the heat source, and thus reduces the exergy loss. When this advantage is eroded, as with pressure loss, it is sensible that this effect is more pronounced with mixtures than with pure fluids.

While this analysis gives a glimpse at the potential for extra power output without pressure loss, it is limited in that it does not take into account other changes accompanied by pressure loss. For example, there is a positive correlation between pressure drop and the heat transfer coefficient, meaning that when the pressure drop is reduced, then so will the heat transfer coefficient. Additionally, the temperature differences that lead to exergy destruction in the heat exchanger also facilitate heat transfer rates, meaning that one would need larger heat exchangers to transfer the same amount of heat. It is therefore likely that the estimates in Table 5.1 exaggerate the increase in cycle performance. Because it is unclear exactly how neglecting pressure

drops will impact the performance of the entire cycle, it is conceivable that decreasing or removing pressure drop may in fact worsen the performance of the cycle. Finally, even if reduced pressure loss does lead to higher net power outputs of the cycle, this must be a result of other heat exchanger geometries that may be more expensive. It is therefore not clear if lowering pressure drop is economical even when it is thermodynamically beneficial.

5.2 Evaluation of the design point

5.2.1 Evaluating the chosen design point

In Section 4.1.1, a methodology for choosing a suitable design point was described. Having chosen a design point, it is important to evaluate this point and investigate whether there are other more suitable alternatives, and whether the assumptions employed when choosing a design point are true.

To evaluate whether the chosen design points is the most optimal, it is compared to the performance across the year with other design points. Naturally, the design point that provides the highest net power is the most optimal point, as this creates the highest value for the owner. The evaluation has only been done for butane and the 50%-50% mixture, to illuminate any potential differences between the design points for pure fluids and mixtures. Butane was chosen in favor of pentane, as this has consistently been the better-performing fluid. For butane, the alternative point that has been investigated is July, and for the mixture second point is mid-August. These points are chosen using the same methodology that has been previously described, as it is not entirely clear from Figure 4.1 alone whether the pressure ratios and mass flows of the previously chosen design point will lead to the highest yearly performance.

Figure 5.3 shows how the net power production varies with these designs points. The performance of the old design points has also been included to compare with the alternative design points.

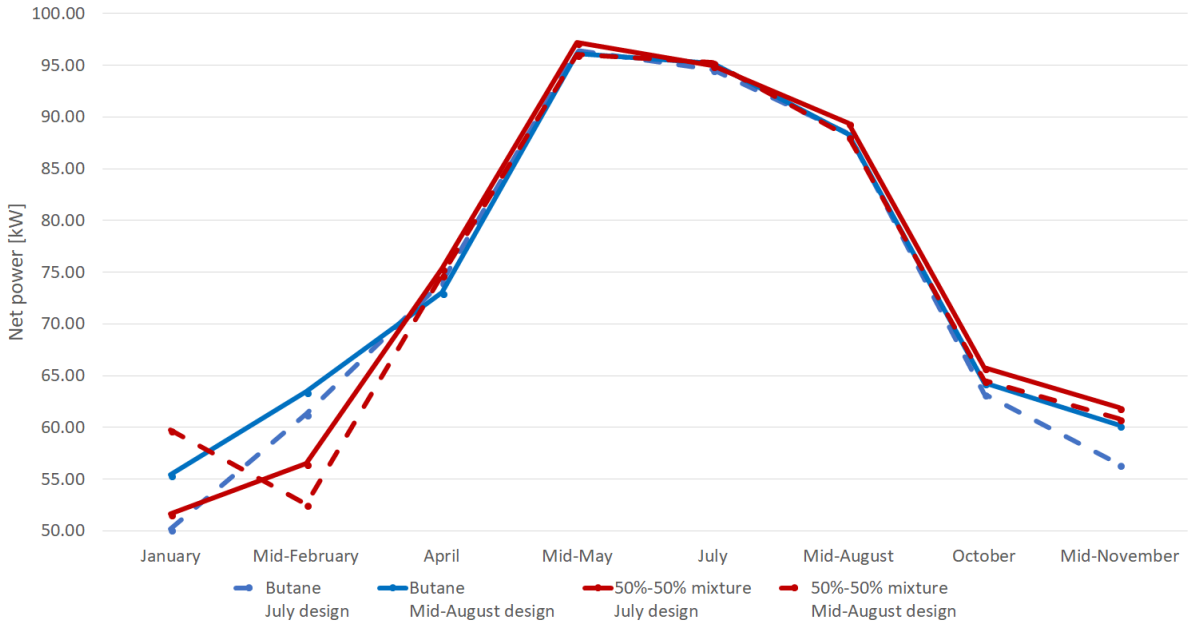

Figure 5.3: Net power developed for alternative design points with butane and 50%-50% mixture

The figure shows that there is not much difference in performance when choosing between these design points, and this is not entirely surprising as the design points are so close to one another. However, significant differences arise in the points at the beginning and end of the year. This is expected with the present model for the expander, where the differences should become more apparent the further away the off-design point is from the design point. The largest differences appear in January, and here Figure 5.3 shows that the alternative design point for the

50%-50% mixture outperforms the original design point, while the reverse is true for butane. In fact, the old design point for butane seems to outperform the alternative design point throughout the year, and so is obviously the better choice.

It is interesting to investigate why the alternative design point for the 50%-50% mixture is so much better than the original design point in January. With the assumption that the optimal pressure ratio and mass flow rate do not change much between on-design and off-design points, Figure 4.1c suggests that the expander performance would deteriorate somewhat, because the design mass flow rate in the alternative design point decreases. As Figure 3.4 shows, having the design mass flow be as large as possible is beneficial for the off-design performance of the expander, so when the flow rate at the design point is lowered, the expander efficiency at off-design points with low flow rates is reduced. The expander performance would also benefit a little because the new design pressure ratio is closer to the optimal pressure ratio in January, thereby reducing the performance loss due to pressure ratio mismatch. However, it seems that the decrease in design mass flow rate is relatively higher than the increase in pressure ratio, so one would expect that the net effect is a decrease of the turbine isentropic efficiency. This is also what is found in the results for the expander: the isentropic efficiency is 82.6% when the design point is in July, and 81.8% when the design is in mid-August. It therefore seems that the performance difference is not due to the expander performance change.

When changing the design point, it is important to remember that one has also rearranged the distribution of the available heat exchanger area. This redistribution will change the process parameters so that the energy balance is still preserved in each heat exchanger. Inspecting the temperature - entropy diagram and the data for the heat exchangers may offer some answers to why the performance of the mid-August design performs better, despite the lower expander efficiency. The temperature - entropy diagrams are plotted in Figure 5.4 for both designs.

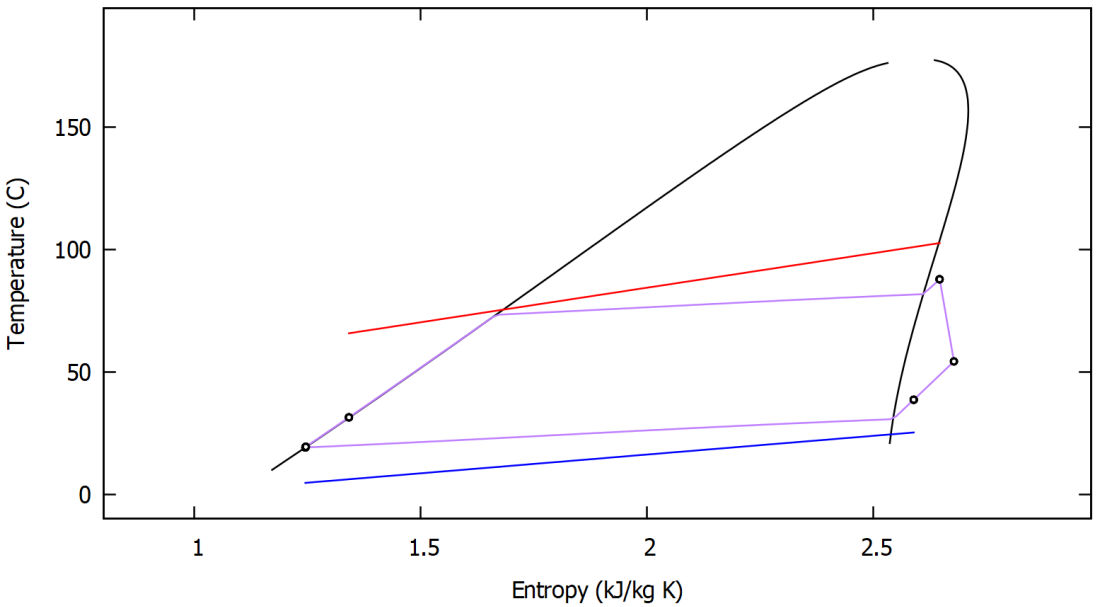

(a) Using July as the design point.

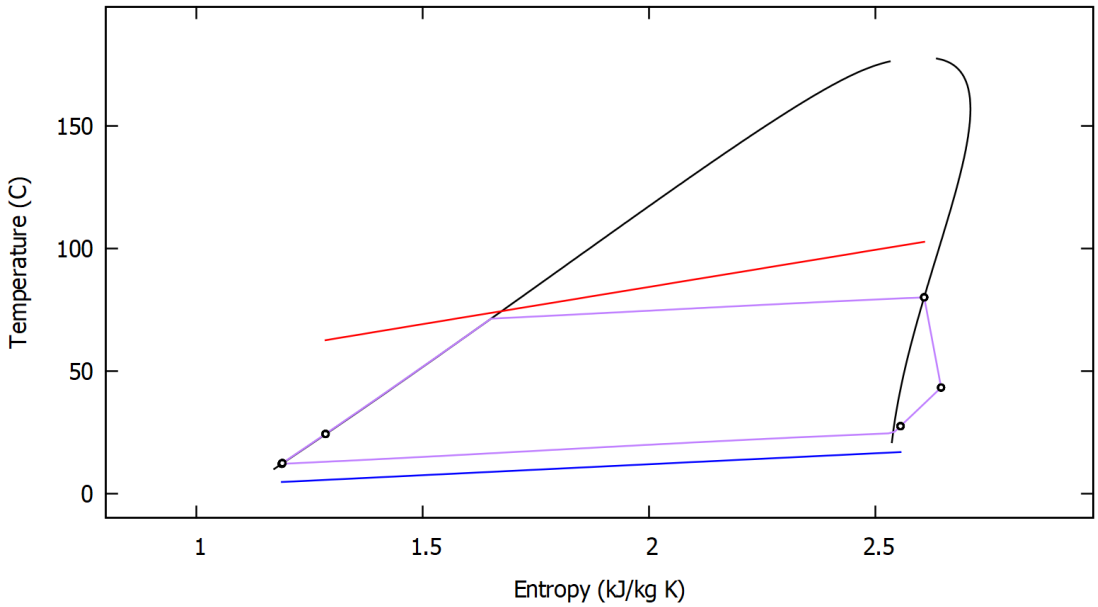

(b) Using mid-August as the design point.

Figure 5.4: Temperature - entropy diagram for the off-design performance of January using the 50%-50% mixture.

Inspecting the temperature - entropy diagrams illuminates several important characteristics that may explain the performance difference. One difference is how the design for July has superheating at the inlet of the exapnder, while the mid-August does not. Furthermore, the average temperature difference in the evaporator is smaller for the July design than for the mid-August design, which suggests that more area has been dedicated to the evaporator in this design. The numerical results from the simulation reaffirm this; while the area in the condenser is almost identical between the two designs, the design for mid-August has less area dedicated to the evaporator, and has instead increased the size of the recuperator. The effect of increasing the size of the recuperator is that the condenser has a smaller heat load, and since the condenser area

is the same as before, this leads to a smaller temperature difference in the condenser, as is clearly seen in Figure 5.4b. A smaller temperature difference in a heat exchanger is associated with reduced exergy destruction, and research by Heberle et al. (2012) has shown that reducing the irreversibilities in the condenser is particularly beneficial to the performance of the entire cycle. Moreover, superheating of the working fluid is associated with a performance degradation of the cycle. Combined, the effects lead to a higher performance for the alternative mid-August design in January than the original July design. This shows that in addition to the off-design performance of the expander, it is also important to consider the design of the heat exchangers.

Despite the higher performance in January when the design point is in mid-August, Figure 5.3 shows that the original July design outperforms the alternative in the other data points, leading to a better overall yearly performance, but only barely. Table 5.2 shows the different yearly electric energy outputs of the various design points for each working fluid.

Table 5.2: Comparison of estimated yearly electric energy output between using original and alternative design point

	Butane	50%-50% mixture
E_{el} at original design point[a] (MWh)	643.64	640.07
E_{el} at alternative design point[b] (MWh)	631.36	639.19
Performance decline (%)	1.91	0.14

[a] Recall that the original design point for butane is in mid-August, and for the mixture it is in July.
[b] Alternative design point for butane is in July, and for the mixture it is in mid-August.

For butane, the performance at the original design point seems to be significantly higher, so that it is favorable to keep the original design point. For the mixture, the results are nearly identical, and it is not clear whether the original case is truly better, or whether it is just a result of numerical noise in the optimizer. Using net power alone, it seems inconsequential to choose either design point for the mixture. However, these design points differ in the geometry of their heat exchangers, and the marginal costs between the different heat exchangers may differ significantly, ultimately favoring one design over the other.

5.2.2 Investigating cases of more net power in off-design mode than on-design mode

Looking at Figure 4.2, one can see that the off-design optimization sometimes outperforms the correspond on-design optimization. For example, investigating the result for butane, it appears that in April, July and October, the off-design optimization was significantly higher than the corresponding on-design optimization. How can that be? Presumably, the on-design optimization should always outperform the on-design optimization, because this optimization has fewer restrictions, allowing the optimizer to find a better result. It is important to analyze what causes these higher performances, as they may indicate that the on-design points are in fact sub-optimal, and that better designs exist for the investigated points. This would mean that the optimizer cannot be relied on to find optimal solutions.

To investigate the source what causes the increased performance in the off-design optimization, one must look at the details of each cycle and evaluate the differences independently. Therefore, Table 5.3 has been made which shows a few characteristics of the on-design and off-design cycles that are chosen as important to the performance of the system. The data point

which is investigated in detail is April, as this is where there is the largest difference of power output between the on-design and off-design optimizations.

Table 5.3: Comparison between parameters for on-design and off-design optimization for April using butane as working fluid

	On-design	Off-Design[a]	Percent difference
Pressure ratio across expander (-)	4.09	5.40	+ 32.1
Mass flow rate ($\frac{kg}{s}$)	1.57	1.49	- 5.6
Isentropic efficiency (%)	80.0	81.2	+ 1.5
Net work (kW)	70.9	73.0	+ 2.9

[a]Design conditions in this optimization were a pressure ratio of 4.32 and a mass flow of 2.12 $\frac{kg}{s}$

The power output of the expander is positively correlated with all of these parameters, and so one would expect the on-design optimization to benefit from the higher mass flow rate, but that the off-design optimization would be advantaged by the higher pressure ratio and isentropic efficiency. However, the interaction between the expander efficiency and the pressure ratio and mass flow rate in off-design optimization is not straight forward, as explained in Section 3.2.1. Table 5.3 shows that the net result of these parameters is that the isentropic efficiency of the expander in the off-design optimization is higher than in the on-design optimization. This will naturally affect the performance of the cycle. Using the same expander inlet conditions as in the on-design optimization, and having it expand to the same outlet pressure, a manual calculation shows that if the expander isentropic efficiency were 81.2%, as in the off-design result, then the expander output would increase with 1.21 kW, or 1.7%. This accounts for 57.9% of the discrepancy found in Figure 3.2.1 and Table 5.3.

The effect of a higher isentropic efficiency is further propagated through the rest of the cycle. For example, with the higher isentropic efficiency in the expander, the enthalpy of the stream at the outlet would be lower than before. This means that the recuperator does not need to extract as much heat on the low pressure side to reach the same conditions at the inlet of the condenser. This will free up some area that the optimizer can allocate to the other heat exchangers. It is unclear how the available area will be redistributed, and the effect of this on the various temperature differences, so instead of calculating a rough estimate, the optimizer is used to optimize a new on-design result, but where the on-design isentropic efficiency of the expander is increased to 81.2%. These results are shown in Table 5.4, and are compared with the off-design results.

Table 5.4: Result from new on-design optimization for butane in April with higher design expander isentropic efficiency

	New on-design	Off-design
Pressure ratio across expander (-)	4.80	5.40
Mass flow rate ($\frac{kg}{s}$)	1.62	1.49
Isentropic efficiency (%)	81.2	81.2
Net work (kW)	74.6	73.0

As Table 5.4 shows, with a higher expander design isentropic efficiency, the on-design result *will* be better than the off-design result at the same data point. These results reaffirm that the performance of the expander has a major role in the performance of the entire cycle. More importantly, they shows that the difference in performance between the on-design and off-design optimization found in Figure 4.2 are the result of unintuitive interactions between the expander isentropic efficiency and other cycle parameters, and not because of poor optimizations.

5.3 Investigating influence of WHRU temperature difference

In this work, it has been assumed that the temperature difference in the WHRU is constant at 17.5 K, which has been calculated using the results from the autumn project work. However, comparing the results from the project work and from this work for July – the period in which the heat source temperature specifications are the same between the this work and the project work – one will see that the net power output from the cycle with the 50%-50% mixture in this work is significantly lower than the corresponding cycle in the fall project work.

The discrepancy may partly be due to including pressure drop in this work, as the project work assumed no pressure drop in the heat exchangers. Another element that is different is how the present model uses correlations to calculate the heat transfer coefficient in a heat exchanger. In literature, such as in the study by Abadi and Kim (2017), it has been reported that mixtures may experience a degradation of the heat transfer coefficient compared to each of the pure fluids, and this has been reflected in the correlations employed in the model. In the project work, the heat transfer coefficients were set as constant and where the same for the mixtures and pure fluids, which may have unrealistically favored mixtures. This may explain why pure butane seems to be more effective in this work, compared to the optimal mixture from the project work. The effects of the pressure drop and the calculation of heat transfer coefficients both lead to differing results between this work and the project work. Another key element of the system is the WHRU. Because the model is unable to influence the performance of the WHRU, it is important to evaluate alternative temperature differences in this heat exchanger, to gain an understanding of how the entire cycle performs with other WHRU characteristics.

Increasing or decreasing ΔT_{WHRU} is implicitly describing changing the size of the WHRU, where one will achieve a lower temperature difference with a larger WHRU and vice versa. Changing the value of ΔT_{WHRU} impacts the maximum and minimum temperature of the indirect water loop which is modelled by the optimizer, but it changes both values equally. For example, decreasing ΔT_{WHRU} from 17.5 K to 10 K will increase both the inlet temperature of the water and its minimum temperature with 7.5 K. This means that the temperature glide of the water will remain the same, so the net effect is an increased increased temperature level for the cycle, but with the same heat content available in the indirect water loop. One has thereby only increased the exergy content available in the indirect water loop.

To investigate the effect of changing ΔT_{WHRU}, the off-design performances of butane and the 50%-50% mixture have been optimized, but with a high ΔT_{WHRU} of 25 K and a low of 10 K, thereby changing the temperature profile from the old constant temperature difference with $\pm$7.5 K. The design points for these optimizations are the same as the previous off-design optimization: mid-August for butane and July for the mixture. Figure 5.5 compares the performance of the cycle with the modified constant temperature differences with that of the cycle when ΔT_{WHRU} was 17.5 K.

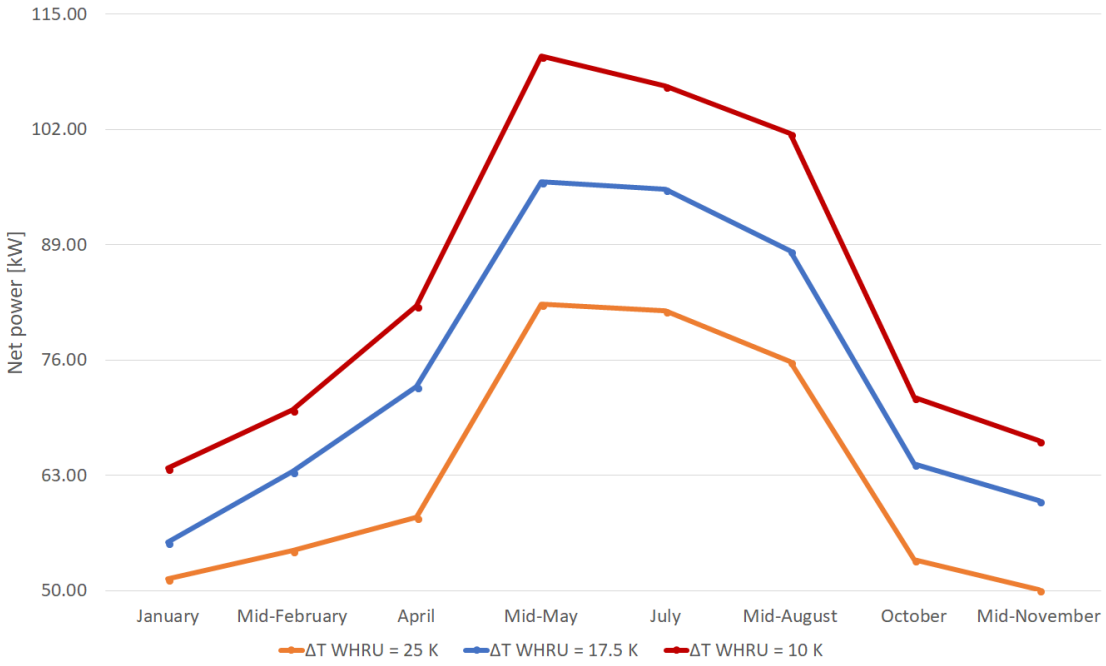

(a) Comparison for butane.

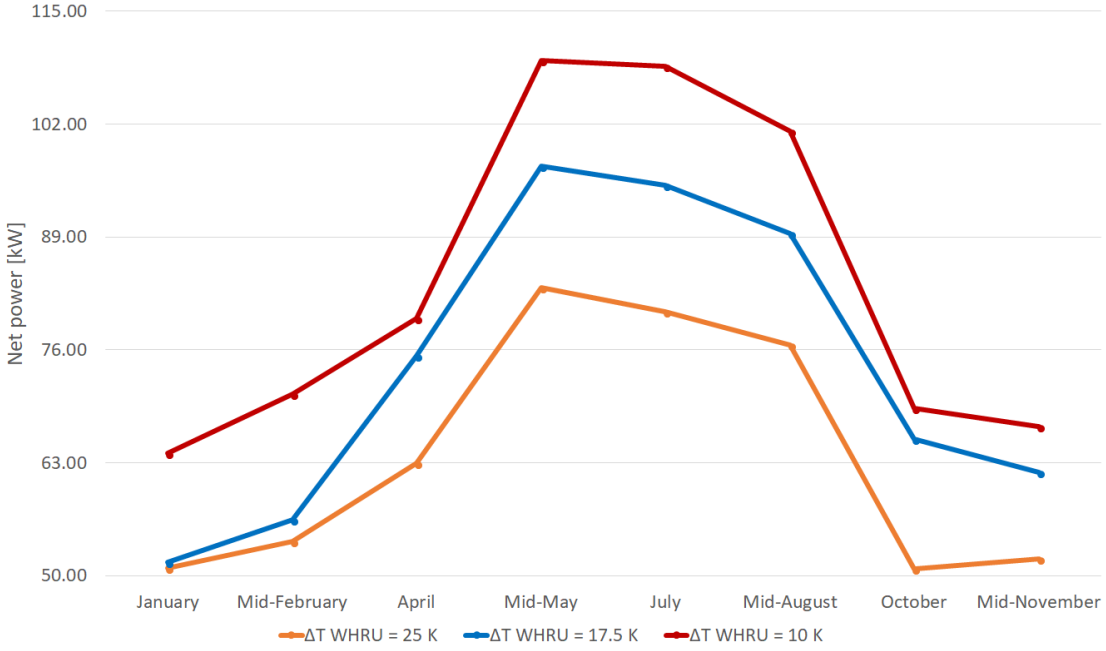

(b) Comparison for the 50%-50% mixture.

Figure 5.5: Comparison between performances of cycle with various ΔT_{WHRU}.

As Figures 5.5a and 5.5b show, the performance of the cycle increases with decreasing ΔT_{WHRU} while the shape of the performance curve across the year remains very similar. The performance increase is to be expected, as the main effect of decreasing ΔT_{WHRU} is to increase the exergy content in the indirect water loop. This increased exergy is subsequently transferred to the working fluid in the evaporator, raising the available exergy for the expander.

It is interesting to explore more precisely what changes as ΔT_{WHRU} is lowered. With this in

mind, the changes in exergy destruction has been investigated for each case in the design point of each fluid. Table 5.5 shows the the temperature characteristics of each fluid in their design month under the different ΔT_{WHRU}.

Table 5.5: Temperature data for the cycle with new WHRU temperature differences.

	Butane	50%-50% mixture
Flue gas inlet temperature (°C)	146.32	150.00
Flue gas minimum temperature (°C)	80.00	80.00
ΔT_{WHRU} = *25 K*		
Indirect water maximum temperature[a] (°C)	121.32	125
Indirect water minimum temperature (°C)	55.00	55.00
ΔT_{WHRU} = *17.5 K*		
Indirect water maximum temperature (°C)	128.82	132.50
Indirect water minimum temperature (°C)	62.50	62.50
ΔT_{WHRU} = *10 K*		
Indirect water maximum temperature (°C)	136.32	140.00
Indirect water minimum temperature (°C)	70.00	70.00

[a]Keep in mind that the value of the maximum water temperature is set, while the lower temperature is an inequality limit. As a result, there is the possibility that some exergy is left in the heat source stream.

Tables 5.6 and 5.7 examine the distribution of available exergy in the cycle for butane and the mixture respectively. Because the WHRU is not modelled in the optimizer, the outlet temperature of the flue gases have been calculated manually, so that the heat balance is preserved. The exergy performance of the WHRU is also evaluated using the calculated temperature profile, and assuming that the pressure in the exhaust gas stream is 1 bar.

Table 5.6: Exergy analysis for cycle using butane in mid-August, with different pinches in WHRU.

	ΔT_{WHRU} = 25 K	ΔT_{WHRU} = 17.5 K	ΔT_{WHRU} = 10 K
Unused $\dot{E}_{x,\,s}$ (kW)	25.0	1.0	0.3
$\dot{I}_{WHRU}$ (kW)	39.5	31.3	17.2
$\dot{I}_{evap}$ (kW)	32.8	40.7	38.6
$\dot{I}_{exp}$ (kW)	19.6	23.0	26.2
$\dot{I}_{recup}$ (kW)	0.8	0.9	1.7
$\dot{I}_{cond}$ (kW)	21.7	25.4	24.8
$\dot{I}_{pump}$ (kW)	1.1	1.3	1.7
$\dot{I}_{gen}$ (kW)	4.7	5.6	6.5
$\dot{E}_x$ to heat sink (kW)	18.5	20.7	19.9
Lossless $\dot{W}_{pump}$	5.1	6.6	7.7
Total $\dot{E}_x$ loss (kW)	169.5	157.6	145.4
$\dot{W}_{net}$ (kW)	75.9	88.3	101.6
η_{E_x} (%)	30.9	35.9	41.1
$\dot{E}_{x,\,tot}$	245.4	246.0	247.0
$\dot{E}_{x\,avail,\,Carnot}$	242.6	242.6	242.6
% Difference	1.1	1.4	1.8

Table 5.7: Exergy analysis for cycle using the 50%-50% mixture in July, with different pinches in WHRU.

	ΔT_{WHRU} = 25 K	ΔT_{WHRU} = 17.5 K	ΔT_{WHRU} = 10 K
Unused $\dot{E}_{x,\,s}$ (kW)	33.7	0.5	4.6
$\dot{I}_{WHRU}$ (kW)	33.2	32.8	17.0
$\dot{I}_{evap}$ (kW)	20.3	46.0	40.5
$\dot{I}_{exp}$ (kW)	20.3	25.0	28.3
$\dot{I}_{recup}$ (kW)	4.9	3.6	5.0
$\dot{I}_{cond}$ (kW)	21.6	23.9	24.5
$\dot{I}_{pump}$ (kW)	0.7	0.8	1.1
$\dot{I}_{gen}$ (kW)	4.7	5.6	6.5
$\dot{E}_x$ to heat sink (kW)	18.6	23.5	20.5
Lossless $\dot{W}_{pump}$	5.1	4.3	4.8
Total $\dot{E}_x$ loss (kW)	180.8	166.8	153.7
$\dot{W}_{net}$ (kW)	80.4	95.0	108.7
η_{E_x} (%)	30.8	36.3	41.4
$\dot{E}_{x,\,tot}$	261.2	261.8	262.4
$\dot{E}_{x\,avail,\,Carnot}$	259.3	259.3	259.3
% Difference	0.7	1.0	1.2

The results show that the main benefit of decreasing ΔT_{WHRU} is to reduce the losses in this heat exchanger, which is a consequence of the reduced temperature difference. When $\Delta T_{WHRU} = 25$ K, there is a lot of exergy left in the heat source that goes unused in the cycle for both fluids. This is a result of the optimizer finding a solution where the the low temperature of the indirect water loop does not reach the limit of 55°C, but instead it reaches 63.7°C and 66.5°C for butane and the mixture respectively. The optimizer is unable to find a better solution in which the minimum temperature of the indirect water is closer to its limit, while still maintaining the energy balance and avoiding temperature crossing in the evaporator. Figure 5.6 shows the temperature glide of the indirect water loop, and what it would have been, had it reached its minimum temperature constraint.

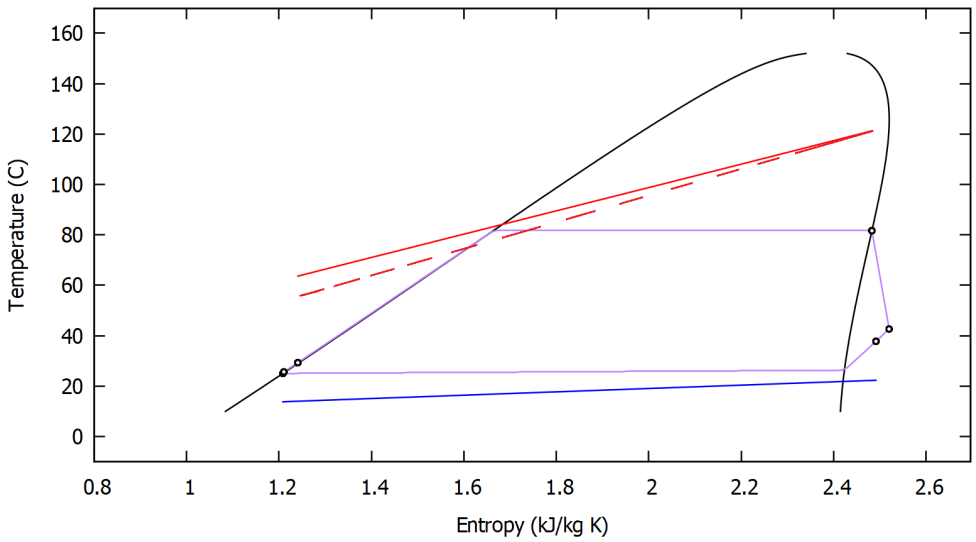

Figure 5.6: Temperature - entropy diagram of a cycle with butane for ΔT_{WHRU}=25 K. Dashed red line represents temperature of indirect water loop if the minimum temperature constraint had been reached.

From Figure 5.6, it is clear that to reach the lower temperature limit of the indirect water, the pressure in the evaporator would have to be reduced. With the reduced pressure at the expander inlet, and therefore a reduced pressure ratio across it, it is unlikely that this would lead to higher net work of the cycle. Thus it is favorable to not utilize all of the available exergy. This problem is avoided when ΔT_{WHRU} is lower, as the temperature curve for the indirect water is shifted upward. This allows the optimizer to fully utilize the available exergy in the heat source.

While it is clearly thermodynamically advantageous to lower ΔT_{WHRU}, it is not certain whether this is always economical. For example, inspecting Table 5.6, it can be seen that by lowering ΔT_{WHRU} from 17.5 K to 10 K, the exergy efficiency of the cycle increases from 35.9% to 41.1%, a relative increase of 14.5%. Assuming that the overall heat transfer coefficient in the WHRU is 100 $\frac{W}{m^2 \times K}$, this would require increasing the heat exchange area of the WHRU from roughly 550 m^2 to 930 m^2, a relative increase of 70%. This may be too costly in terms of capital or even volume, as WHRUs are known to be large to begin with.

The previous analysis has investigated the effect of having different constant ΔT_{WHRU}, but a real cycle may not operate such that this is the case. The results for the WHRU in the project work did not have a constant ΔT_{WHRU}. Instead, the temperature difference at the cold side of the WHRU was much smaller than at the hot side, and the mass flow was significantly higher to uphold the energy balance. Inspecting Figure 5.7, which is the temperature - entropy diagram for the on-design optimization of the mixture in July with constant ΔT_{WHRU} = 17.5 K, one can deduce some advantages with using a different temperature profile for the indirect water loop. With a higher temperature at the cold end, and a lower temperature at the hot end, the gradient of the temperature curve for the indirect water is smaller. This may allow for a higher pressure in the evaporator. Had the WHRU been a part of the model, the optimizer could vary these parameters itself, but since this is not the case, this must be evaluated manually.

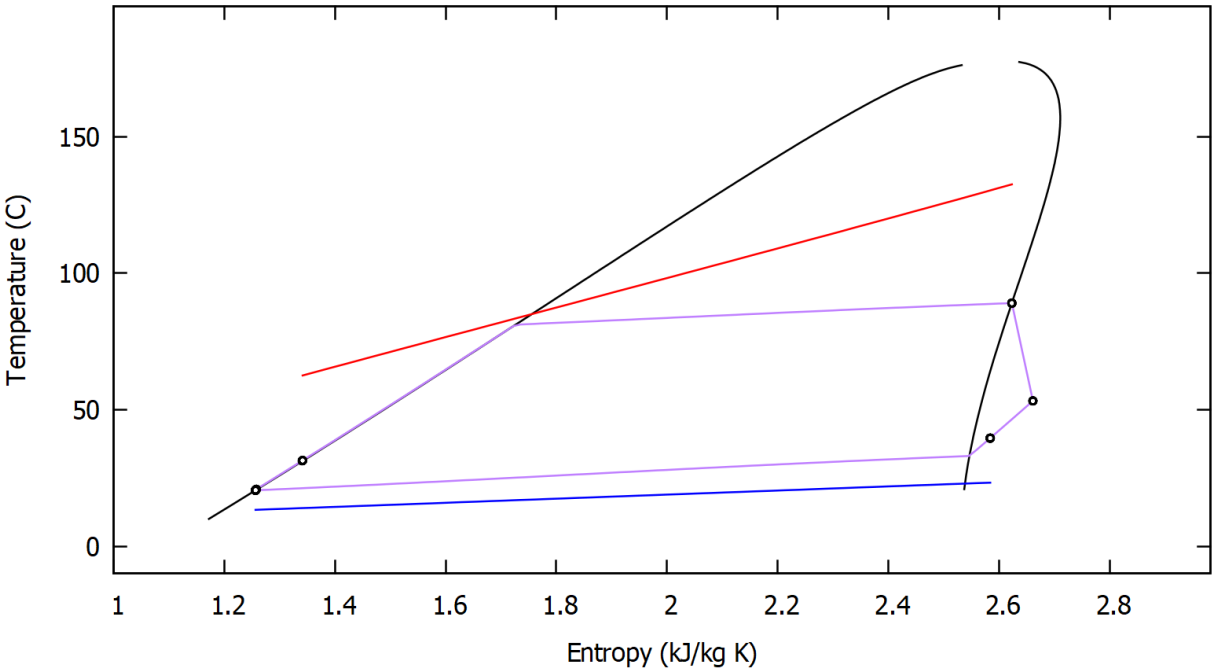

Figure 5.7: Temperature - entropy diagram for the on-design optimization for the 50%-50% mixture in July, with ΔT_{WHRU} = 17.5 K

The performance of a system in which the temperature difference in the WHRU is non-constant has been evaluated for the mixture. The optimized data for the indirect loop from the project work have been used, and are displayed in Table 5.8. The analysis is done for the data point in July, as this is where the heat source temperatures match between this work and the project work. Table 5.8 shows that the LMTD in the WHRU with these temperature characteristics is 18.93 K, and so the results are compared with the case where $\Delta T_{WHRU} = 17.5$ K , as these are so similar.

Table 5.8: Temperature specifications in the WHRU for a non-constant ΔT_{WHRU}

	Non-constant ΔT_{WHRU} temperature details
Flue gas inlet temperature (°C)	150.00
Flue gas minimum temperature (°C)	89.9
Indirect water maximum temperature (°C)	117.58
Indirect water minimum temperature (°C)	80.08
LMTD in WHRU (K)	18.93

Using the present optimizer to evaluate the performance of such a cycle shows that this cycle produces 92.2 kW of power, compared to 95.0 of the cycle with a constant 17.5 K temperature difference. Table 5.9 shows the distribution of exergy for the cycle with a non-constant ΔT_{WHRU} and the cycle with a constant $\Delta T_{WHRU} = 17.5$ K. Additionally, because the cycle with non-constant ΔT_{WHRU} does not utilize all the available heat in the heat source – as the cycle with a constant ΔT_{WHRU} almost does – a third column is included to show the performance of the former cycle had it used all the available heat. This has assumed that the extra exergy has been distributed to the other entries in the table in such a way that their proportion relative to their sum remains the same.

Table 5.9: Exergy analysis for cycle using the 50%-50% mixture, comparing the constant 17.5 K temperature difference with a non-constant temperature profile. (Estimate of performance with no unused exergy in shaded table entries.)

	ΔT_{WHRU} = NC	ΔT_{WHRU} = 17.5 K	Scaled ΔT_{WHRU} = NC
Unused $\dot{E}_{x,\,s}$ (kW)	28.6	0.5	0.0
$\dot{I}_{WHRU}$ (kW)	33.2	32.8	37.3[a]
$\dot{I}_{evap}$ (kW)	32.2	46.0	36.2
$\dot{I}_{exp}$ (kW)	24.2	25.0	27.2
$\dot{I}_{recup}$ (kW)	4.3	3.6	4.8
$\dot{I}_{cond}$ (kW)	17.3	23.9	19.5
$\dot{I}_{pump}$ (kW)	1.6	1.6	1.8
$\dot{I}_{gen}$ (kW)	5.5	5.6	6.1
$\dot{E}_x$ to heat sink (kW)	18.8	23.5	21.1
Lossless $\dot{W}_{pump}$ (kW)	4.1	4.3	4.6
Total $\dot{E}_x$ loss (kW)	169.7	166.8	158.6
$\dot{W}_{net}$ (kW)	92.2	95.0	103.6
η_{E_x} (%)	35.2	36.3	39.5
$\dot{E}_{x,\,tot}$	261.9	261.8	261.9
$\dot{E}_{x\,avail,\,Carnot}$	259.3	259.3	259.3
% Difference	1.0	1.0	1.0

[a]This number is likely very erroneous. If the flue gases were cooled to 80°C, the temperature difference in the cold end of the WHRU would be 0.15 K, down from 10.05 K. This decrease in temperature difference would most likely lower the irreversibility in the WHRU, not increase it.

Comparing the cycle performance when ΔT_{WHRU} is non-constant, what is immediately clear is that this cycle is not able to extract all the available exergy in the heat source. This is however somewhat offset by a much lower exergy destruction rate in the evaporator. This lower irreversibility rate is to be expected, as the temperature change from the hot end to the cold end for the indirect water loop is much smaller. This means that the temperature profile of the working fluid matches that of the working fluid much better. While the temperature difference increases somewhat on the cold end, this increase is smaller than the reduction on the hot end, resulting in the LMTD being lowered from 36.95 K to 31.82 K.

The estimate for the performance of the cycle with non-constant ΔT_{WHRU} and with no unused exergy shows that having a smaller gradient on the temperature profile of the indirect water loop may be beneficial, if it is able to extract all the available heat from the heat source. To extract the remaining exergy for the system with a non-constant temperature difference in the WHRU, one would most likely need larger heat exchange areas.

The values that were approximated in Table 5.9 most likely overestimate the potential of a system with this temperature profile for the indirect water loop. This is because the minimum temperature of this loop is 79.85°C, which is barely lower than 80°C, the minimum allowable temperature of the exhaust gas. It is therefore likely that the minimum temperature of the indirect water loop would have to be lower than what is specified in this estimate. Despite the limitations of the estimation, this analysis still shows that having a non-constant temperature profile may lead to performance improvements of the cycle, primarily by eliminating irreversibilities in the evaporator, and allowing the working fluid to reach a higher pressure level in the evaporator.

5.4 Performance impact of district heating

It natural to imagine that the district heating requirement worsens the performance of the organic Rankine cycle in this work. Figure 3.7 shows how much of the available energy that district heating uses, but it is challenging to judge just how large this impact is from Figure 3.7 alone. A more helpful measure to investigate is the amount of exergy that the district heating siphons from the power generating cycle. As explained in section 3.1, the heat for the district heating is extracted upstream of the ORC, and so it utilizes the high-temperature region of the available heat. Figure 5.8 shows how much of available exergy is taken by district heating for each period. Comparing with Figure 3.7, one can see that the exergy content in the heat source is significantly lower than the energy content, where roughly only a quarter of the total available total heat can be converted to work. Additionally, because the exergy is primarily concentrated in the high-temperature part of the flow, the energy extracted for district heating uses a higher share of the available exergy than it does of the available energy. This further worsens the performance during the colder months.

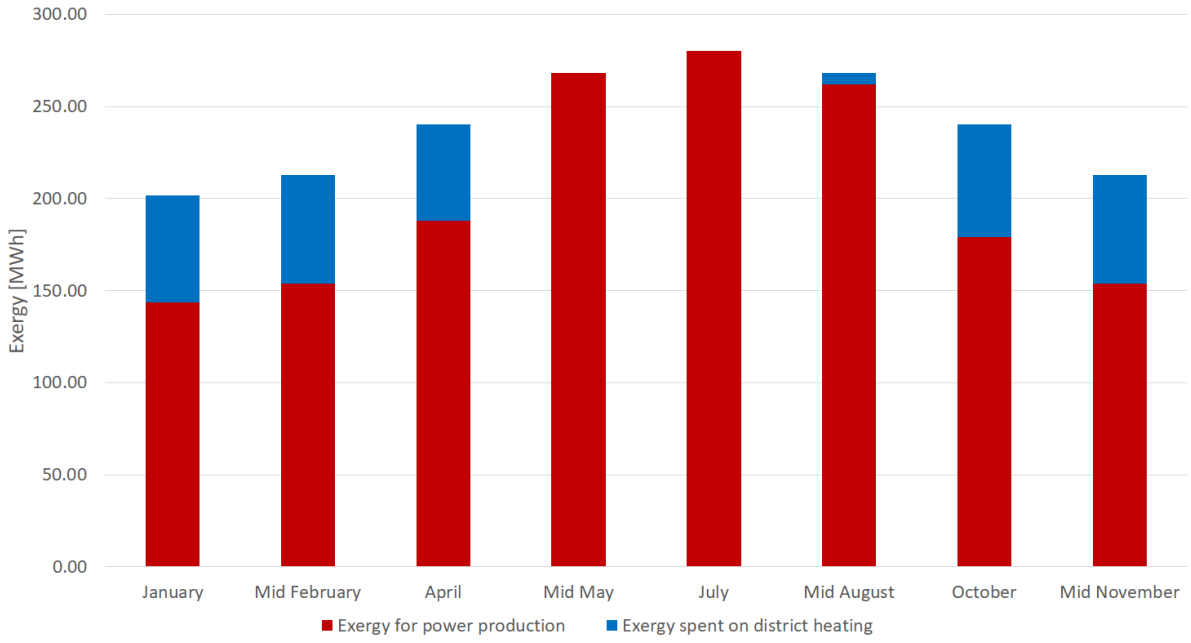

Figure 5.8: Distribution of available exergy.

Having simulated the off-design fluctuation in power production without district heating, it is possible to compare the cycle performance and other parameters between when district heating is present and when it is not. The off-design optimization without district heating has only been done for butane and the 50%-50% mixture in this work. With the same design points as in Chapter 4, the net power output increases when district heating is neglected. Tables 5.10 and 5.11 show the yearly output of net power and district heating – when the latter is included – for butane and the 50%-50% mixture, respectively.

Table 5.10: Comparison of performance between cycle with and without district heating for butane.

	With district heating		Without district heating	
Period	E_{el}	E_{DH}	E_{el}	E_{el} Increase
(-)	(MWh)	(MWh)	(MWh)	(%)
January to mid-February	64.19	198.75	86.09	34.1
Mid-February to April	73.68	198.75	91.85	24.7
April to mid-May	91.31	168.75	97.18	6.4
Mid-May to July	103.31	0.00	103.31	0.0
July to mid-August	99.45	0.00	99.45	0.0
Mid-August to October	82.40	18.75	91.78	11.4
October to mid-November	67.21	198.75	87.80	30.6
Mid-November to January	62.42	198.75	85.95	37.7
Total	643.64	982.5	741.06	15.1
Total E (MWh)	1626.14		741.06	

Table 5.11: Comparison of performance between cycle with and without district heating for the 50%-50% mixture.

	With district heating		Without district heating	
Period	E_{el}	E_{DH}	E_{el}	E_{el} Increase
(-)	(MWh)	(MWh)	(MWh)	(%)
January to mid-February	58.37	198.75	89.09	52.6
Mid-February to April	71.18	198.75	94.92	33.4
April to mid-May	93.17	168.75	102.60	10.1
Mid-May to July	103.77	0	103.77	0.0
July to mid-August	99.57	0	99.35	0.0
Mid-August to October	83.79	18.75	94.57	12.7
October to mid-November	68.93	198.75	90.61	31.4
Mid-November to January	61.30	198.75	88.52	44.4
Total	640.08	982.5	763.29	19.3
Total E (MWh)	1622.58		763.29	

Because the prices for the electricity and district heat fluctuate significantly and are not readily available, it is difficult to conclusively decide whether to include a system for district heating when designing a new process. Despite this limitation, it is still possible to make some more general observations from the data in the two preceding tables. For butane, the case without district heating produces 15.1% more power, but when district heating is included, much more energy is exported. One would expect that the price for electricity is higher than for district heating, but including district heating may still be profitable simply because the amount of additional energy that the owner can sell. In fact, using the data in Table 5.10, it is calculated that the price for the district heat would have to be less than roughly 10% of the price for electricity for the case without district heating to become profitable. One must also consider that the equipment for the district heating is an additional investment cost when building the entire system, potentially increasing the time to break-even for the owner. This again depends on the price of the various equipment and the price of the heat sold.

Moreover, even if the price of the thermal energy in the district heating loop were that low

compared to the price of electricity, it may still be beneficial to export district heating. As Tables 5.10 and 5.11 show, more energy is exported to be used outside the facility. Also, it seems wasteful to use electricity for heat when one could use district heating instead. Because district heating exports so much heat, and it reduces the use of electricity for heating, it seems more environmentally friendly to have district heating.

What should also be considered are other designs for extracting the district heating and simultaneously producing power. It seems wasteful to use the high temperature heat on district heating, as this is better utilized in the ORC. At the same time, the district heating has a minimum temperature at which it has to leave the facility, so it cannot be heated using whatever heat is left after the exhaust gasses have passed the WHRU for the ORC. It therefore seems reasonable that a system where the high and low ends of the temperature range is used for power production, where the medium temperature region is used for district heating. This allows the system to take advantage of the high temperature heat, while still meeting the temperature requirements of the district heating system.

One example of such a system is one in which there are two separate Rankine cycles, each designed specifically for either the high-temperature heat or for the low temperature heat, with the district heating utilizing the temperature range between these cycles. While relatively high efficiencies can be reached with this approach, it is most likely very costly, as one would need two evaporators, condensers, expanders and pumps, as well as the recuperators if these are included. Another option is to have only one Rankine cycle which is heated by both the low temperature and high temperature sections of the heat source. This can also be solved in more than one way. One way may be using two turbines and reheating the working fluid between each turbine stage. Another design may be using two pumps instead, where the working fluid is heated at two separate pressure levels, before being expanded in a single stage. This design may require a separator to avoid two phase flow in the second pump, in case the working fluid starts to evaporate during the first heating stage. The simplest design may be to just have the flow evaporate at one pressure level, but in two heat exchangers, that are connected by a well insulated pipe. Such a system may be difficult to control if the working fluid is heated directly. If one uses an indirect design instead, where the indirect loop is heated by the two temperature regions of the heat source, which subsequently heats the ORC in a single evaporator, then one can operate with higher stability in the Rankine cycle. It would be interesting to evaluate and compare these designs with the design used in this work, but unfortunately the optimizer only has the capability to model the elementary Rankine cycle, and so none of these suggestions can be quantitatively evaluated. If the operator of a similar facility has a similar case to the one described here, then it may be worthwhile to investigate the options described here to increase the efficiency and profitability of the system.

5.5 Investigating effect of increased heat source temperatures and heat exchanger area

For the operator of an aluminum plant, it is possible to increase the temperature of the flue gases while maintaining the same heat content with reference to the ambient conditions. This is because in an aluminum plant, the high temperature flue gases leaving the cells are immediately mixed with some ambient air, before passing them further downstream the system. The temperature of the flue gases is increased by reducing the amount of air that is mixed with the flue gases, but the mass flow simultaneously decreases. This maintains the same heat content in the flue gas stream, but increases the exergy available for power production. In this section, the performance benefits of increasing the temperature of the flue gases are considered. Additionally, the effect of increasing the total allowable heat exchanger area is also investigated, both with the normal and increased temperature of the flue gas.

Table 5.12 shows the difference between the investigated cases in this section. A_{tot} refers to the total area employed by the evaporator, recuperator and condenser, as the WHRU is not modelled in the optimizer. However, as these three heat exchangers can use more area, it is reasonable that the WHRU will also have its heat exchange area increased to improve performance, so ΔT_{WHRU} is lowered to 10 K in the high area cases. As calculated in Section 5.3, this would correspond to a 70% increase in area for this heat exchanger. This relative increase is much higher than the relative increase for the cumulative heat exchanger areas for the other heat exchangers, but it is chosen as working with a 10 K temperature difference is easier in the model. The mass flow rates of the heat source and indirect water have been modified in the high temperature cases to maintain the same heat content relative to the ambient.

Table 5.12: System parameters in increasing the heat exchange area and heat source temperature

	Normal	High T_s	High area	High area and T_s
A_{tot} (m^2)	230	230	300	300
T_s (°C)	150	180	150	180
ΔT_{WHRU} (K)	17.5	17.5	10.0	10.0
$\dot{m}_{indirect}$ ($\frac{kg}{s}$)	3.275	2.631	3.275	2.631
$\dot{m}_s$ ($\frac{kg}{s}$)	13.614	11.198	13.614	11.198

Figure 5.9 shows the exergy efficiency of each of these cases. For the normal case, each point has been simulated, whereas only the design point[2] has been simulated for the other three cases. To find the other points, the ratio of exergy efficiency at design point for a given case to the normal case is calculated, and this ratio is multiplied to all the other points in the year. For example, for butane at the design point it was found that the exergy efficiency in the high temperature case was 8.8% higher than in the normal case. Therefore, the other data points for the high temperature case are 8.8% higher relative to the corresponding data point for the normal case. This is the reason that the shape of the other cases match that of the normal case so closely. The lines for the non-normal cases in Figure 5.9 are dashed to illustrate that they are estimates, and not simulated results.

[2]Design points: mid-August for butane and July for the mixture.

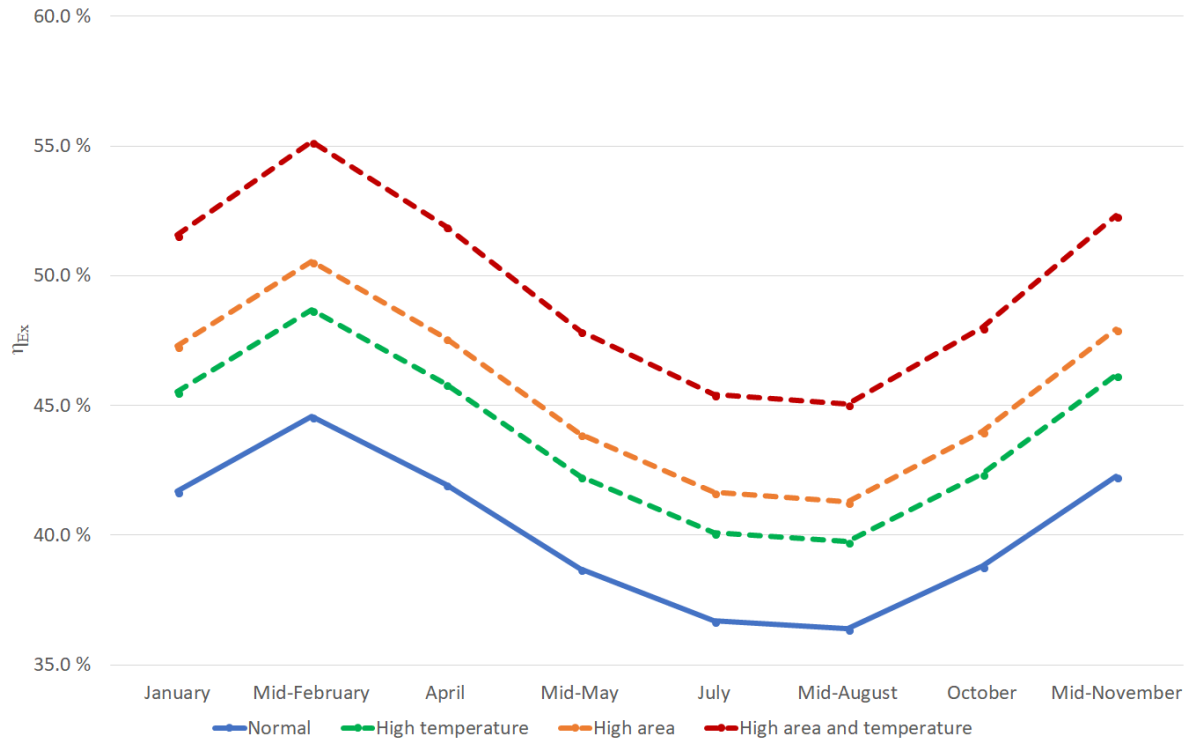

(a) Cycle using butane.

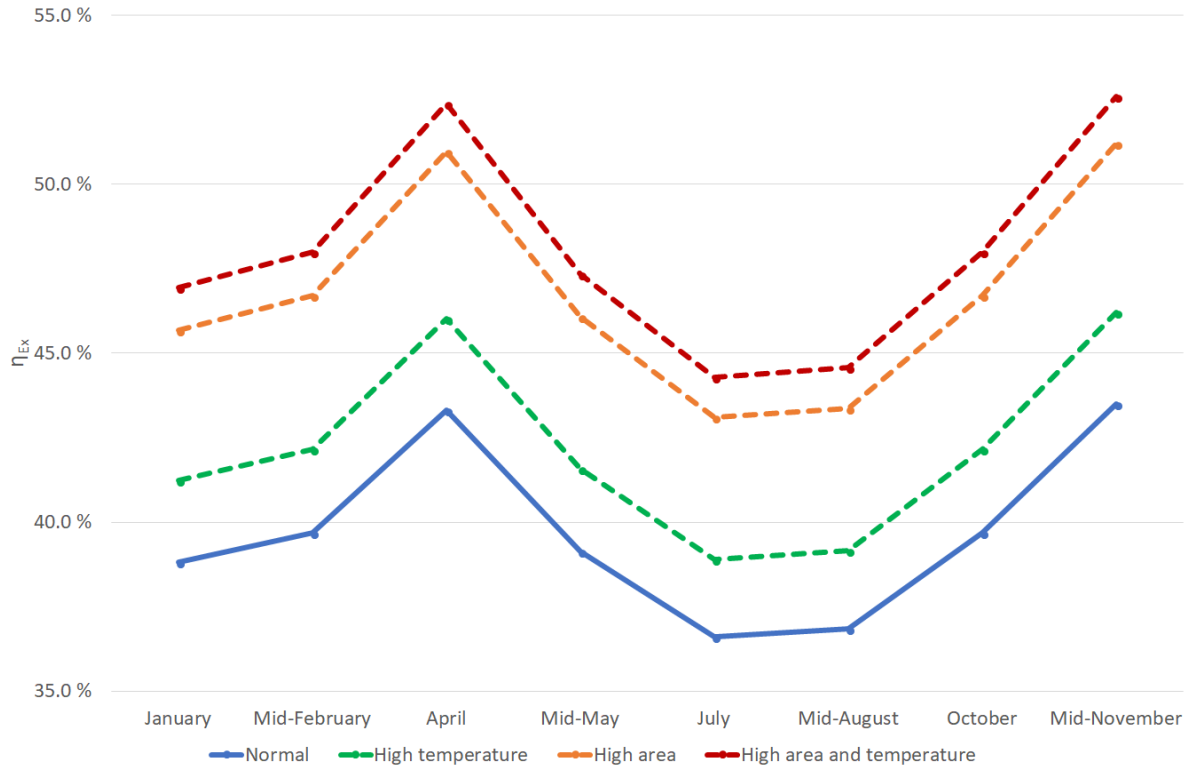

(b) Cycle using the mixture.

Figure 5.9: Exergy efficiency of the cycle under normal optimization, with higher temperature, with higher area and with higher area and temperature. (Dashed lines for estimates.)

The results show that the exergy efficiency of the cycle increases as the heat source temperature and the heat exchanger area increase. The largest gain is naturally found when both are increased simultaneously, and the next best improvement is found by increasing area, followed by increasing the temperature. This is true for both fluids. Curiously, the exergy efficiency seems to increase for the colder months. To investigate why this occurs, Table 5.13 has been constructed, which shows how the exergy available in the heat source is distributed for the points of maximum exergy efficiency for each fluid. This analysis has been done only for when the heat source inlet temperature and area have their normal values, as there are simulation data only for these parameter settings. Compare the values in Table 5.13 with those found in the design point for each fluid, found in Table 5.14.

Table 5.13: Exergy analysis in the maximum exergy efficiency points for butane and the 50%-50% mixture. (Percent relative to total used exergy in parentheses.)

	Butane in mid-February		Mixture in April	
Unused $\dot{E}_{x,\,s}$ (kW) (% of $\dot{E}_{x,\,tot}$)	0.3	(0.2)	0.1	(0.0)
$\dot{I}_{WHRU}$ (kW) (% of $\dot{E}_{x,\,tot}$)	21.7	(15.1)	25.3	(14.4)
$\dot{I}_{evap}$ (kW) (% of $\dot{E}_{x,\,tot}$)	20.7	(14.4)	27.2	(15.5)
$\dot{I}_{exp}$ (kW) (% of $\dot{E}_{x,\,tot}$)	14.4	(10.0)	18.6	(10.6)
$\dot{I}_{recup}$ (kW) (% of $\dot{E}_{x,\,tot}$)	2.5	(1.8)	2.6	(1.5)
$\dot{I}_{cond}$ (kW) (% of $\dot{E}_{x,\,tot}$)	18.3	(12.7)	17.6	(10.0)
$\dot{I}_{pump}$ (kW) (% of $\dot{E}_{x,\,tot}$)	1.3	(0.9)	1.1	(0.6)
$\dot{I}_{gen}$ (kW) (% of $\dot{E}_{x,\,tot}$)	3.8	(2.7)	4.3	(2.5)
$\dot{E}_x$ to heat sink (kW)	-5.8[a]	(-4.1)	0.3	(0.2)
Lossless $\dot{W}_{pump}$ (kW) (% of $\dot{E}_{x,\,tot}$)	3.1	(2.1)	2.8	(1.6)
Total $\dot{E}_x$ loss (kW) (% of $\dot{E}_{x,\,tot}$)	80.4	(55.9)	100.0	(57.0)
$\dot{W}_{net}$ (kW)	63.4		75.3	
η_{E_x} (%)	44.1		43.0	
$\dot{E}_{x,\,tot}$ (kW)	143.81		175.3	
$\dot{E}_{x\,avail,\,Carnot}$ (kW)	142.35		174.0	
% Difference	1.02		0.8	

[a]The reason for the negative exergy increase in the heat sink is due to the ambient being set to 10°C. In this month, the ambient water arrives in the condenser at 4.17°C, and is heated to 11.6°C. Because the difference from the reference point is decreased, there is a net loss of exergy for the heat sink.

Table 5.14: Exergy analysis of the design points for butane and the 50%-50% mixture. (Percent relative to total used exergy in parentheses.)

	Butane in mid-August		Mixture in July	
Unused $\dot{E}_{x,\,s}$ (kW) (% of $\dot{E}_{x,\,tot}$)	1.0	(0.4)	0.4	(0.2)
$\dot{I}_{WHRU}$ (kW) (% of $\dot{E}_{x,\,tot}$)	31.3	(12.7)	32.8	(12.5)
$\dot{I}_{evap}$ (kW) (% of $\dot{E}_{x,\,tot}$)	40.7	(16.5)	46.0	(17.6)
$\dot{I}_{exp}$ (kW) (% of $\dot{E}_{x,\,tot}$)	23.0	(9.3)	25.0	(9.5)
$\dot{I}_{recup}$ (kW) (% of $\dot{E}_{x,\,tot}$)	0.9	(0.4)	3.6	(1.4)
$\dot{I}_{cond}$ (kW) (% of $\dot{E}_{x,\,tot}$)	25.4	(10.3)	23.9	(9.1)
$\dot{I}_{pump}$ (kW) (% of $\dot{E}_{x,\,tot}$)	2.5	(1.0)	1.6	(0.6)
$\dot{I}_{gen}$ (kW) (% of $\dot{E}_{x,\,tot}$)	5.6	(2.3)	5.6	(2.2)
$\dot{E}_x$ to heat sink (kW) (% of $\dot{E}_{x,\,tot}$)	20.7	(8.4)	23.5	(9.0)
Lossless $\dot{W}_{pump}$ (kW) (% of $\dot{E}_{x,\,tot}$)	6.6	(2.7)	4.3	(1.7)
Total $\dot{E}_x$ loss (kW) (% of $\dot{E}_{x,\,tot}$)	157.6	(64.1)	166.8	(63.7)
$\dot{W}_{net}$ (kW)	88.3		95.0	
η_{E_x} (%)	35.9		36.3	
$\dot{E}_{x,\,tot}$ (kW)	246.0		261.8	
$\dot{E}_{x\,avail,\,Carnot}$ (kW)	242.6		259.3	
% Difference	1.4		1.0	

Comparing the relative values, what is clear is that in the colder months, much less of the relative exergy leaves the system through the heat sink. This is likely a result of the choice of base state for the exergy calculations; because the heat sink starts at below the base temperature, the increase in temperature leads to an exergy reduction in this stream, rather than an increase. Consequently, the calculated exergy loss to the heat sink is much lower during the colder months compared to the design months. This leads to a misleading exergy efficiency increase, where it seems the cycle performs much better during these months. However, the cycle does operate more efficiently in these months, as seen when investigating the first law efficiency of the system. This is done in Table 5.15, below:

Table 5.15: Comparing the first law efficiency of the cycle in the best efficiency off-design point with the design point for butane and the 50%-50% mixture

	Butane		Mixture	
	Mid-February	Mid-August	April	July
$\dot{E}_{t,\,avail}$ (kW)	585.9	914.6	694.3	965.5
$\dot{W}_{net}$ (kW)	63.4	88.3	75.3	95.0
η_t (%)	10.8	9.7	10.9	9.8

This shows that the effect of losing less exergy to the heat sink is significant, if somewhat exaggerated in Table 5.13. Because the temperature in the heat sink is so low to start with, the cycle is able to expand the working fluid to a lower pressure, increasing the net power output. Moreover, the relative irreversibility in the evaporator has also decreased for the colder months, likely because of an oversized evaporator.

A similar exergy analysis can be applied to the high temperature and high area cases as well. Figure 5.10 is made to show how the available exergy in each case is distributed, for both butane and the mixture. This is done for the respective fluid's design month, as this is where the simulation results are available.

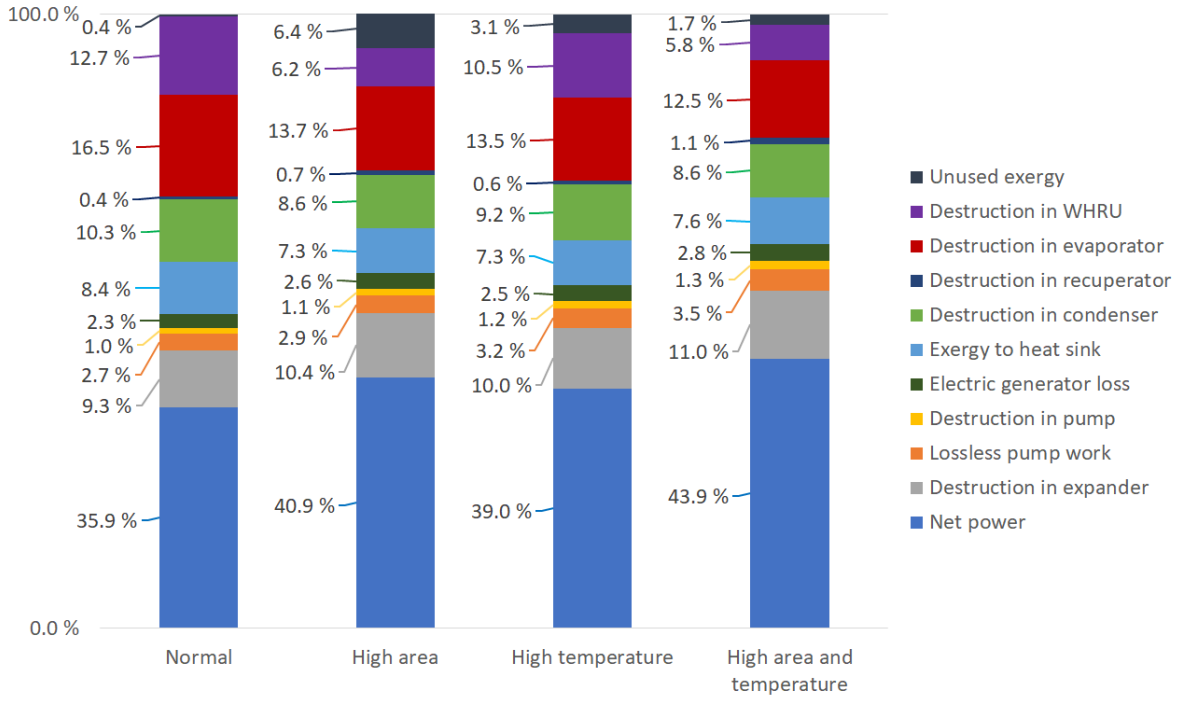

(a) Cycle using butane.

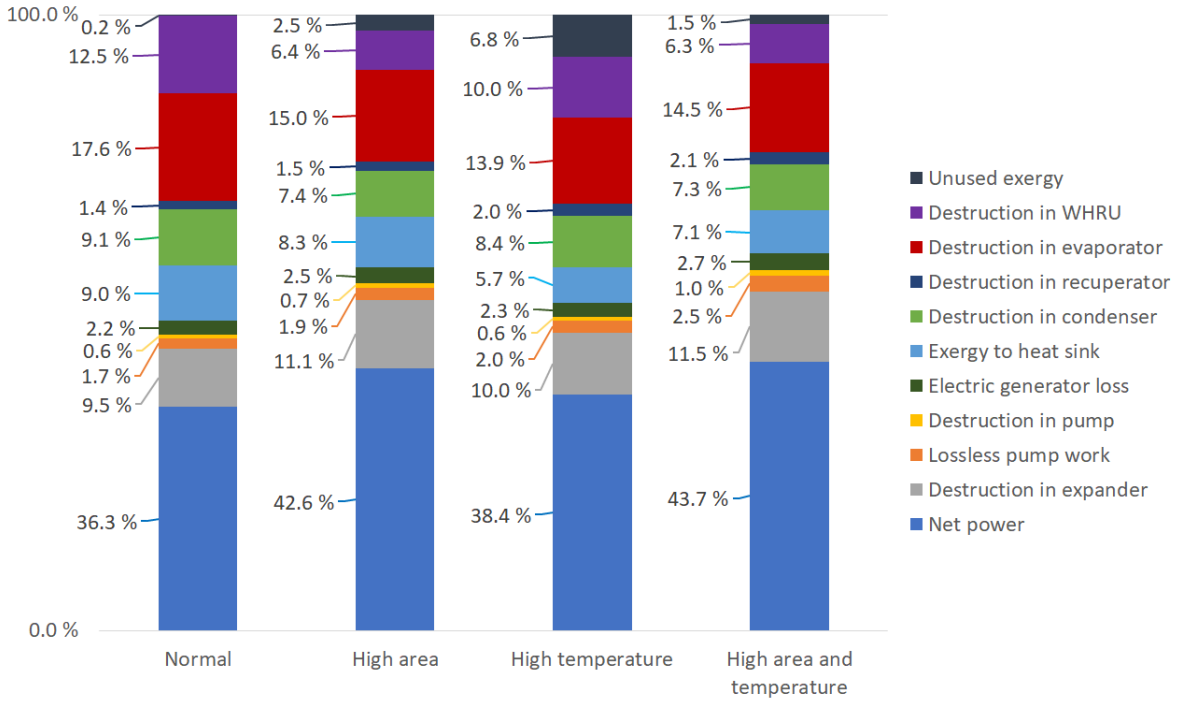

(b) Cycle using the mixture.

Figure 5.10: Distribution of exergy for the normal case, the high area case, the high temperature case and high area and temperature case.

Inspecting Figure 5.10 reveals that as the area increases, the losses in the heat exchangers generally decrease. Curiously, the unused exergy content increases when moving from the normal case to the case of higher area. Additionally, for both fluids, the recuperator breaks the trend of decreasing exergy loss in this step. Both of these are the result of the heat load on the recuperator increasing significantly when the area is increased from the normal case. This increase in load is enabled by the higher area, as most of the new available area is dedicated to the recuperator. Because of the higher heat load on the recuperator, the temperature of the working fluid entering the evaporator is increased, lowering the temperature difference here. This makes it more challenging for the water in the indirect loop to reach its minimum temperature constraint. When the indirect water loop does not reach its minimum temperature constraint, then neither will the heat source due to the assumption of constant ΔT_{WHRU}. This results in unused exergy in the heat source. However, the exergy destruction rate in the evaporator will also decrease because of the reduced temperature difference in this heat exchanger, and combined with the reduced losses in the other heat exchangers, there is ultimately a net gain of exergy to the expander.

It is important to remember that when the heat source temperature increases, the available exergy increases significantly. Figure 5.10 may thus be somewhat misleading, as the exergy efficiency does not change much between the cases. Also, it appears that the heat exchangers have had their exergy destruction rates reduced when only the temperature has increased, and that the improvement to the heat exchangers is similar to that of just increasing the area. However, inspecting the absolute values of the irreversibilities in the heat exchangers shows that this is not the case, and that all the heat exchangers experienced an increase in their respective exergy destruction rates. To better illustrate the benefits of increasing the heat source temperature, Figure 5.11 is made, which shows how much the net power increased for each case.

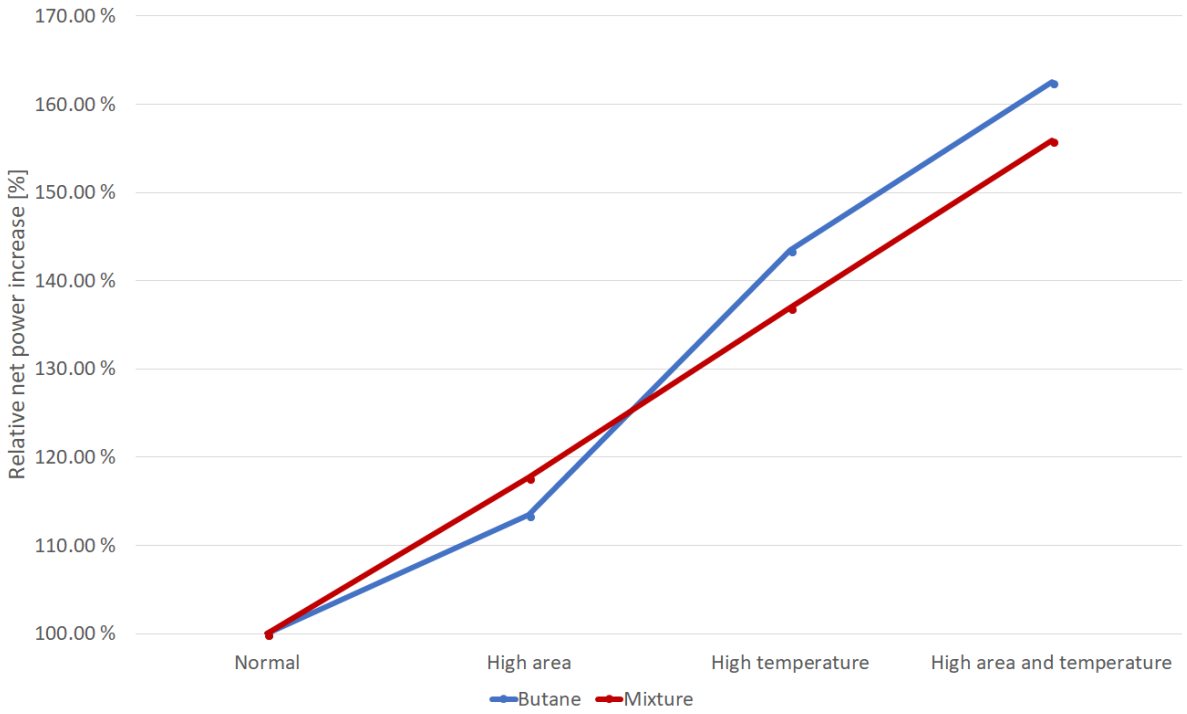

Figure 5.11: Net power for each case of area and heat source temperature.

Figure 5.11 shows that considerable gains can be made by making the adjustments shown in Table 5.12. While increasing the heat exchanger area of the system may be costly, increasing the temperature does not require additional investments as it only involves mixing the flue gases with less ambient air. By only increasing the temperature of the flue gases, the net power from the cycle may increase with 37% to 43%, depending on the working fluid. Increasing both the area and temperature, the net power increases by 56% to 63%. This shows that other, far more preferable solutions can be reached if surrounding process parameters are changed.

Chapter 6

Conclusion and future work

6.1 Conclusion

This work has investigated the yearly performance of an organic Rankine cycle using butane, pentane and a 50%-50% mixture of the two, and has identified how this performance varies with the characteristics of the cycle itself and the surrounding system. The off-design performance of the system is quantified using a geometric model for the heat exchangers and a numerical model for the expander off-design performance. The off-design performance is found by first optimizing for a design point, and then using the design data for the off-design optimization. For butane, the design point was in mid-August, and for the mixture, it was in July. The design points were evaluated on the grounds of operational feasibility and thermodynamic performance. Neither design point seemed to present variations in operational characteristics that would not be attainable in reality, and are therefore not rejected based on this. In terms of thermodynamic performance, the chosen design points were each compared to an alternative design point which could perhaps outperform the original design point. For both fluids, the original design point performed better, but not by much. For the mixture in particular, the alternative design point decreased the yearly energy output with only 0.14%, suggesting that one can freely choose between these based on this criterion. However, there may be other factors that influence this decision, such as the cost and size of the heat exchangers for example.

The owner of the aluminum production facility also has a contractual obligation to provide district heating to customers outside the facility. This heat is extracted upstream of the ORC, and the impact of this is evaluated. It was found that for butane, one could increase the yearly electric energy output with 15.1% if the district heating duty were not there. For the mixture, this increase was 19.3%. The alternative is to produce less electricity, but far more heat. With district heating, the cycle with butane has a yearly export of 643.7 MWh of electric energy and 982.5 MWh of thermal energy, compared with 741.0 MWh of electric energy without district heating. In order for the case without district heating to become profitable, the cost of the district heat must be less than 10% of the price of electricity. Even in such a case, it may be favorable to include the district heating for environmental reasons alone.

The impact of the WHRU is quantified. Because this component is not included in the model, it has had to be manually estimated, where the performance of the cycle was evaluated with the temperature difference in the WHRU being locked to 25 K, 17.5 K and 10 K throughout the heat exchanger. It was found that the WHRU performance is one of the key characteristics of the ORC, and as the WHRU temperature difference decreased from 25 K to 10 K, the net power

developed increased by 33.9% for butane and 35.1% for the mixture. The relative increase in heat exchange area for this performance is estimated to be 286.3%, and may not be economical, even if thermodynamically favorable.

Increasing the temperature of the heat source while maintaining the same heat content relative to the ambient has also been evaluated, alongside the effect of increasing the total heat exchanger area for the entire system. It was found that by just increasing the temperature, one could increase the net power output of the system by between 37% and 43% in the design month for the mixture and butane, respectively. If the total heat exchanger area is also high, the net power increase relative to the normal case is increased to 56% for the mixture and 63% for butane. It is not clear if the latter case is economical, as the price for the increase in heat exchanger area is not evaluated, but increasing just the temperature does not require the investment of capital, and leads to significant improvements. This change is therefore recommended.

While results from the preceding project indicated that mixtures were favorable to pure fluids, this work, with its more developed heat exchanger and expander models, seem to contradict that conclusion. In most scenarios evaluated in this work, butane outperforms the corresponding system with the 50%-50% mixture, and it therefore seems natural to favor butane as a working fluid. One exception to this is when comparing the performance of the cycle without district heating. In this case, the yearly electric energy output of the mixture is higher than the corresponding value for butane by roughly 3%. Also, in investigating the performance with different WHRU temperature differences, it was found that for the lowest WHRU temperature difference, the exergy efficiency for the cycles using butane and the mixture were equal. It seems that the mixture becomes more favorable as a working fluid as the temperature of the indirect water increases. However, because only butane and the 50%-50% mixture are compared, it cannot be concluded that for higher temperatures, the mixture becomes the favorable working fluid, because another pure fluid might become better at those temperature ranges. It may also be possible that a mixture between butane and pentane other than the 50%-50% mixture would be more favorable than the mixture in this work, but that is not investigated here.

6.2 Further work

It would be interesting to investigate other pure fluids and mixtures than butane, pentane and the 50%-50% mixture. This work neglected pentane because it performed so poorly, but investigating using propane and its isomers may be fruitful to see if the trends in this work continue or are just an anomaly of these particular fluids. It would also be interesting to analyze the performance with working fluids other than the alkanes, as alcohols, alkenes and aromatics may have properties that make them favorable as working fluids in these scenarios. Working fluids that may become transcritical for the heat source specifications may be interesting to investigate. A transcritical cycle may have significantly smaller exergy losses in the evaporator, thereby allowing higher expander power outputs. While neither butane nor the mixture are close to being transcritical, results from the project work showed that mixtures with cyclopropane and propane were close to transcritical. Investigating their performance in the event they did become transcritical could show that their performance is even better than that of butane in this work.

Another worthwhile addition to the repertoire of mixtures may be mixtures that are non-flammable. Because these cycles operate in close proximity to high-temperature heat sources, it may be reassuring for the operator of the facility to know that the working fluid in the ORC does not present a safety hazard. One alternative for achieving a non-flammable working fluid is to add CO_2 to the mixture. With a sufficiently high mass fraction, the presence of CO_2 will prevent the working fluid from igniting under the conditions in the aluminum production facility.

The analyses in this work would also be improved with a better models for the heat exchangers and expander. While the present model for the heat exchangers is advantaged in the sense that it calculates pressure drops and heat transfer coefficients while optimizing, it is hindered by the fact that the modelled heat exchangers are not actual heat exchanger designs. The results would be closer to reality if the model were able to simulate and optimize real heat exchanger designs, with the user choosing which design to use for the various heat exchangers. As for the expander, the present model requires the design isentropic efficiency to be input by the user, and the off-design efficiency is calculated based on this. It would be better if the expander sub-model instead took into account geometrical parameters, and calculated the losses due to e.g. leakage and friction under optimization. This would yield more accurate results, while also providing the actual expander geometries, meaning that one would not have to spend resources trying to develop the expander with the specified performances afterwards.

Finally, this work has only evaluated the thermodynamic performance of the ORC, and has not taken into account any costs involved in the system. Before an owner can conclusively choose a working fluid and a design for the facility, one must perform an extensive economic analysis to ensure that the system, and the components that are required for that system, are profitable in the long term. One characteristic that may influence this profitability is for example the pressure ratio across the expander and pump, where a higher pressure ratio may lead to more expensive equipment. Other aspects to consider are also the cost of the chosen working fluid, and the maintenance on the system with that fluid that is required to ensure a safe operation. Even the cost of heat exchangers vary significantly, and these depend very much on the chosen type of heat exchanger and its size. These are all factors that will have a significant impact on whether or not this system should be implemented in a facility, and must be evaluated before making a final decision.

Bibliography

Abadi, G. B., Kim, K. C., 2017. Investigation of organic rankine cycles with zeotropic mixtures as a working fluid: Advantages and issues. Renewable and Sustainable Energy Reviews 73, 1000–1013.

Calise, F., Capuozzo, C., Carotenuto, A., Vanoli, L., 2014. Thermoeconomic analysis and off-design performance of an organic rankine cycle powered by medium-temperature heat sources. Solar Energy 103, 595–609.

Cho, S.-Y., Cho, C.-H., Ahn, K.-Y., Lee, Y. D., 2014. A study of the optimal operating conditions in the organic rankine cycle using a turbo-expander for fluctuations of the available thermal energy. Energy 64, 900–911.

He, Z., Zhang, Y., Dong, S., Ma, H., Yu, X., Zhang, Y., Ma, X., Deng, N., Sheng, Y., 2017. Thermodynamic analysis of a low-temperature organic rankine cycle power plant operating at off-design conditions. Applied Thermal Engineering 113, 937–951.

Heberle, F., Preißinger, M., Brüggemann, D., 2012. Zeotropic mixtures as working fluids in organic rankine cycles for low-enthalpy geothermal resources. Renewable Energy 37, 364–370.

Hsu, S.-W., Chiang, H.-W. D., Yen, C.-W., 2014. Experimental investigation of the performance of a hermetic screw-expander organic rankine cycle. Energies 7, 6172–6185.

Hu, D., Zheng, Y., Wu, Y., Li, S., Yiping, D., 2015. Off-design performance comparison of an organic rankine cycle under different control strategies. Applied Energy 156, 268–279.

Hu, F., Zhang, Z., Chen, W., He, Z., Wang, X., Xing, Z., 2017. Experimental investigation on the performance of a twin-screw expander used in an orc system. Energy Procedia 110, 210–215.

Ibarra, M., Rovira, A., Alarcón-Padilla, D.-C., Blanco, J., 2014. Performance of a 5 kwe organic rankine cycle at part-load operation. Applied Energy 120, 147–158.

Kim, D.-Y., Kim, Y.-T., 2017. Preliminary design and performance analysis of a radial inflow turbine for organic rankine cycles. Applied Thermal Engineering 120, 549–559.

Lemort, V., Guillaume, L., Legros, A., Declaye, S., Quoilin, S., Apr. 2013. A comparison of piston, screw and scroll expanders for small-scale rankine cycle systems. In: Proceedings of the 3rd International Conference on Microgeneration and Related Technologies.

Lemort, V., Legros, A., 2017. Organic Rankine Cycle (ORC) Power Systems, 1st Edition. Woodhead Publishing Series in Energy, Ch. 12, p. 361.

Li, G., Lei, B., Wu, Y., Zhi, R., Zhao, Y., Guo, Z., Liu, G., Ma, C., 2018. Influence of inlet pressure and rotational speed on the performance of high pressure single screw expander prototype. Energy 147, 279–285.

Liu, L., Zhu, T., Ma, J., 2017. Working fluid charge oriented off-design modeling of a small scale organic rankine cycle system. Energy Conversion and Management 148, 944–953.

Manente, G., Toffolo, A., Lazzaretto, A., Paci, M., 2013. An organic rankine cycle off-design model for the search of the optimal control strategy. Energy 58, 97–106.

Mazzi, N., Rech, S., Lazzaretto, A., 2015. Off-design dynamic model of a real organic rankine cycle system fuelled by exhaust gases from industrial processes. Energy 90, 537–551.

Tang, H., Wu, H., Wang, X., Xing, Z., 2015. Performance study of a twin-screw expander used in a geothermal organic rankine cycle power generator. Energy 90, 631–642.

Tian, Y., Xing, Z., He, Z., Wu, H., 2017. Modeling and performance analysis of twin-screw steam expander under fluctuating operating conditions in steam pipeline pressure energy recovery applications. Energy 141, 692–701.

Walnum, H. T., Ladam, Y., Nekså, P., Andresen, T., 2011. Off-design operation of orc and co2 power production cycles for low temperature surplus heat recovery. International Journal of Low-Carbon Technologies 6, 134–140.

Walnum, H. T., Rohde, D., Ladam, Y., 2013. Off-design analysis of orc and co2 power production cycles for low-temperature surplus heat recovery. International Journal of Low-Carbon Technologies 8, 29–36.

Wang, J., Yan, Z., Zhao, P., Dai, Y., 2014. Off-design performance analysis of a solar-powered organic rankine cycle. Energy Conversion and Management 80, 150–157.

Yr.no, 2018. Weather statistics for sunndalsøra. `https://www.yr.no/place/Norway/M%C3%B8re_og_Romsdal/Sunndal/Sunndals%C3%B8ra/statistics.html`, Accessed: 12-03-2018.

Zeleny, Z., Vodicka, V., Novotny, V., Mescuch, J., 2017. Gear pump for low power output orc – an efficiency analysis. Energy Procedia 129, 1002–1009.

Zheng, Y., Hu, D., Cao, Y., Dai, Y., 2017. Preliminary design and off-design performance analysis of an organic rankine cycle radial-inflow turbine based on mathematic method and cfd method. Applied Thermal Engineering 112, 25–37.

Zhu, Y., Jiang, L., Jin, V., Yu, L., 2014. Impact of built-in and actual expansion ratio difference of expander on orc system performance. Applied Thermal Engineering 71, 548–558.

Appendix A

Draft article

One of the tasks in this thesis is to summarize the work in a draft scientific article. This draft can be found starting on the next page. A large focus has been placed on keeping the draft short, and so not all of the analysis is included. The topics that have been included are the effect of changing the temperature difference in the WHRU, and the performance gains when the heat exchanger area and heat source temperature are increased. These were chosen as it is thought that these are the most general results, and therefore applicable to a wider audience compared to the other topics investigated in this work.

Effect of design specifications for off-design operation of low temperature Rankine cycles using zeotropic mixtures and pure working fluids

Goran Durakovic
NTNU: Norwegian University of Science and Technology

Trond Andresen, Brede Andre Larsen Hagen & Petter Nekså
SINTEF Energy Research

Abstract

The organic Rankine cycle is an attractive technology to use on low temperature heat sources in order to develop power. It is important to evaluate the performance of these cycles through the entire year, as ambient conditions can experience large fluctuations between seasons. This work models the off-design performance of an indirectly heated organic Rankine cycles using butane, pentane and a 50%-50% mixture of these fluids, and investigates their sensitivities to the design specifications. It is found that the temperature of the heat source and the sizes of the heat exchangers play a large role in how much power the cycle is able to produce. For example, the results show that increasing the temperature of the heat source from 150°C to 180°C, but lowering the mass flow so that the heat content relative to the ambient remains the same, increases the net power output by 37% and 43%, depending on if the working fluid is the mixture or butane, respectively. Increasing the sum of the heat exchanger areas for the condenser, recuperator and evaporator from 230 m^2 to 300 m^3 leads to a net power increase of 18% for the mixture and 13% for butane. It is important to balance the cost of the increasing the size of the heat exchangers and the corresponding performance increase, as it is not always economical to enlarge the heat exchangers. Also, the temperature of the heat source should be maximized in order to increase the available exergy, wherever this is possible to do cheaply.

1 Introduction

The use of energy has received widespread attention in recent decades, following a growing understanding of the environmental consequences of our collective consumption of fossil fuels. To limit our reliance on non-renewable fuel sources, it is important to explore more environmentally friendly alternative sources of energy. One possibility for such a source is the exploitation of low-temperature waste heat from industrial processes, but technology for harnessing this for power production is underdeveloped. SINTEF Energy Research and their industrial partners have initiated the project CO-PRO, aimed at exploring and improving available solutions for utilizing waste heat for power production, in order to make this technology more attractive to the industry.

The organic Rankine cycle (ORC) seems like a fitting technology for using low-temperature heat sources for power production, and the use of zeotropic mixtures may further improve the performance of this cycle. The use of mixtures in ORCs have been documented in literature. [1] found that for heat sources at 150°C and 250°C, the use of zeotropic mixtures increased the net power output of the system by 12.3% and 5.5% respectively. [5] studied cycles using pure R601a and R600a, and mixtures that combined these with R245fa, R277ea, R1234yf and R1234ze. They found that the mixtures always outperformed both pure fluids, with the largest difference having the best mixture doubling the net power output of the best pure fluid. [2] found that a zeotropic mixture could increase the thermal efficiency of a system by up to 17.96%, compared to the constituting pure fluids. [6] investigated the exergy efficiency of subcritical ORCs using eight pure fluids and various mixtures that combined these, and found that using a mixture would increase the exergy efficiency of the cycle by at least 7.1%. [1] and [9] studied the effect of using more than two fluids in a mixture. [1] found that adding more fluids had a marginal effect, while [9] found that adding a third component could increase the net work of the system by 3.3% compared to the output of the binary mixture. Adding a fourth component increased the power output by 0.03% compared to the ternary mixture.

Exploring the use of ORCs using both pure fluids and zeotropic mixtures with one set of heat source characteristics is valuable work to illuminate the potential of zeotropic mixtures. The application of the results to

the industry is limited, however, because real cycles are exposed to many parameters that experience significant variations throughout the year, either as a result of differing activity levels or changing ambient conditions. An off-design analysis of a proposed system must be conducted in order to make the results more relevant to the industry. [4] modelled using R245fa and Solkatherm ES36 in an ORC that used a scroll expander to develop work. They varied the maximum temperature of the working fluid, the evaporation pressure of the cycle, the condensation temperature and the rotational speed of the expander, in order to investigate how these parameters influenced the system performance. They found that the thermal efficiency increased with increasing maximum temperature and decreasing condensation temperature. Additionally, they find that the performance of the expander plays a critical role in the performance of the cycle. [7] investigated the off-design analysis of an ORC incorporating R123 as the working fluid and a scroll expander. The design output of the expander is 3000 W, and using their model, they constrained the power output of the expander. They modelled expander power outputs between 1500 W and 3000 W, and investigated how the thermal efficiency of the cycle changed as the power requirement varied. They also investigated the influence of working fluid charge, modelled as the sum of mass in the condenser and evaporator. They found that the lowest thermal efficiency was reached when the power output was 1500 W, and that the charge had little effect. The highest efficiency was reached when the power output was 3000 W, and that this varied significantly with working fluid charge.

[12] modelled applying R245fa to a cycle using a turbine as the expander. The system was indirectly heated, where solar radiation would heat thermal oil, which subsequently heated the R245fa. They studied the effect of ambient temperatures on the system performance, and how the system reacted the flow of thermal oil changed. When the ambient temperature increased, the system performance decreased, mainly due to increased condensation pressure, which lowered the enthalpy difference in the expander. Increasing the flow rate of thermal oil increased the available heat in the evaporator, and thus increased the power output. [8] studied the off-design performance of a system using geothermal fluid as the heat source, where the flow rate of the geothermal fluid was constant, but the temperature varied between 130°C and 180°C. The heat sink of this investigation is air, and so the system is sensitive to changes in ambient temperature as well. The working fluids that are investigated are isobutane and R134a, with a radial turbine as the expander for both. For both fluids, the net power increases with increasing heat source temperature and decreasing ambient temperature. In one result, where the heat source temperature increased from 160°C to 180°C, the net power output of the cycle increased with 59%.

Off-design analyses have been given limited attention in literature, and off-design investigations into ORCs with zeotropic mixtures in appear to be entirely missing. The main objective of this work is therefore to examine the yearly performance of ORCs with zeotropic mixtures, and compare this to the performance of ORCs with pure fluids. This is done by investigating the effect of design specifications and changes in heat source and heat sink characteristics, for cycles with both pure fluids and mixtures.

2 System description

The heat source in this work is exhaust gases from aluminum production cells. These gases indirectly heat the ORC, with water acting as an intermediary fluid. The process diagram for this is shown in Figure 1, consisting of a waste heat recovery unit (WHRU), evaporator, recuperator, condenser, expander and pump. The expander used in this work is a twin-screw expander. The heat source has a lower temperature limit of 80°C to avoid reaching the acid dew point. The heat sink in this work is modelled to be water from a river. The temperature - entropy diagram is given in Figure 2, with the numbered state points included.

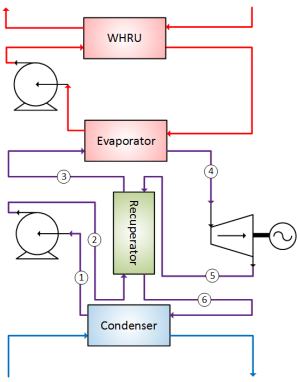

Figure 1: Process diagram of the system.

The weather data of Sunndalsøra have been used to capture the yearly variations in ambient temperature. The temperature of the ambient air and cooling water is modelled to vary sinusoidally between the maximum and minimum temperature throughout the year, and so the average monthly temperatures have been used.[13] In this work, it is assumed that the temperature of the heat source varies with the ambient air temperature such that a 1 K drop in the ambient temperature results in a 1 K drop in the heat source.

The changes in water temperature are delayed by one month compared to the ambient air, so the maximum temperature of water is reached one month after the maximum temperature of air. Figure 3 shows the variation of heat source and sink in this work. The heat source referred to in Figure 3 is the indirect water, as this is the heat source in the evaporator of the ORC.

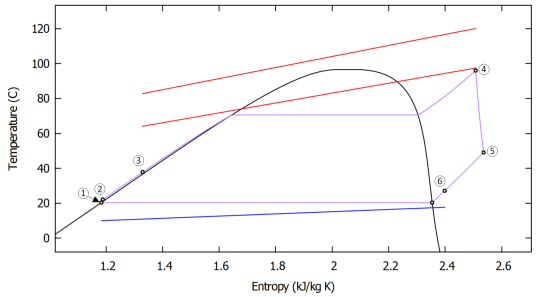

Figure 2: Temperature - entropy diagram of the ORC

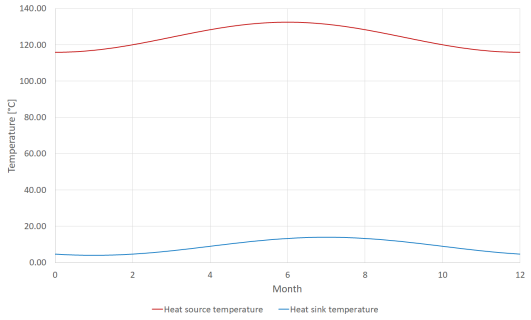

Figure 3: Yearly variation in heat source and sink temperatures.

Table 1 shows the parameters of the system that do not change between the on-design and off-design optimizations. The heat transfer coefficient of the heat source is set to 5000 $\frac{W}{m^2 \times K}$, due to model instability when this was geometrically evaluated. It is set so high to ensure that it is not the limiting factor in the evaporator. This value is most likely too high, so the results are somewhat overestimated. The number of tubes for the heat sink in the condenser is locked to 150 to increase the probability for a successful optimization. This number is very similar to the number of hot tubes in the condenser, and so it is unlikely that it affects the results much.

3 Methodology

3.1 Heat exchangers

This work uses a model developed by SINTEF Energy Research, which uses the NLPQL routine to find the set of parameters that optimize the net work for the system. Included in the model is a geometric evaluation of the heat exchangers. The details of the model and its geometric evaluations can be read about in detail in [10] and [3][2]. This model is only able to evaluate a directly heated ORC, and so it is unable to optimize the performance of the WHRU. To remedy this deficiency, it has been assumed that the temperature difference in the WHRU is

Table 1: System parameters.

Parameter	Value	Unit
Heat source characteristics		
Heat source medium	Air	-
Heat source flow rate	40000	$\frac{Nm^3}{h}$
Heat source inlet pressure	1	bar
$T_{s,min}$	80	°C
WHRU constant ΔT	17.5	K
Intermediate fluid characteristics		
Intermediate fluid medium	Water	-
Intermediate fluid flow rate	3.275	$\frac{kg}{s}$
Heat sink characteristics		
Heat sink medium	Water	-
Heat sink inlet pressure	5[1]	bar
Investigated working fluids		
Butane		
Pentane		
50%-50% mixture of butane and pentane		
Other constants		
Pump isentropic efficiency	70	%
Generator efficiency	95	%
Motor efficiency	95	%
Evaporator hot side HTC	5000	$\frac{W}{m^2 \times K}$
Condenser cold side number of tubes	150	-

17.5 K in the entire heat exchanger, which allows the temperature range of the indirect water loop to be specified. During on-design optimization, the geometries of the heat exchangers are set as variables, meaning that the optimizer can vary these to improve net work. When the off-design performance is optimized, the heat exchangers are locked to a specific design.

3.2 Expander

The expander employed in this work is a twin-screw expander. During optimization, two phase flow in the expander is disallowed, meaning that only gaseous flow in the expander is deemed an acceptable result. The off-design performance of the expander takes into account the effect of changing pressure ratios and varying volume flow rates through the expander. The expander sub-model is based on the findings of [11] and [14], where the results of the former is used to model the performance change due to changing flow rates, and the latter evaluates the performance degradation due to non-design pressure ratios. Using the expander sub-model, it is possible to create a performance map for the expander, which can be applied to an off-design scenario. Such a map is shown in Figure 4. The expander's off-design performance is evaluated during optimization by the model.

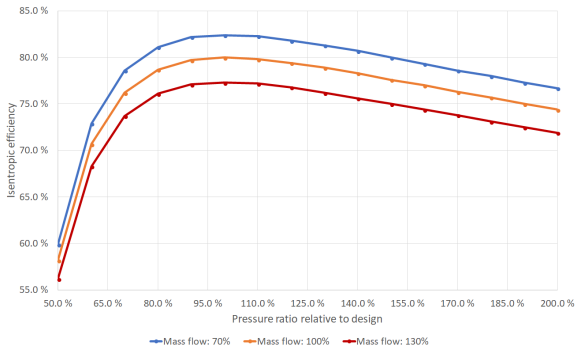

Figure 4: Performance map of the expander.

3.3 Exergy analysis

The distribution of available exergy in the cycle is evaluated in this work. The exergy of a system is the maximum amount of energy that can be converted to work before the system reaches a base state. The base state in this work is 10°C and 1 bar, which are atmospheric conditions. Equation 1 shows how the exergy is calculated at a point, and Equation 2 shows the exergy balance in a control volume, which must always be upheld. The exergy efficiency of the cycle is the ratio of net work to the available exergy, represented algebraically in Equation 3.

$$\dot{E}_x = \dot{m} \times [(h - h_0) - T_0 \times (s - s_0)] \tag{1}$$

$$\sum \dot{E}_{x\,in} - \sum \dot{E}_{x\,out} - \dot{W}_{net} - \dot{I} = 0 \tag{2}$$

$$\eta_{Ex} = \frac{\dot{W}_{net}}{\dot{E}_{x\,s,\,in} - \dot{E}_{x\,s,\,out,\,min}} \tag{3}$$

The Carnot efficiency of the system is calculated to have a reference of how much exergy is available in the system. This is done to ensure that the exergy calculations are correct. Equation 4 gives the Carnot efficiency of a cycle that has a temperature difference of the heat source, and has a minimum heat source temperature. Using the Carnot efficiency, the maximum available exergy from the heat source is calculated using Equation 5.

$$\eta_{Carnot} = 1 - \left(\frac{T_0}{T_{s,\,in} - T_{s,\,min}}\right) \times \ln\left(\frac{T_{s,\,in}}{T_{s,\,min}}\right) \tag{4}$$

$$\dot{E}_{x\,avail,\,Carnot} = \eta_{Carnot} \times \dot{m}_s \times (h_{s,\,in} - h_{s,\,min}) \tag{5}$$

3.4 Choosing a design point

The year is split into eight evenly spaced data points in this work, for which the performance is evaluated. To find the design point for each working fluid, first every data point is optimized as on-design points, meaning that the optimizer finds the optimal geometry of the heat exchangers. One of these on-design optimization results are picked as the design point for that fluid. The design specifications for each fluid is given in Table 2.

When the model is optimizing a design point, it is able to change the geometrical parameters of the heat exchangers, and it must balance the trade-off between pressure drop and increased heat transfer. With a very large heat exchanger, it is possible to transfer all the required heat and have little pressure drop, but this is unrealistic for practical applications. Therefore, the total heat exchanger area is restricted to 230 m^2 in this work. This particular value is chosen based on other preceding work, that showed that this number offered a good balance between performance and area investment.[3]

4 Results and discussion

Figure 5 displays how much net power each fluid develops in every data point using the chosen design points given in Table 2.

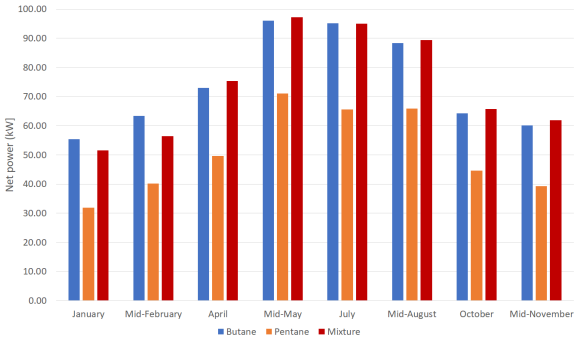

Figure 5: Net power for each data point, with each working fluid

It is clear from Figure 5 that pentane is significantly outperformed by the other two working fluids, and it is therefore not analyzed further. Figure 5 also shows how in January and mid-February, butane outperforms the mixture by a large margin, whereas the mixture is slightly better than butane in all the other data points. The yearly energy output is estimated by applying the trapezoid rule to these data points. Table 3 shows the estimated yearly electric energy output for butane and the mixture. It shows that across the entire year, butane is able to deliver the most electric energy. The fact that butane is able to provide more electrical energy on a yearly basis means that the higher power output during January and mid-February is enough to offset the small advantage the mixture has in the other data points.

Table 2: Design parameters for each fluid.

	Butane	Pentane	50%-50% mixture
Design point	Mid-August	April	July
Working fluid maximum pressure (bar)	11.07	3.10	6.80
Working fluid maximum temperature (°C)	84.08	73.35	89.02
Working fluid flow rate ($\frac{kg}{s}$)	2.12	1.67	2.16
Working fluid minimum pressure (bar)	2.45	1	1.33
Heat sink mass flow rate ($\frac{kg}{s}$)	23.64	13.87	21.73
Evaporator length (m)	25.77	25.81	23.81
Evaporator cold side number of tubes (-)	104	202	107
Condenser length (m)	26.11	7.39	22.46
Condenser hot side number of tubes (-)	85	142	97
Recuperator length (m)	1.34	0.09	2.38
Recuperator cold side number of tubes (-)	67	61	51
Recuperator hot side number of tubes (-)	126	100	141
Expander design isentropic efficiency (%)	80	80	80

Table 3: Estimated yearly electric energy output for butane and the 50%-50% mixture.

	Butane	50%-50% mixture
Yearly E_{el} (MWh)	643.6	640.0

It is important to investigate the effect of the assumption with the constant WHRU temperature difference, as this is not part of the model. The effect of changing this temperature difference from 17.5 K to 10 K and 25 K is investigated for butane and the mixture. Table 4 shows the temperature specifications for the indirect fluid with the new temperature differences in the WHRU.

Table 4: Temperature data for the cycle with new WHRU temperature differences.

	Butane	50%-50% mixture
$T_{s,in}$ (°C)	146.32	150.00
$T_{s,min}$ (°C)	80.00	80.00
$\Delta T_{WHRU} = 25\ K$		
$T_{indirect,max}$ (°C)	121.32	125
$T_{indirect,min}$ (°C)	55.00	55.00
$\Delta T_{WHRU} = 17.5\ K$		
$T_{indirect,max}$ (°C)	128.82	132.50
$T_{indirect,min}$ (°C)	62.50	62.50
$\Delta T_{WHRU} = 10\ K$		
$T_{indirect,max}$ (°C)	136.32	140.00
$T_{indirect,min}$ (°C)	70.00	70.00

Figure 6 shows how the performance changes when the temperature difference in the WHRU is varied. It is important to realize that by changing the temperature difference in the WHRU, one is also implicitly changing the size of the heat exchanger. It is therefore not clear whether decreasing the WHRU temperature difference will be economical, even if it thermodynamically superior. Using the result for butane as an example, in mid-August the performance of the cycle is increased by 15% when the temperature difference is lowered from 17.5 K to 10 K. Assuming that the overall heat transfer coefficient in the WHRU is 100 $\frac{W}{m^2 \times K}$, to reach such a low temperature difference, one would have to increase the heat exchange area from roughly 500 m^2 to 900 m^2 – a relative increase of 80%. A more in-depth techno-economic study must be performed to deem whether this is a worthwhile investment.

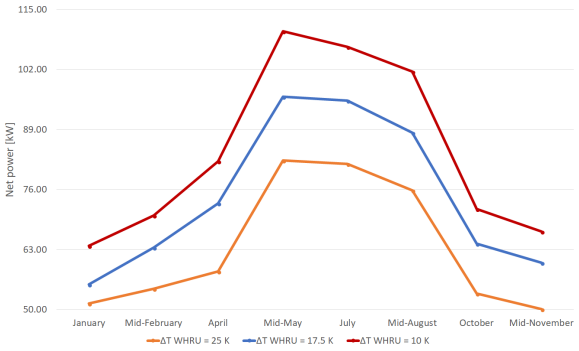

(a) For butane.

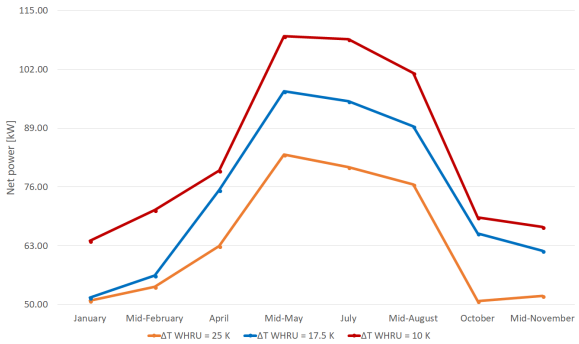

(b) For the mixture.

Figure 6: Performance changes with different ΔT_{WHRU} for butane and the mixture.

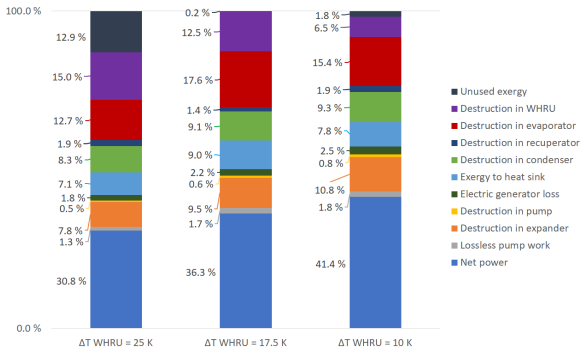

(b) For the mixture in July.

Figure 7: Distribution of available exergy with different ΔT_{WHRU} for butane and the mixture

An exergy analysis of the cycle components is performed to investigate what causes the increase in power output with lower temperature difference in the WHRU. This traces the exergy in the exhaust gases from when it enters the system, and discovers how it leaves the system. The exergy analysis is only performed for the design points for butane and the mixture, but the findings should be general enough so that they give an insight into what occurs in the other data points as well. This is shown in Figure 7.

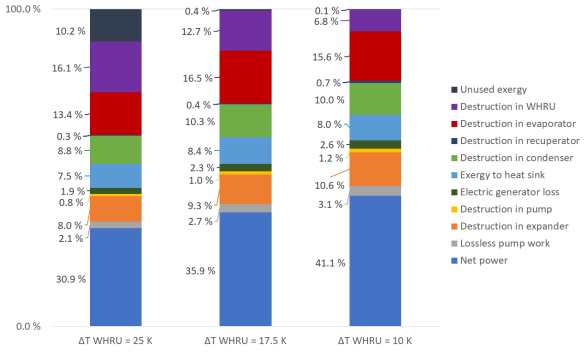

(a) For butane in mid-August.

It is clear that by decreasing the WHRU temperature difference (and thus increasing the size of this heat exchanger,) the major benefit is that the cycle wastes far less of the available exergy. The exergy that was unused when the temperature difference was 25 K is distributed into the cycle in various ways as the temperature difference is lowered to 17.5 K, with roughly half becoming additional work produced by the expander for both working fluids. Further reducing the temperature difference results in reducing the exergy destruction in the WHRU, because the intermediate fluid leaves the WHRU with a temperature that is closer to the inlet temperature of the heat source.

It is also interesting to investigate the effect of increasing the temperature of the heat source, but maintaining the same heat content in reference to the ambient by reducing the mass flow of the exhaust gases. This is a realistic modification of the system, as the exhaust gas is immediately mixed with ambient air to cool it as it exits the aluminum cell. By reducing the intake of ambient air, the temperature of the gas is increased. It is also worthwhile to investigate increasing the areas of the three heat exchangers that are present in the model, especially as the temperature of the heat source increases. With the higher temperature, there will be more exergy in the stream, and to extract most of it one needs larger heat exchangers. Thus it becomes more reasonable to consider increasing the size of the heat exchangers. Here, when modelling the cases where the heat exchangers have their areas increased, the temperature difference in the WHRU is again lowered to 10 K, rather than 17.5 K. This is done to simulate that the WHRU also has its heat exchanger area increased. The distribution of area between the other three heat exchangers is left to the optimizer, as it is able to find the best solution. Table 5 shows how the heat source temperature and total heat exchanger area are changed for each of the cases investigated in this section.

Table 5: System parameters in increasing the heat exchange area and heat source temperature

	Normal	High T_s	High A	High A and T_s
A_{tot} (m^2)	230	230	300	300
T_s (°C)	150	180	150	180
ΔT_{WHRU} (K)	17.5	17.5	10	10
$\dot{m}_{indirect}$ ($\frac{kg}{s}$)	3.275	2.631	3.275	2.631
$\dot{m}_s$ ($\frac{kg}{s}$)	13.614	11.198	13.614	11.198

The effect of the changes listed in Table 5 were only

investigated for the design months of butane and the mixture. The results are shown in Figure 8.

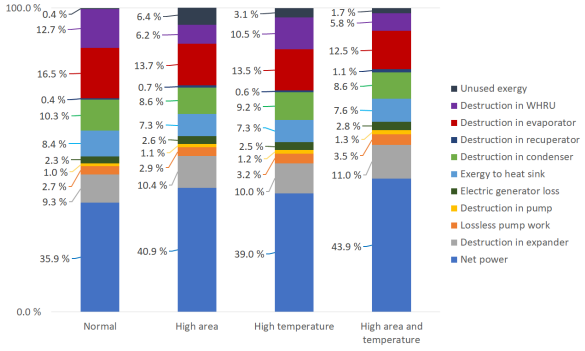

(a) Cycle using butane.

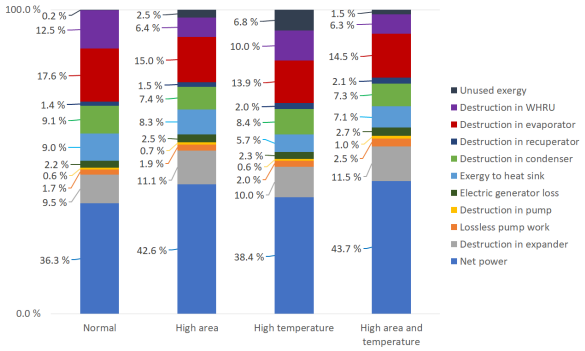

(b) Cycle using the mixture.

Figure 8: Distribution of exergy for the normal case, the high area case, the high temperature case and high area and temperature case.

It is clear that increasing the area will lead to a higher exergy efficiency, both when the temperature is normal and high. Curiously, when the temperature is normal, the unused exergy increases when the area is increased. This occurs because the majority of the larger heat exchanger budget goes to the recuperator. With the larger heat exchanger area in the recuperator, the temperature of the working fluid at the inlet of the evaporator will increase. This reduces the temperature difference in the evaporator, and thereby making it more challenging to have the indirect water loop reach its minimum temperature. As a result, the indirect water loop is further from its minimum temperature limit than when the heat exchanger area budget is lower.

Figure 8 may be somewhat misleading, as it appears from the exergy efficiency that the differences are very small between the cases when the heat source temperature is normal and when it is high. However, it is important to keep in mind that the exergy content has increased considerably when the temperature of the heat source is increased. Investigating the increase in net power will paint a more realistic picture. This is shown in Figure 9.

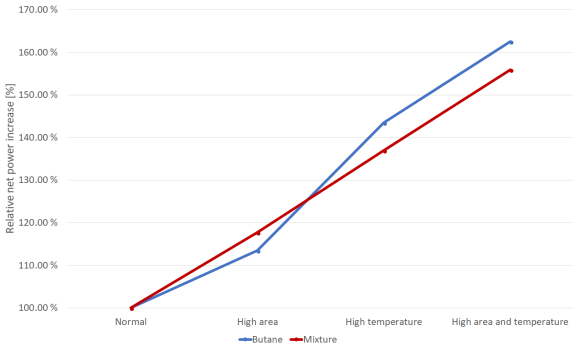

Figure 9: Net power for each case of area and heat source temperature.

It can be seen in Figure 9 that just by increasing the temperature, the net power developed can be increased by 37% to 43% compared to the normal case, depending on the working fluid. This change seems recommendable, as it does not cost anything to the operator of the aluminum facility – it only requires decreasing the amount of air that is mixed with the exhaust gases as they exit the aluminum cells. Increasing both the area and the temperature results in a net power increase of 56% to 63%, again depending on the working fluid. Whether it is worth it to invest in higher heat exchanger areas is not clear from this data alone, and more thorough economic analyses should be made before this is conclusively decided.

5 Conclusion

This work has investigated the impact of the design specifications on the performance of a low-temperature ORC using either butane or a 50%-50% mixture of butane and pentane. A simulation model capable of optimizing the distribution of heat exchanger area during on-design mode, and estimating the performance changes in the expander in off-design mode has been developed and utilized in this work. This has allowed for a realistic estimate of the off-design performance of the cycles.

The results show that the dimensions of the heat exchangers and the temperature of the heat source play a large role in the performance of the cycle. In investigating the WHRU alone, it was found that by decreasing the temperature difference from 17.5 K to 10 K, the power development of the cycle with butane would increase by 15%. This was primarily attributed to reduced exergy irreversibilities in the WHRU. Investigating how the system responded when the temperature difference in the WHRU was decreased from 25 K to 17.5 revealed that the primary reason for the increase in performance was

that much less exergy went unused. Unused exergy in the heat source is particularly unfortunate, as this is almost wasted pure work. That the amount of wasted exergy is lowered when the WHRU size is increased highlights the importance of the WHRU.

Changing the heat source characteristics as well as the areas for the evaporator, recuperator and condenser were also investigated. It was found that the net power would increase by 37% to 43% for the mixture and butane, respectively, just by increasing the heat source temperature. Increasing both the heat exchanger area and heat source temperature lead to a net power increase of 56% to 63% for the mixture and butane, respectively.

References

[1] Chys, M., van den Broek, M., Vanslambrouck, B., and De Paepe, M. Potential of zeotropic mixtures as working fluids in organic rankine cycles. *Energy 44* (2012), 623–632.

[2] Dong, B., Xu, G., Luo, X., Zhuang, L., and Quan, Y. Potential of low temperature organic rankine cycle with zeotropic mixtures as working fluid. *Energy Procedia 105* (2017), 1489–1494.

[3] Hagen, B., and Nikolaisen, M. Detailed analysis of promising working fluids for COPRO technology. Tech. rep., SINTEF Energy Research, 2017.

[4] Ibarra, M., Rovira, A., Alarcón-Padilla, D.-C., and Blanco, J. Performance of a 5 kwe organic rankine cycle at part-load operation. *Applied Energy 120* (2014), 147–158.

[5] Kang, Z., Zhu, J., Lu, X., Li, T., and Wu, X. Parametric optimization and performance analysis of zeotropic mixtures for an organic rankine cycle driven by low-medium temperature geothermal fluids. *Applied Thermal Engineering 89* (2015), 323–331.

[6] Lecompte, S., Ameel, B., Ziviani, D., van den Broek, M., and De Paepe, M. Exergy analysis of zeotropic mixtures as working fluids in organic rankine cycles. *Energy Conversion and Management 85* (2014), 727–739.

[7] Liu, L., Zhu, T., and Ma, J. Working fluid charge oriented off-design modeling of a small scale organic rankine cycle system. *Energy Conversion and Management 148* (2017), 944–953.

[8] Manente, G., Toffolo, A., Lazzaretto, A., and Paci, M. An organic rankine cycle off-design model for the search of the optimal control strategy. *Energy 58* (2013), 97–106.

[9] Satanphol, K., Pridasawas, W., and Suphanit, B. A study on optimal composition of zeotropic working fluid in an organic rankine cycle (orc) for low grade heat recovery. *Energy 123* (2017), 326–339.

[10] Skaugen, G. Thermodynamic framework for cycle and component analysis and optimisation. Tech. rep., SINTEF Energy Research, 2016.

[11] Tian, Y., Xing, Z., He, Z., and Wu, H. Modeling and performance analysis of twin-screw steam expander under fluctuating operating conditions in steam pipeline pressure energy recovery applications. *Energy 141* (2017), 692–701.

[12] Wang, J., Yan, Z., Zhao, P., and Dai, Y. Off-design performance analysis of a solar-powered organic rankine cycle. *Energy Conversion and Management 80* (2014), 150–157.

[13] Yr.no. Weather statistics for Sunndalsøra. `https://www.yr.no/place/Norway/M%C3%B8re_og_Romsdal/Sunndal/Sunndals%C3%B8ra/statistics.html`, 2018. Accessed: 12-03-2018.

[14] Zhu, Y., Jiang, L., Jin, V., and Yu, L. Impact of built-in and actual expansion ratio difference of expander on orc system performance. *Applied Thermal Engineering 71* (2014), 548–558.

Nomenclature

Abbreviations

HTC	Heat transfer coefficient
ORC	Organic Rankine cycle
WHRU	Waste heat recovery unit

Symbols

A	Area, m^2
$\dot{E}_x$	Exergy, kW
E	Energy, MWh
h	Enthalpy, $\frac{kJ}{kg}$
h_0	Enthalpy at base state, $\frac{kJ}{kg}$
$\dot{I}$	Exergy destruction rate, kW
$\dot{m}$	Mass flow, $\frac{kg}{s}$
s	Entropy, $\frac{kJ}{kg \times K}$
s_0	Entropy at base state, $\frac{kJ}{kg \times K}$
T	Temperature, K
T_0	Ambient temperature, K
$\dot{W}$	Work, kW

Greek symbols

Δ	Difference
η	Efficiency

Subscripts

0	Ambient
avail	Available
cond	Condenser
el	Electric
evap	Evaporator
ex	Exergy
exp	Expander
gen	Generator
in	Inlet
indirect	Indirect fluid
min	Minimum
net	Net
out	Outlet
pump	Pump
recup	Recuperator
s	Heat source
tot	Total
WHRU	Waste heat recovery unit

Notes

[1] 5 bar was chosen to avoid issues with high pressure loss in the model. In evaluating the pump work for the heat sink, the model only takes into account the work needed to sustain the pressure loss, so a high inlet pressure here does not affect the result. In reality, the inlet pressure here would most likely be much lower to avoid having to needlessly pump the heat sink fluid to a high pressure.

[2] Don't think I can reference these internal memos?

[3] Reference project work?